POLITECNICO DI MILANO

School of Industrial and Information Engineering

Master of Science in Materials Engineering and Nanotechnology

Analysis of surface acoustic waves-based devices for particles trapping and sorting

Supervisor: Prof. Stefano Mariani

Co-Supervisor: Prof. Olivier Français

Candidate:

Gianluca Mezzanzanica, 943782

Academic Year 2020-2021

Abstract

The separation and manipulation of particles and bioparticles are important operations for biological analyses. Microfluidic devices can be considered as low cost and low consumption of power and resources portable solutions. The integration of microfluidics with different fields of physics, brought the possibility to control particles in a more precise way, compared to centrifugation for example, exploiting their mechanical, electric and magnetic properties. Acoustofluidics has been considered in recent years as a very effective solution for particle control and isolation: the development of acoustic waves inside the microfluidic channel generates acoustic radiation forces (ARFs) to move particles. The specific kind of waves studied are standing surface acoustic waves (SSAWs). Considering acoustic pressure field, solid particles are moved towards the pressure nodes (points of null acoustic pressure): the name of this phenomenon is acoustophoresis.

In this thesis, microfluidics is coupled with acoustics through a multi-physics numerical solution. Exploiting interdigital transducers (IDTs), waves are generated on the surface of a lithium niobate piezoelectric substrate. These waves interfere constructively where a microfluidic channel, made on polydimethylsiloxane (PDMS), is placed to generate SSAWs in the channel. To demonstrate pressure waves development and particles motion, a 2D transversal cross-section of the device was studied both with frequency and time domain analyses. Keeping a rectangular section rectilinear channel, different geometric features (width and height) were considered to investigate the sensitivity of the acoustic pressure field to geometrical changes. Then, a 3D complete device simulation was done to see particles focusing on pressure nodes due to acoustic radiation force. Further analyses were related to IDTs positioning to investigate surface waves interactions on an anisotropic material as lithium niobate. With these simulations a squared pressure waves “pool” made on PDMS was considered to demonstrate the possibility to immobilize particles inside pressure nodes.

Riassunto

La separazione e la manipolazione di particelle e bioparticelle sono importanti operazioni per le analisi biologiche. I dispositivi di microfluidica possono essere considerati come soluzioni portatili a basso costo e a basso consumo di risorse e potenza. L'integrazione della microfluidica con diversi campi della fisica ha portato alla possibilità di controllare le particelle in modo più preciso, rispetto alla centrifugazione per esempio, sfruttando le loro caratteristiche meccaniche, elettriche e magnetiche. L'acustofluidica è stata considerata, negli anni recenti, una soluzione molto efficace per il controllo e l'isolamento delle particelle: lo sviluppo di onde acustiche all'interno di un canale di microfluidica genera forze di radiazione acustica per muovere le particelle. La tipologia specifica di onde acustiche studiata è quella delle onde acustiche di superficie stazionarie. Considerando un campo di pressione acustica, particelle solide sono mosse verso i nodi di pressione (punti dove la pressione acustica è nulla): il nome di questo fenomeno è acustoforesi.

In questa tesi, la microfluidica è accoppiata con l'acustica attraverso una soluzione numerica di multi-fisica. Sfruttando trasduttori interdigitali, le onde sono generate sulla superficie di un substrato di niobato di litio piezoelettrico. Queste onde interferiscono costruttivamente dove è posizionato un canale in PDMS per generare onde acustiche di superficie stazionarie nel canale. Per dimostrare lo sviluppo di onde di pressione e il movimento delle particelle, è stata studiata una sezione 2D trasversale del dispositivo sia con analisi in frequenza sia tempo dipendenti. Mantenendo un canale rettilineo a sezione rettangolare, diverse proprietà geometriche (larghezza e altezza) sono state considerate per investigare la sensibilità del campo di pressione acustica a variazioni geometriche. Poi, è stata fatta una simulazione 3D del dispositivo completo per vedere la focalizzazione delle particelle nei nodi di pressione acustica. Ulteriori simulazioni sono relative al posizionamento dei trasduttori interdigitali per investigare l'interazione delle onde di superficie su un materiale anisotropo come il niobato di litio. Con queste simulazioni una "piscina" quadrata di onde di pressione in PDMS è stata considerata per dimostrare la possibilità di immobilizzare le particelle nei nodi di pressione.

Contents

List of figures

List of tables

1 Introduction

The possibility to manipulate and separate particles and bioparticles is fundamental for chemical and biomedical analyses. These operations can lead to a precise diagnosis of diseases for patients. Fast and precise technologies are always required to improve the control and the study of specific cells or biological species.
Several examples can be found related to specific problems of biological samples handling. Exosomes are membrane-bound extracellular vesicles of between 30-200 nm diameter, they act as biomarkers for diagnosis of diseases and play an important role in regenerative medicine [1]. These nanoparticles are typically collected from moderate fluid volumes with ultra-centrifugation or ultra-filtration which are time-consuming and can damage the structural integrity of bioparticles. Escherichia coli O157:H7 is a serotype of enterohemorrhagic Escherichia coli (EHEC). As the most harmful food-borne pathogenic bacterium, it can destroy cells. This bacterium can cause many life-treating diseases. Many methods have been developed for detecting Escherichia coli, but these are tedious and include pre-enrichment, selective planting, biochemical screening and serological confirmation [2]. The two proposed examples highlight the need of new efficient technologies to deal with specific issues in biomedical and chemical research.

Microfluidic technology is considered as a valid solution to these issues for particles and cells manipulation. Microfluidics is the science of systems that process small amounts of fluids, using channels with dimensions from tens to hundreds of micrometres [3]. Several advantages are reported considering microfluidics: first of all, the reduction in size of technological analyses devices, leading to lower costs for production and the design of portable ones; the use of small amounts of samples and reagents, reducing the cost and the waste of chemicals; the reduction of time required for reactions and analyses; the possibility of integration of different chemical analyses in parallel on the same sample [4], [5]. Another important advantage is related to fluid dynamics. At microscale the fluid flow is always laminar in rectilinear structures, not disturbed by any kind of spontaneous turbulences [6]. These advantages can be directly connected with a technology

called Lab-on-chip (LoC). Lab-on-chip is basically the integration of microfluidics, electronics, optics and biosensors on a single portable device. The very first idea was to design a portable device to perform usual laboratory activities such as mixing or filtering. The platforms provide a solid way for miniaturization, integration, automation and parallelization of chemical processes [7]. Microfluidics properties, such as low cost and portable devices and low waste of chemicals, are specifically needed to design point-of-care (POC) systems. This term is associated to the development of inexpensive but reliable and accurate systems for medical analyses to be done near the patient, without need to go in a laboratory to perform them. A further step is thinking these devices to be easy-to-use without a high level of training, becoming simpler to guarantee global public health control [8].

The coupling of microfluidics with other fields of physics is considered to overcome some of the limitations induced by the micrometric size of the devices and by the particles nature. For example, contact techniques have been developed exploiting microfluidic channels to investigate cells and particles characteristics. Chen et al. [9] designed a microfluidic platform which can park specific particles, considering their mechanical properties, in hydrodynamic traps with the possibility to recollect them after the analyses. The micrometric size of channels limits fluid manipulation. At this scale viscous forces overcome inertial ones, limiting basic fluidics operations such as pumping or mixing. For these specific purposes microfluidics was coupled with acoustics to develop the field of acoustofluidics. The interaction of acoustic waves with fluids enables fluids and particles manipulation and control due to development of specific effects (the acoustic radiation force, ARF, and the acoustic streaming). Although the two fields are deeply studied as stand-alone branches of physics, the coupling between them is complicated and generates many effects not so easy to be controlled [10].

The first experimental observation of acoustic interactions on particles dates back to the 1860s, when German physicist August Kundt measured the velocity of sound. Kundt designed an acoustic resonator chamber, later known as Kundt's tube, to establish a standing acoustic wave field. The position of the pressure nodes was then visualized by adding dust into the chamber, which aggregated at the location of the pressure nodes [11]. His tube is nowadays still used to demonstrate the

presence of longitudinal waves in gases and measure acoustic forces. From that work up to now there was a great development in the field exploiting microfluidics advantages. Hill et al [12], [13] exploited acoustofluidics to separate particles flowing in a fluid. They developed a device based on bulk acoustic waves (BAWs) with piezoelectric materials to generate ultrasound waves in a silicon microfabricated channel. More recent BAWs technology designs follow the "Lund method", developed by a research group at Lund university, which proposes the actuation to be done from below, with standing acoustic waves generated between the channel side walls exploiting the use of a reflector at the opposite side [14].

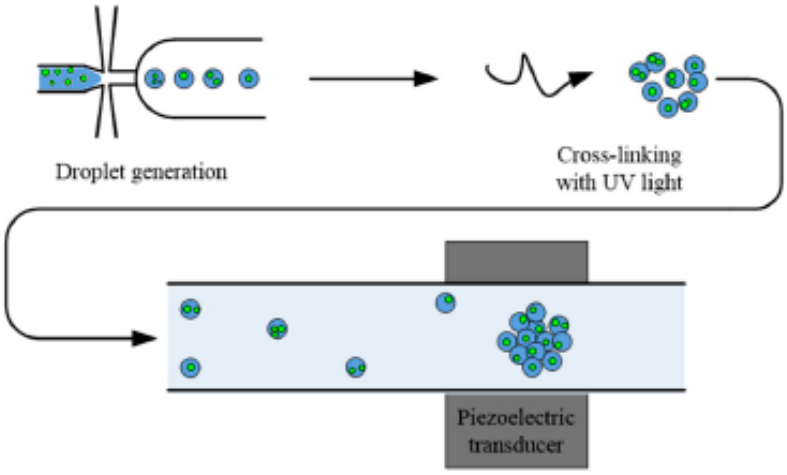

Figure 1.1: Flow chart of acoustic trapping of hydrogel droplets. A piezoelectric transducer is placed below the microchannel to generate the acoustic waves [15].

Also surface acoustic waves (SAWs) are exploited for acoustofluidics, providing an easier design of systems and no need of wave reflectors. One of the first experimental evidence of acoustic streaming induced by SAWs is contained in the work of Shiokawa et al [16] in 1988. Then many studies were done both for fluid manipulation (controlled motion of droplets [17], acoustic streaming [18]) and particle manipulation (heterogeneous particles separation [19]) with SAWs.

The aim of this work is to study the interaction of standing surface acoustic waves (SSAWs) with fluids for particles manipulation. To do it, numerical simulations of acoustofluidic devices have been done to highlight the effect of the acoustic radiation force, resulting from the scattering of acoustic waves on particles, for particles being dragged by fluid flow in a microchannel. The simulations were performed first considering a two-dimensional transversal cross section of the

microfluidic device and then with a complete three-dimensional device structure. In addition, a parametric analysis on channel geometrical features was done to investigate the sensitivity of the pressure field being developed inside the fluid. To conclude, further analysis has been performed considering different interdigital transducers (IDTs), array of metallic electrodes deposed on a piezoelectric substate, geometries and disposition on a piezoelectric substrate, where IDTs are deposited, to indagate the anisotropic mechanical response of these materials. The results of these analyses have shown the possibility to use SSAWs to generate specific pressure patterns inside microchannels and with them different possibilities for particles manipulation (focusing or trapping).

1.1 Thesis outline

In this chapter, a brief introduction on the problem was given. In Chapter 2, an overview on acoustofluidics is reported. After a description of the fundamentals of microfluidics, the acoustic manipulation is introduced through the description of the generation of acoustic waves and their use in microfluidics. Both BAW-based and SAW-based systems are presented considering the design of the devices and the specific fabrication techniques. The chapter is focused on SAWs, being distinct between travelling (TSAWs) and standing (SSAWs), and their specific applications on microfluidic technologies. The chapter concludes presenting some limits and future trends related to this problem.

Chapter 3 provides a theoretical description of the physics involved in the acoustofluidic problem. The governing equations related to fluid and solid mechanics are presented. Rayleigh waves and their transmission to fluids are also described. Moreover, the formulation of the acoustic radiation force is reported to see the parameters on which it depends.

In chapter 4, the numerical analyses performed on a SSAW-based acoustophoretic device are described and the results are reported. First, a two-dimensional analysis on the cross-section of the device is done to manage the physics involved and investigate the effect of the boundary conditions and the channel geometry on the pressure field. Then, a three-dimensional device is modelled to simulate a complete interaction between the components of the device. Finally, to investigate the

propagation and the interaction between counter-propagating waves, different IDTs configurations are modelled. Using the results obtained by this last simulation, a water "pool" containing particles is modelled to achieve particle trapping. Furthermore, the fabrication steps, related to soft-lithography (which name is associated to the use of soft materials to fabricate microstructures), followed to build a PDMS microchannel are described.

Finally, Chapter 5 reports the final considerations and the possible future developments correlated the analyses.

2 Acoustofluidics

Acoustofluidics is the specific coupling between acoustics and microfluidics. The integration of these fields opens a complex and manifold branch: not only having to handle the phenomena by coupling fluid mechanics and acoustics, but also design precise micro-fabrication processes. In the first part of a thematic tutorial series on this topic [20], acoustofluidics is defined as "ultrasound-based external forcing of microparticles in microfluidics". Therefore, the definition itself states the fundamental building blocks and the aims of this science.

To explain what acoustofluidics is, first microfluidics is introduced defining some dimensionless numbers to explain the phenomena governing fluid dynamics at the microscale. Acoustic waves for particles manipulation are described considering the use of piezoelectric materials for the actuation of waves and the great biocompatibility of this technology for bio-samples handling. Different kinds of devices are introduced, exploiting both BAW and SAW-based configurations. Microfabrication is the main fabrication technique used to produce these systems: a focus on the soft-lithographic technique is given as a cheap and easy solution for SAW-based devices production. Then, three different possibilities are introduced and compared as surface acoustic wave modes: traveling SAWs, standing SAWs and Love waves. Even if Love waves are not considered for the manipulation of microparticles, in this work are introduced as a possible mode of actuation of piezoelectric materials to be used in microfluidics as biosensors. Finally, a brief review on the specific applications of SAW-based systems is provided to show the versatility of acoustofluidics.

2.1 Microfluidics

Microfluidics is the branch of fluidics related to processing and manipulation of small amounts of fluids contained in micrometric size channels. Dealing with microfluidics, also the fabrication process and the design of the entire device for fluid handling must be considered. Typical structures are channels and chambers, which can have different geometries correlated to specific applications. There are several reasons which have brought microfluidics to become a standalone science,

going alongside microfabrication development. In the review by Convery et al. [6] on history and development of microfluidics, the steps related to the growth of the field are reported. One of the first works exploiting microfabrication for microfluidics was done by Terry et al. [21] to construct a gas chromatography system. Gas-phase chromatography and other microanalytical methods (liquid chromatography, capillary electrophoresis) were detected by Whitesides as the first reason for microfluidic improvement [3], due to the possibility to create capillary structures and to make analyses using small amounts of samples, achieving high sensitivity and high resolution. The second reason was related to a different request: after the end of cold war, an increasing interest was developed in study of detectors for chemical and biological threats. The Defense Advanced Research Project Agency (DARPA) supported a series of programmes for this research field which were stimulus for a rapid growth of academic technologies [3]. The idea of this research project arises when μTAS (miniaturized total analysis system) were invented as innovative systems that could carry out all the functions required for analysis: sampling, transport of the sample, any sample preparation steps including chemical reactions and separations, as well as detection [6]. The third motivational force is related to molecular biology. In 1990 the Human Genome Project (HGP) was launched with the aim of mapping the entire human genome. More efficient and low-cost technologies for DNA sequencing were required, leading to a fast improvement in microfluidics, seen as useful instrument to achieve these features [3]. The fourth and last contribution was from microfabrication related to microelectronics. Initially, silicon and glass were used to exploit known technologies, such as photolithography (microfabrication technique to pattern thin films or bulk materials exploiting the use of UV-light sensible photoresist). The requirement for biocompatible, transparent and easy to fabricate materials, drives technologies to use polymers. PDMS (Poly-dimethylsiloxane) was quickly substituted to other materials in microfluidics due to its properties: transparency, non-toxicity, biocompatibility, reversibility to deformations and elastomeric properties [22]. With this kind of materials there is no need for microfabrication in a clean room. The technique of soft-lithography is used, based on rapid prototyping and replica molding, which is simpler and more accessible than standard

microfabrication technologies. Nowadays, microfluidics is exploited for several applications. Droplet microfluidics exploits the use of immiscible phases to generate droplets in another steady or flowing fluid. With this solution, it is possible to treat single drops as microreactors to perform chemical reactions, being controlled on very small amounts of samples [23], [24]. Particles and bioparticles manipulation can be done both with active (exploiting external fields as electric, magnetic or acoustic) or passive (hydrodynamics) methods. In this work only the active acoustic manipulation is described (see Section 2.2), to have a complete overview on this classification the reader is suggested to consider the reference [4].

2.1.1 Fluid dynamics at the microscale

At sub-millimetre channel scale, some phenomena, unimportant at the macroscale, become an important force to be consider when designing microfluidic systems. The decrease in fluid mass causes the effects of viscosity to overcome the influence of inertia. Turbulent flow cannot be achieved at any realistic fluid velocity, making mixing a challenging task. The only phenomenon capable of blending liquids at microscale is diffusion. The decrease in the channel size also leads to an increased surface-to-volume ratio, which increases the importance of surface effects, including adsorption, capillary action and surface wetting [25]. To describe the effects of size downscaling, some dimensionless numbers, introduced in the following sections, are used in microfluidics.

2.1.1.1 Reynolds number

Reynolds number (Re) is defined as the ratio between inertial and viscous forces in a fluid. This dimensionless number is useful to discriminate between laminar or turbulent regimes for fluid flow. Its mathematical expression is given as:

$$Re = \frac{\rho v L}{\eta} \tag{2.1}$$

where ρ is the density of the fluid, v is the average velocity of the fluid, L is the characteristic linear dimension of the system and η is the dynamic viscosity. The characteristic linear dimension of non-circular channels is measured with the

hydraulic diameter $D_H = 4A/C$ where A is the cross-sectional area of the flow while C is the wetted perimeter of the cross-section.

When Re value is above 4000 fluid flow is considered as turbulent, while if the value is below 2300 the flow is laminar. The regime in between is called as transition regime [26]. Considering the reduction in characteristic dimensions for microfluidics systems, low values of Reynolds number are expected and, accordingly, a laminar flow. In fluid dynamics, laminar flow is characterized by fluid particles following smooth paths in layers, with each layer moving smoothly past the adjacent layers with no mixing. No crosscurrents perpendicular to the direction of flow, nor eddies or swirls are present. Laminar flow behaviour, for these reasons, is easy to be predicted.

2.1.1.2 Péclet number

Pèclet number (Pe) describes the fluid behaviour at the microscale distinguishing between diffusion and advection:

$$Pe = \frac{vL}{D} \tag{2.2}$$

where v is the average velocity of the fluid, L is the characteristic linear dimension of the system and D is the diffusion coefficient. As said for the Reynolds number, reducing the dimensions of the system, also the Pèclet number is reduced [27].

To recall, diffusion is the net movement of particles from high to low concentration zones, advection is the motion of particles along the bulk flow. Having small values of Pe means that diffusive effects overcome advection in microfluidics.

2.1.1.3 Capillary number

Capillary number (Ca) expresses the relation between viscous and surface tension forces. The number is defined as [27]:

$$Ca = \frac{\eta v}{\gamma} \tag{2.3}$$

where η is the dynamic viscosity, v is the velocity and γ is the surface tension between immiscible phases. Surface tension is exploited in microfluidics for droplet formation and transport. One of the most used channel configurations for droplet

generation is the T-junction (Figure 2.1). Separated streams of immiscible fluids, coming from separated inlets pumping the fluids towards the junction, become in contact at the junction where they come up against: the equilibrium between surface tension (acting on reducing the interface) and viscous forces (acting on increasing the interface) generates the droplet shape. A critical droplet radius can be found from this balance of forces:

$$R \sim \frac{\gamma h}{\eta v} = \frac{h}{Ca} \tag{2.4}$$

where h is the height of the channel.

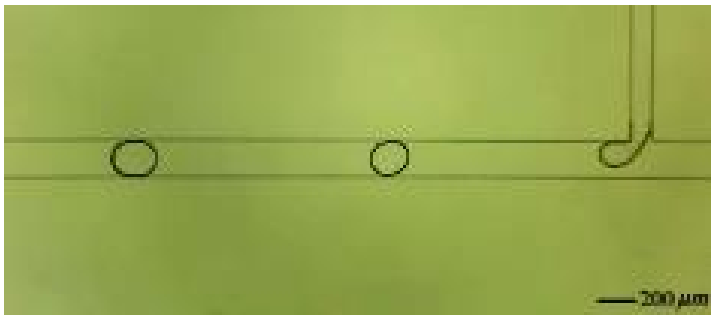

Figure 2.1: Experimental images of droplet generation with a T-junction [28]

2.2 Acoustic manipulation

Several techniques have been used for particles and bioparticles manipulation. A major classification exists, dividing them into active or passive techniques. Passive systems utilize the flow field together with the channel geometry or topology changes to manipulate the motion of particles. On the other hand, active systems utilize an external force field such as electric, acoustic, magnetic and optic to manipulate the motion of particles [4]. An additional categorization is made between label-based or label-free techniques, depending on the need of any labelling for particles to be recognised. Label-free methods exploit the intrinsic properties of the particles such as size, shape, density, dielectric properties, acoustic properties, and refractive index to discriminate the effect of the field on particles. For example, acoustic manipulation can be considered for particles separation based

on their dimensions. On the other hand, the label-based techniques require additional labels (such as fluorescent markers) to activate particles and let them be influenced by specific fields [4].

In particular, the acoustic-based technique is active, exploiting the generation of ultrasound waves externally, and label-free, exploiting the mechanical properties of particles for manipulation. Acoustophoresis and acoustic streaming are the main phenomena involved in particles manipulation. Acoustophoresis literally means "acoustic transport" and is related to the possibility of exploiting ultrasound waves in a fluid to develop acoustic radiation forces (ARFs) interacting with particles to be displaced. ARF depends on physical properties of particles such as size, density and compressibility [29]. Acoustic streaming is associated to viscous attenuation of sound in a fluid generating fluid flow. The phenomenon can be considered as a disturbance of the acoustic radiation force for particle manipulation, but it can be useful if intended for fluid motion or mixing [30].

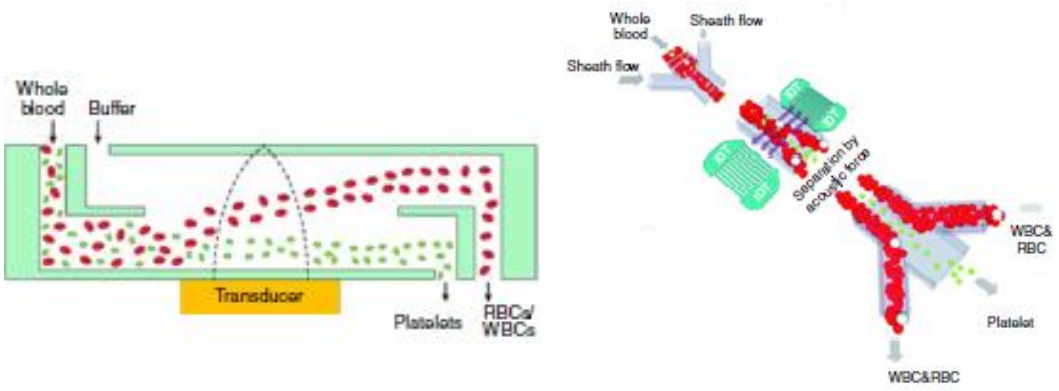

Figure 2.2: BAW-based (left) and SAW-based (right) devices for bio-particles separation [32].

Several examples and different configurations have been studied to exploit acoustofluidics for particles manipulation [31]. As can be seen in Figure 2.2, different designs of microfluidic devices can be exploited leading to the same effect (in this case heterogenous particle separation). The example on the left shows a BAW-based device, which generates acoustic waves in the fluid with bottom actuation of a piezoelectric transducer, while on the right a SAW-based device is shown, exploiting interdigital transducers (IDTs) deposed on a piezoelectric substrate for ultrasound waves generation. The difference between the two devices

is related to the kind of waves exploited: bulk waves are used in the first case, they propagate through the walls of the device to reach the fluid medium exploiting waves transmission between materials, while surface waves are propagating on the surface of the substrate of the device and develop acoustic pressure waves in a fluid in contact with this surface interacting with it. The particles are forced to move towards pressure nodes or antinodes, generated in the pressure field, depending on their physical properties [31].

2.2.1 Biocompatibility

Manipulation of biological cells by acoustic radiation forces is often motivated by its biocompatibility. On the other hand, acoustic exposure can cause damage to tissue or cells, primarily due to heating or cavitation effects. The effect of the pressure field can also shake or squeeze the bio-particles, phenomena which can be considered as a source of damage [32]. There are two main effects causing heat development: electromechanical losses in the piezoelectric layer of the transducer and heat losses in thin glue layers in between supporting solid layers. Heat losses related to the materials to construct the devices are not considered typically due to the use of silicon, glass and water-based fluids which are low-losses materials. High temperatures are critical dealing with bio-samples, they can be affected and partially lose their properties, therefore system temperature must be controlled throughout the experiments (for example the best temperature for cell cultures is around 37°C) [32]. Another important effect to be considered is cavitation, defined as the formation and activity of bubbles in fluid medium. Stable cavitation is defined as the continuous oscillation of bubbles for a large number of cycles driven by pressure fluctuations. This type of cavitation typically produces highly localized acoustic streaming preventing cells aggregation in standing fields. Inertial cavitation consists in heavy oscillations of bubbles for a few cycles causing collapse or implosion. Fortunately, considering standing waves, small bubbles (being moved towards pressure antinodes) can be separated from cells or particles. This separation avoids particles and cells to be injured by cavitation [32].

2.2.2 Acoustic waves

A wave, with a general definition, is a propagating dynamic disturbance (oscillation around equilibrium) of a quantity or a field. Sound is an example of mechanical wave: an oscillating pressure wave which is transmitted through a physical medium, such as air or water, with a characteristic velocity [33]. Wave propagation velocity is related to the elastic properties of the medium: the particles that constitute the medium material do not travel with the wave but they experience oscillations around their equilibrium positions. Waves can be mainly divided into longitudinal, causing the medium to vibrate along the propagation direction of the wave, and transversal, when medium particles oscillate perpendicularly with respect to wave propagation direction. There exist also surface waves travelling along the surface or an interface between two media. When two waves with the same frequency and amplitude traveling in opposite directions interact, they generate a standing wave. Standing acoustic field is exploited in acoustofluidics to manipulate particles due to the presence of pressure nodes (when the wave amplitude is null) and antinodes (when the pressure amplitude is maximum) causing the development of ARF moving particles towards nodes or antinodes depending on physical properties.

In an acoustofluidic device, acoustic waves are generated through piezoelectric transducers exploiting the converse piezoelectric effect, phenomenon in which a mechanical strain is generated in a material through the application of an external electrical field. Acoustic waves can be categorized in two types (see Figure 2.3): surface acoustic waves (SAWs) and bulk acoustic waves (BAWs). SAWs, generated by IDTs deposed on a piezoelectric substrate, propagates on the surface of an elastic material. There are two types of SAWs: traveling SAWs (TSAWs) and standing SAWs (SSAWs). Traveling surface acoustic waves are defined as SAWs that propagate in one direction and radiate away from the acoustic sources. Standing surface acoustic waves are generated by two opposite traveling SAWs interfering or reflecting traveling SAWs, creating fixed nodes and antinodes in an open or confined domain [34]. On the contrary, BAWs propagate inside the bulk of a material. The waves are generated by the actuation of a piezoelectric material bonded to the wall of the microchannel. Usually BAW-based devices exploit the

use of a reflector, placed on the opposite side wall of the channel, to generate standing waves inside the channel for particles manipulation [34].

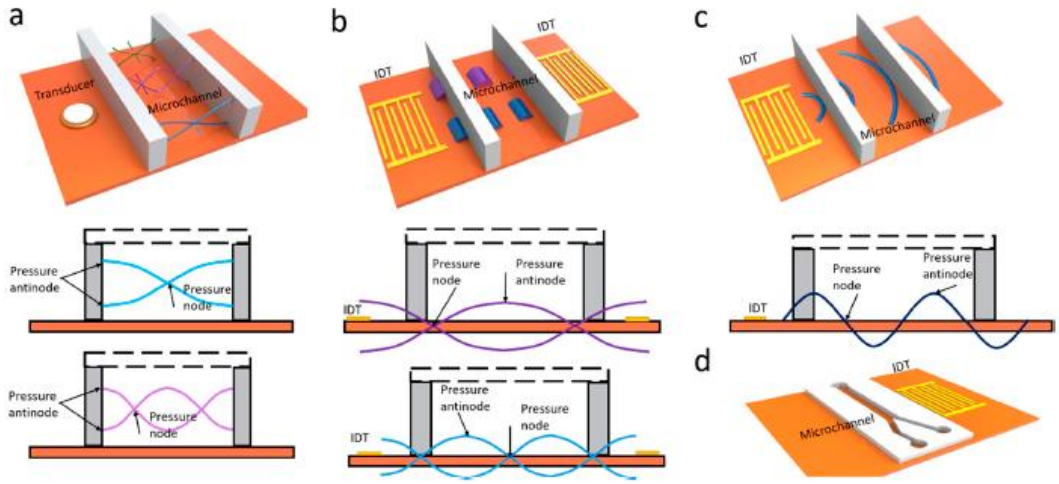

Figure 2.3: Schematic illustration of propagation of (a) BAWs, (b) SSAWs and (c) TSAWs in a microchannel [34].

2.2.3 Piezoelectricity

The word piezoelectricity comes from the Greek and means "electricity by pressure" and was introduced by Henkel in 1881 to name the phenomenon discovered one year before by the Pierre and Jacques Curie. They observed that positive and negative charges appear on several parts of crystalline material surfaces when deforming the crystal in different directions [35]. This phenomenon is called direct piezoelectric effect: generation of electrical charges due to the application of a mechanical stimulus. As schematized in Figure 2.4, before subjecting the material to some external stress, negative and positive charges are disposed in equilibrium. Therefore, the external effects of the negative and positive charges are reciprocally cancelled. As a result, an electrically neutral molecule or crystal appears. When applying some pressure on the material, its internal reticular structure can be deformed, causing the separation of the positive and negative charges of the molecules and generating little dipoles. The facing poles inside the material are mutually cancelled and a distribution of a linked charge appears at the material surfaces. After the process, the material is polarized [35]. The opposite effect, called converse piezoelectric effect, can be obtained by applying an electrical

field to generate mechanical strains in a material. This phenomenon is exploited for the generation of acoustic waves.

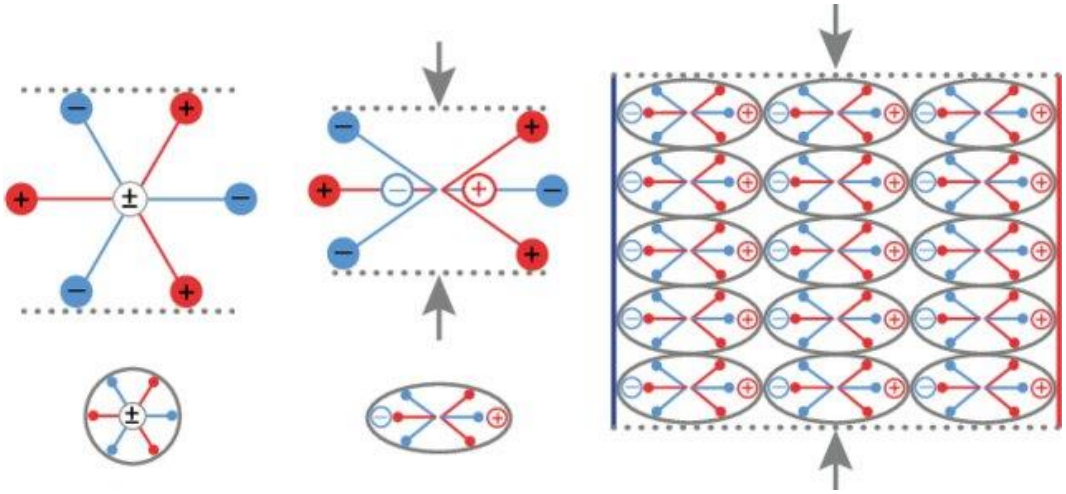

Figure 2.4: Molecular model of direct piezoelectric effect [36].

2.2.4 Piezoelectric materials

Piezoelectric materials are a class of dielectric materials, electrical insulators, that can be polarized not only by the application of an electric field but also from the application of a mechanical stress. Piezoelectric materials can be divided into classes according to their properties and response to external stimuli. Polar piezoelectric materials are characterized by a net dipole moment and then an intrinsic polarization. They can be considered as ferroelectric materials, which provide the ability to reverse their polarization through the application of an external field. A subclass of them are pyroelectric materials showing a change in polarization when subjected to a temperature change.

Piezoelectric materials can be classified into the following categories: single crystalline materials (quartz), piezoceramics (lead zirconate titanate, PZT), piezoelectric semiconductors (zinc dioxide, ZnO_2), polymers (polyvinylidene fluoride, PVDF), piezoelectric composites and glass ceramics (lithium niobate, $LiNbO_3$) [37].

Piezoceramics are widely used for their properties. They are characterized by a perovskite crystalline structure, with general chemical formula ABX_3 where A and B are cations while X is the anion. A famous example is PZT. Above a critical

temperature, the Curie temperature T_C, each perovskite crystal shows a cubic symmetry with no dipole moment. However, at temperatures below the T_C each crystal has tetragonal symmetry and, associated with that, a dipole moment [38]. One typical procedure done on non-polar piezoelectric materials is poling. This treatment consists in the application of a strong external electric field to the material, slightly below T_C, to align dipole domains (zones of net dipole moment) present in the material. After removing the external forcing field, the domains remain aligned along poling direction generating a dipole moment on the material (Figure 2.5) [38].

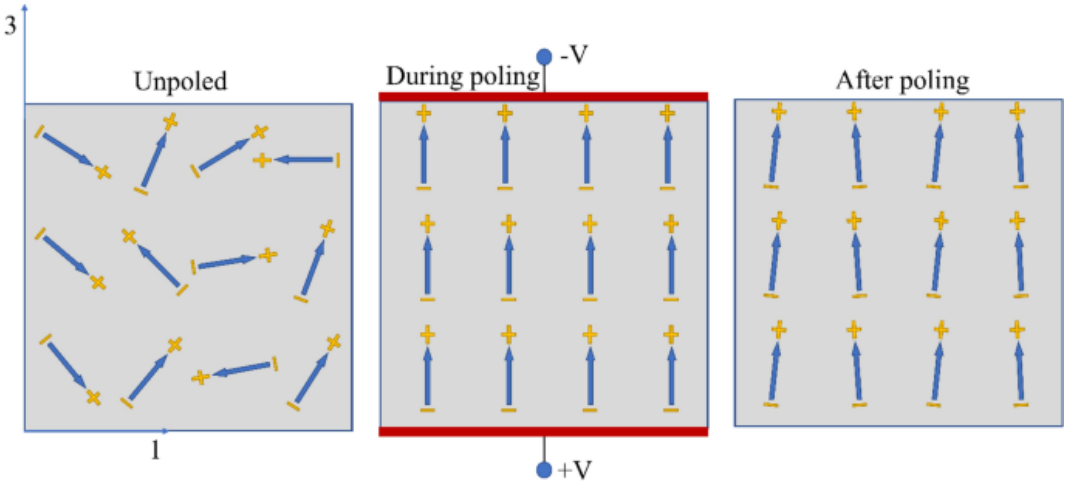

Figure 2.5: Sequence of steps of poling treatment for piezoelectric materials [39].

Dealing with acoustofluidic devices, materials as lithium niobate ($LiNbO_3$) or lithium tantalate ($LiTaO_3$) are typically used due to their capability of generating SAWs exploiting interdigital transducers. Lithium niobate is a human-made dielectric material discovered to be ferroelectric. The material has a trigonal crystal structure and is characterized by large pyroelectric, piezoelectric, electro-optic, and photo-elastic coefficients [40]. Its structure below T_C (near 1210 °C) consists of planar sheets of oxygen atoms in a distorted hexagonal close-packed configuration. The atomic arrangement below the Curie temperature causes the material to be polarized, feature not shown above T_C when niobium atoms are centred between oxygen layers. Lithium tantalate exhibits nearly the same properties of lithium niobate, even though lithium niobate is more used for its better coupling coefficients [41]. Single crystal lithium niobate (Figure 2.6) can be purchased in different cuts,

widely used in transducer application are YZ $LiNbO_3$ or 128° rotated YX $LiNbO_3$, giving the possibility to develop Rayleigh waves (a description is given in Chapter 3).

Figure 2.6: (a, b) A boule of lithium niobate, with (c, d, e) wafers and (d, f) other shapes for typical applications [41].

2.3 Devices

The design of devices at the microscale is done taking into account not only the specific application but also the fabrication technique and its steps. Microfluidic devices can be realized using different materials, always considering the required properties (for example transparency). In this section, a description of microfabrication techniques involved in microfluidics are described, focusing on specific solutions developed for SAW devices (microchannel fabrication, IDTs deposition). Then, a classification of acoustofluidic devices (both BAW-based and SAW-based) is considered.

2.3.1 Microfabrication

Microfabrication is the process of fabricating structures at the microscale (from micrometres to millimetres). The first processes of microfabrication were used in semiconductors manufacturing for integrated circuits fabrication. In this field, a wide use of silicon is made, due to its semiconductive properties with the possibility

to be doped making it to be conductive. In recent years, the technologies were adapted or extended to fit to new fields as MEMS (micro-electromechanical systems) fabrication or microfluidics. Considering microfluidics, great effort was made to develop new and practical solutions which exploit the use of disposable and easy to make devices. Semiconductors microfabrication was just the principle to use well-known technologies but changing and improving them.

The most used technologies for SAW-based microfluidic devices fabrication are reported. The main technology related to microfabrication is photolithography, which exploit the impression of a photosensitive material to imprint the wanted pattern on it. This technique relies on masks, glass structures with transparent and opaque spots to define the pattern to be impressed. A great feature is that, simply by changing masks, is possible to achieve several different patterns. Microfluidics introduced the soft-lithographic technique, and alongside that the use of polymeric materials for the realization of devices. PDMS is presented as an important material for microfluidic devices, being transparent and biocompatible [22].

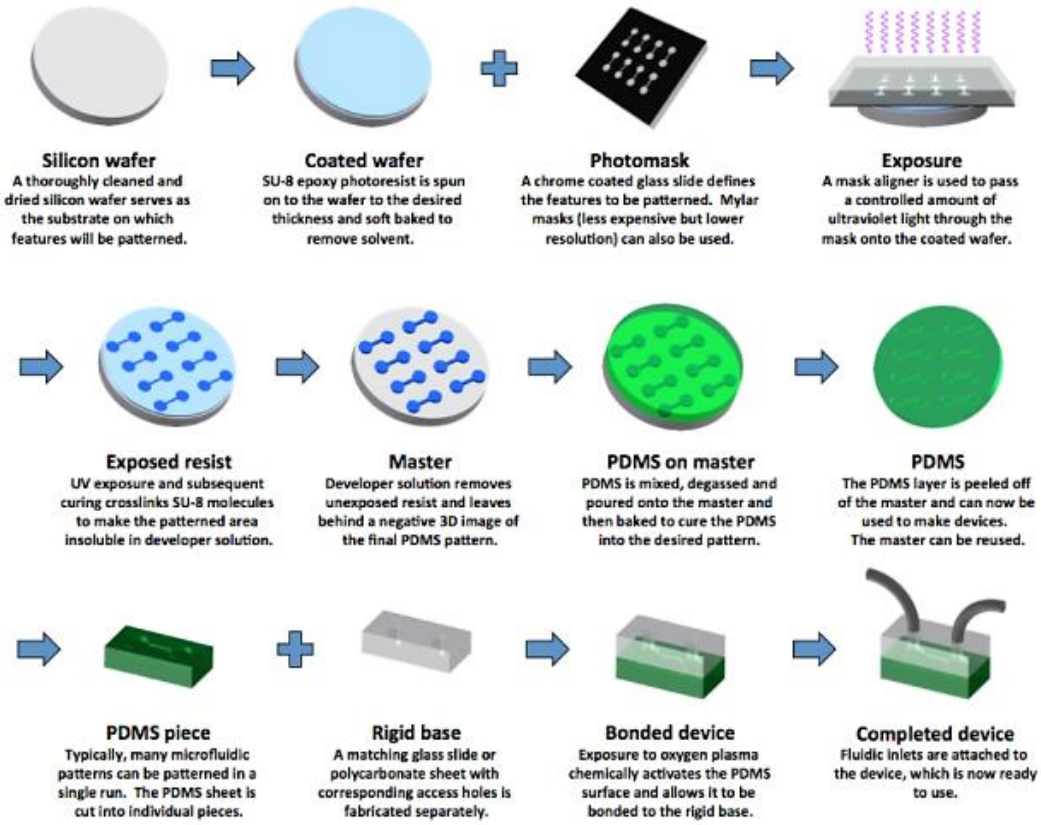

Figure 2.7: PDMS microfluidics fabrication steps [42].

2.3.1.1 Photolithography

Photolithography is introduced to fabricate the master that serves for the creation of a PDMS structure with soft-lithographic techniques. The technique is based on the use of light to impress a photosensitive material (which changes its solubility to specific solvents when impressed by UV-light) to generate precise patterns on its surface.

The wanted pattern is created with CAD software on a computer and is transferred to a mask, a glass disk covered with a photo-definable material (chrome) where the pattern is transferred. The mask contains opaque areas where light is blocked, and transparent area where light can pass: the design of the mask defines the final pattern transferred on the photoresist (SU-8 is typically used). This material must be deposed by spin-coating on the substrate: the wafer is kept on rotation while the photoresist is poured on it, the rotation causes the homogeneous spreading of the material. Photoresist can be divided in positive or negative. The exposure of the UV-light to the positive photoresist causes a change in its chemical structure, making it more soluble in the developing solution. The exposed photoresist is removed by this solution granting direct access to the underlying material. The mask replicates the wanted pattern on the wafer. On the contrary, a negative photoresist, after the exposure to UV light, polymerizes or cross-links (SU-8 is an example). Only the areas that are not exposed to light are removed. Finally, the remaining photoresist layer is stripped and the wanted mold is obtained [43]. To obtain a good quality result in terms of resolution and pattern definition, the mask should be aligned with the substrate using an aligner. All these steps can be seen in the Figure 2.7.

A good alternative technique for research is maskless lithography. It follows the same concept of standard photolithography but no masks are used. Electron-beam and direct laser writing are the main form used. A key advantage of maskless lithography is the ability to change lithography patterns from one run to the next, without incurring the cost of generating a new photomask. This technique, compared to optical projection lithography (OPL) which exploits the same idea using a complex configuration of lenses, provides good results with the possibility to obtain good resolution [44]. Of course, throughput can be considered as a limit

dealing with industrial processes. Maskless lithography equipment based on μLCD projection technologies are now used in research for rapid prototyping [45].

2.3.1.2 PDMS soft lithography

Soft lithography can process a wide range of elastomeric materials, such as mechanically soft materials. This is the reason to call it with the term “soft”. Soft lithography relies on soft materials that are appropriate for stamping, molding, and embossing. For instance, it is well suited for polymers, gels, and organic monolayers. Those polymers that have a low interfacial energy, are chemically inert, have a high thermal stability, and can be easily modified appear to be the best candidates [46]. The most used material for microfluidics is poly-dimethylsiloxane (PDMS). It provides a surface with a low interfacial free energy, is chemically inert, has good gas permeability, good thermal stability and is optically transparent. The surface properties of PDMS are also relatively easy to be modified (great use is done in oxygen plasma treatment).

For basic soft lithography, the base and the curing agent (mixed in sold products) are poured over a rigid master, typically realized using photolithography. To remove the bubbles in the liquid-state PDMS, the mold with the liquid PDMS is put into a vacuum chamber until the bubbles are completely removed. The PDMS can then be cured at room temperature (for nearly 2 days) or at elevated temperatures (for a few hours at 70°C) and be finally stripped from the mold [46]. This technique presents a few advantages: working with polymeric materials reduces the general costs of production, the produced masters can be used to construct several devices. Finally, inlets and outlets must be punched to provide access to the channel, step which can be done manually using a small punch or positioning the tubes during PDMS casting.

Another essential feature of soft lithography is the possibility to obtain a sealed microfluidic device. Typically, the microchannels imprinted in the PDMS layer are closed with a glass slide. Alternatively, another piece of PDMS can be used. PDMS bonding is required to obtain a strong permanent bonding between parts. The most common used technique is oxygen or air plasma activation. Under plasma conditions (pressures lower than 1torr and frequencies greater than 1 MHz), electrons possess high kinetic energy, breaking and ionizing the incorporated gas

molecules. Reactive species and photons produced by gas discharge imping to the surface causing chemical reactions on the substrate. Structural and bulk properties of the polymers are not influenced by this process. The silanol groups (-Si-OH) of the plasma activated PDMS layers can covalently bind to each other creating siloxane bonds (Si-O-Si), by bringing PDMS parts into contact. This is usually followed by a heat treatment step to promote bonding strength [47], [48]. It is important to note that the plasma activated silanol groups on the PDMS surface are thermodynamically unstable, and hydrophobicity can be fully recovered in less than an hour. Then, PDMS bonding should be done immediately after the treatment. Furthermore, it has been shown that plasma activation of PDMS with nitrogen gas allows for PDMS bonding to SU-8 substrates through the covalent reactions between the plasma induced amine groups on the PDMS surface and the epoxy rings present on a SU-8 substrate. Nevertheless, it requires advanced plasma equipment and the repeatability of the process is questionable [48]. Alternatively, other techniques can be used to activate PDMS surface to generate sealed microfluidic devices, such as Ultraviolet/Ozone (UVO) treatment, piranha etching (an extremely strong oxidizer made of hydrogen peroxide and usually sulfuric acid) or corona discharge (another kind of plasma treatment) [48].

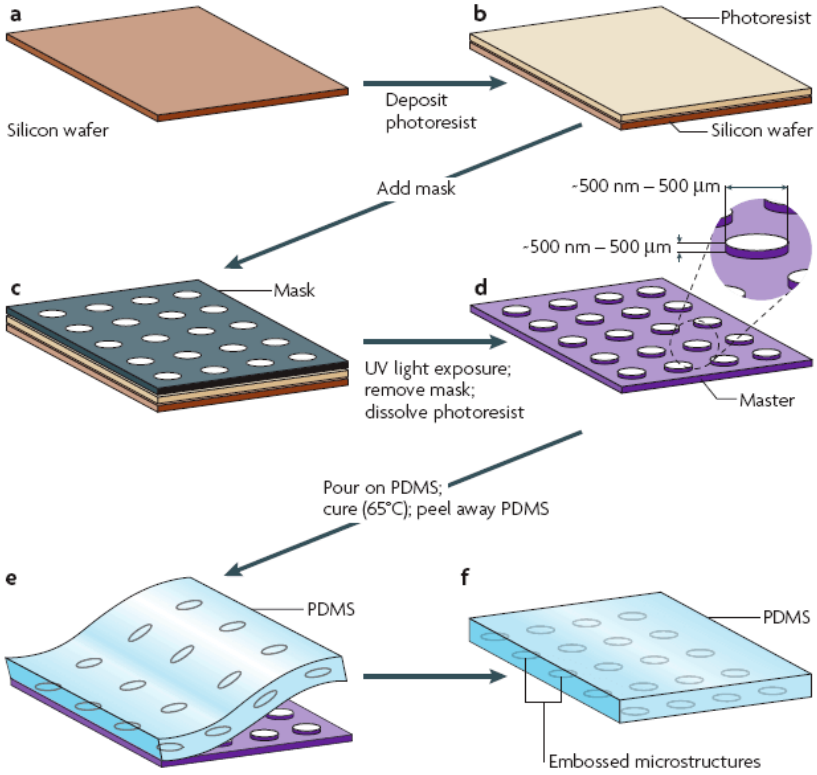

Figure 2.8: Fabrication of a PDMS layer incorporating microstructures [47].

2.3.1.3 Deposition

Several techniques have been developed for thin film materials deposition. To obtain good quality products, two common deposition techniques are considered: chemical and physical depositions [49]. Chemical deposition processes rely on chemical reactions of volatile precursors species on the substrate in a specific atmosphere (for example oxygen or nitrogen). Chemical vapour deposition (CVD) is used, for example, to deposit silicon dioxide on silicon in MEMS fabrication.

Evaporation methods are considered as the common deposition of materials in the form of thin-layer films. The general mechanism of these methods is obtained by changing the phase of the material from solid phase to vapor phase and converting again to solid phase on the specific substrate. It takes place under vacuum or controlled atmospheric condition to grant free travelling of molecules from target to substrate [49].

Considering acoustofluidics devices, IDTs are depose exploiting the lift-off technique. This is a cleanroom process used for applying a patterned thin film on

substrate surface. Lift-off is done by performing photolithography on a wafer before performing a deposition (typically with electron-beam evaporation or sputtering for metals deposition) and then removing the photoresist with a chemical etching step. In this way, the film deposed on the photoresist is washed away by etching, while the material deposed on the substrate should remain attached with the wanted pattern [50].

2.3.2 Device classification

A successful assembly of an acoustophoresis system is based on the design of acoustic resonators (Figure 3.9), involving fabrication techniques, materials choice and actuation modes [51].

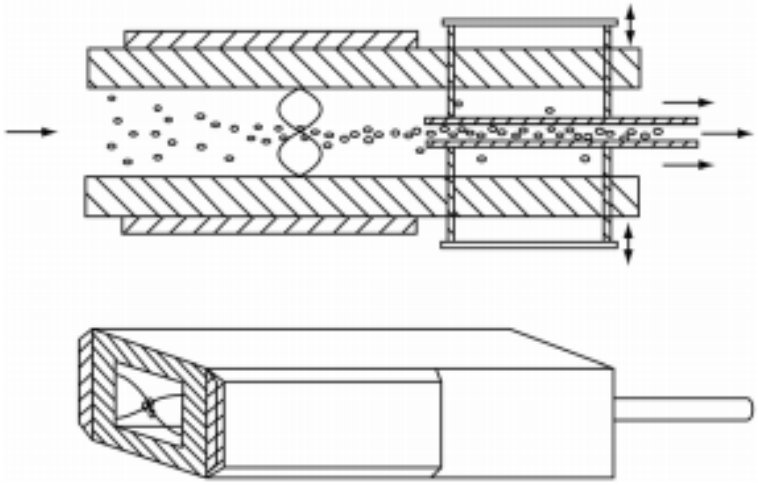

Figure 2.9: Half wavelength acoustic resonator for particle and cell focusing [51].

One classical way of designing an acoustic resonator for cell and particle handling requires a piezoelectric transducer to be glued to a coupling layer of glass or metal, to transfer the waves to the cavity where the fluid flows, while the opposing wall serves as reflector, which reflects back the acoustic waves to generate a standing wave. The same result can be obtained by connecting another transducer, driven at the same frequency, on the opposed face of the cavity [51]. Modifying the actuation frequency of the piezoelectric transducers, multiple pressure nodes can be obtained inside the cavity. For particle and cell focusing, the half-wavelength configuration is used, which develops just one single pressure node in the centre of the channel.

The choice of material is important while designing an acoustic resonator. The different configurations of resonators influence the possible materials to be used. One parameter to be considered is the acoustic impedance Z, a measure of the resistance that a material opposes to acoustic disturbance propagation [51]:

$$Z = \rho c \tag{2.5}$$

where ρ is the density of the medium and c is the longitudinal speed of sound in the material. This material parameter is useful for calculating the reflection (R_p) and transmission (T_p) coefficients for normal incidence [51]:

$$R_p = \frac{Z_2 - Z_1}{Z_1 + Z_2} \tag{2.6}$$

$$T_p = 1 - R_p \tag{2.7}$$

where Z_1 is the characteristic acoustic impedance of the first medium and Z_2 is the characteristic acoustic impedance of the second medium. In case of non-normal incidence of longitudinal waves, a correction should be introduced in the formulations taking into account the angle of incidence. To avoid acoustic losses due to reflection, the acoustic impedances of two adjacent layers should be carefully matched so that the acoustic energy density in the fluidic layer is maximised. For instance, when designing the matching layer, the characteristic acoustic impedance of the layer should be lower than that of the transducer but higher than the material comprising the fluidic cavity [51]. Considering SAW devices, the material constituting the microchannel should have a similar acoustic impedance with respect to the fluid to avoid interferences. Acoustic waves developed inside the fluid travel tilted by a characteristic angle (called Rayleigh angle, see Section 2.4.1) and they are favourably being transmitted than reflected due to materials having similar acoustic impedance values. There are three main types of acoustophoretic systems, layered resonator, transversal resonator and surface acoustic wave (SAW) devices. The first two configurations exploit the use of BAWs while the last works using SAWs.

2.3.2.1 Layered resonators

A layered resonator is a structure composed of different layers having a very specific role in the resonator system. The different layers can be seen in Figure 2.10. Sound is generated through a transducer which is followed by a coupling layer, ensuring good waves transmission. The coupling layer is made by an adhesive material which must be well bonded with the other layers to avoid losses caused by the presence of air voids. Then, a matching layer is used for waves transmission to the fluid layer, containing the fluid with particles. The matching layer, being the bottom part of the resonator chamber, acts also as a reflector to generate standing waves inside the fluid layer. At the other end of the system a reflector layer is positioned to reflect back the waves giving rise to standing waves in the fluid layer [51].

The thickness of the different layers in layered resonators are of great importance to get as powerful resonance as possible. Both materials properties and wave properties (such as the wavelength λ, which is the distance between two successive crests of a wave) must be considered. Hawkes et al. have shown with simulations a good rule to build a half-wavelength resonator, with the development of a single pressure node in the centre of the fluid layer [52]. By changing the thickness of the layers or the actuation frequency, other results can be found, with the presence of more pressure nodes and antinodes in the fluid layer. The typical material used as matching layer is silicon, for the possibility to use microfabrication to obtain the channels, but stainless steel is also used for its high density, good sound propagating properties and good heat transport capabilities. Hawkes and Coakley reported a layered steel resonator used as a continuous flow particles filter exploiting megahertz frequency ultrasonic standing waves. Experimental tests achieved >1000-fold clearance of 5μm yeast cells [53].

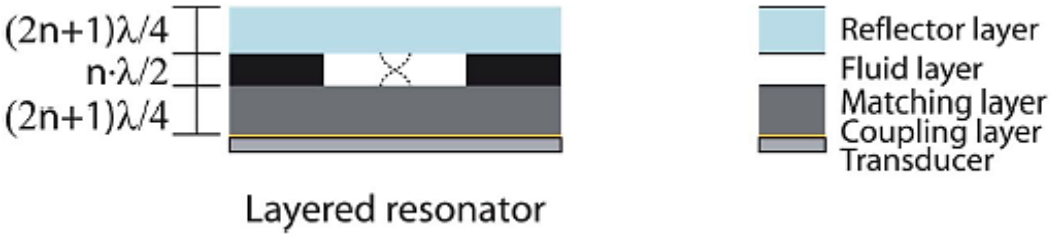

Figure 2.10: The structure of a layered resonator [51].

2.3.2.2 Transversal resonators

Transversal resonators work in a similar way compared to layered resonators. The difference is that a standing wave perpendicular to the incident direction of actuation is obtained [51]. Since the entire microfluidic component is actuated in the transversal mode, a general advice is that the resonator in this case should be made of materials with low acoustic losses displaying a high difference in characteristic acoustic impedance with respect to the fluid. Silicon and glass can be used for transversal resonators. Silicon shows a good reflectivity and ensures the possibility to fabricate channel with vertical walls. Glass has a high density, good acoustic properties and is chemically inert. Evander et al. worked on the development of acoustofluidic systems using glass, comparing the results with silicon-based devices and showing some possible solutions for the design [54]. Polymers are not used to build transversal resonators due to their similar acoustic impedance compared with aqueous solutions and their high acoustic attenuation.

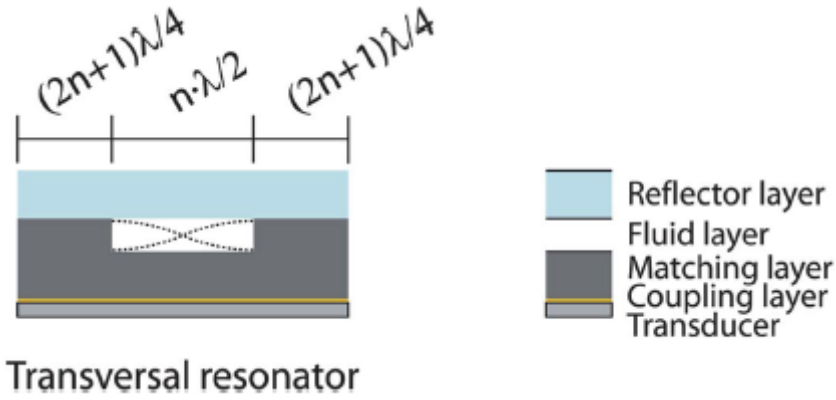

Figure 2.11: The structure of a transversal resonator [51].

2.3.2.3 Surface acoustic waves devices

SAW devices utilise surface waves to manipulate particles in a channel. Generation of surface acoustic waves is achieved by the surface actuation of a piezoelectric material (typically lithium niobate) through deposed interdigital electrode transducers. Different designs of electrode patterns for acoustic wave devices are used to achieve different applications. Mamishev et al. have reported on the design and patterning of different electrodes to enhance the sensing performance to improve microfluidic functions [55].

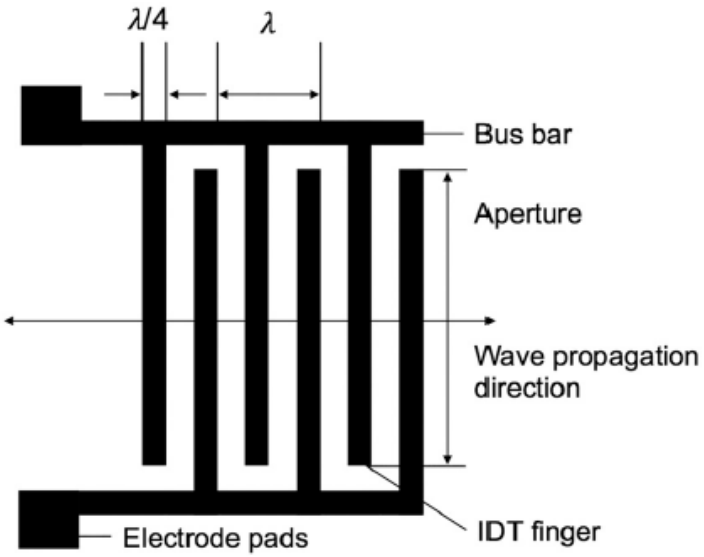

Figure 2.12: Structure and parameters of a single electrode IDT [41].

IDTs are made of several metal bars, named fingers for their slender shape. The fingers are connected to contact pads (through bus-bars to link them): an oscillating voltage signal is applied alternatively on fingers, with a scheme source-ground-source, with ground meaning zero voltage. The application of an electric field generates a strain field in the piezoelectric substrate for waves propagation. Number of fingers, spacing between them and aperture (length of the fingers) of the structure are the characteristic properties of IDTs correlated to waves features. The wavelength of SAWs is equal to the pitch of IDT (choosing a design with spacing equal to fingers width). Then the width of one finger is $\lambda_{SAW}/4$:

$$\lambda_{SAW} = \frac{v_{SAW}}{f} \tag{2.8}$$

where v_{SAW} is the velocity of the surface waves on the substrate and f is the resonance frequency. Waves can propagate in both directions, unless a reflector is positioned at one side to reflect the waves letting them travel in a single direction.

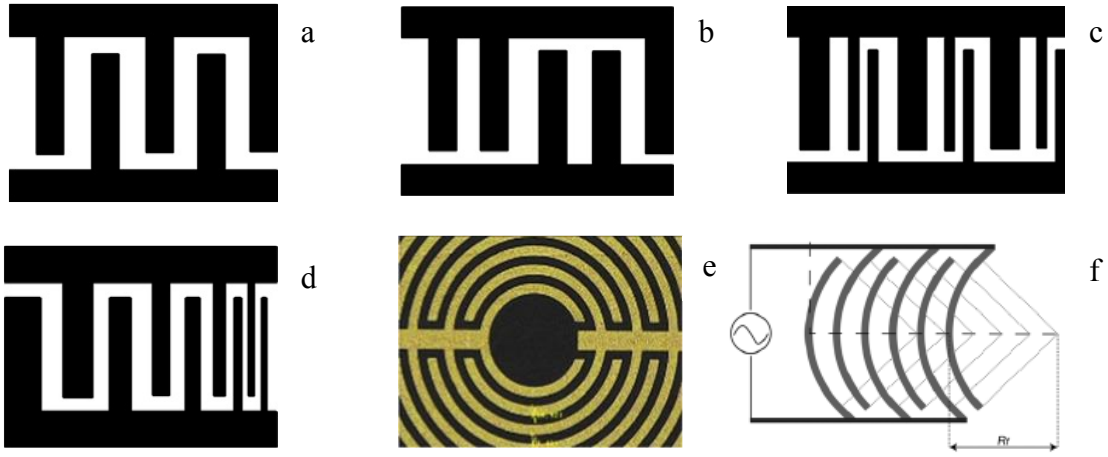

Figure 2.13: Different IDTs configurations. (a) Standard bidirectional IDT, (b) Split IDT, (c) Single phase unidirectional transducer (SPUDT), (d) Chirped IDT, (e) Circular IDT, (f) Focused IDT (FIDT) [41, 56].

The simple structure in Figure 2.12 is called "single electrode". Several kinds of IDTs exist, some examples are shown in Figure 2.13. Split IDTs (b) have the advantage to reflect back some of the waves reducing the reflections. SPUDTs (single phase unidirectional transducers) (c) reflect back or cancel regenerated waves using the internally tuned reflectors within the IDT to form a unidirectional SAW propagation. Chirped IDTs (d) present the same concept of "single electrode" structure but gradually changing the fingers width in one direction. The advantage of this configuration is the possibility to exploit a wide frequency range for actuation and so different SAW wavelengths. Focused and circular IDTs (e, f) are used to focus acoustic force or energy along the IDT main axis. These structures are typically used for fluid pumping or mixing [56].

Differently than BAW systems, polymers are used for SAW devices. In that case, to avoid interfering resonances, the acoustic impedance of the material constituting the channel and the fluid should be similar. PDMS is selected as a valid material because its acoustic impedance is matching with water.

According to what was described in the previous sections, the design and the fabrication of acoustofluidic devices must be carefully defined in their steps and characteristics to achieve the wanted properties for specific applications. All the considerations seen in this section were taken into account to design a SAW-based device to be investigated through numerical simulations and to fabricate a PDMS channel using the soft lithographic technique (described in Chapter 4).

2.4 Surface acoustic waves for microfluidics

The existence of surface waves was demonstrated by Lord Rayleigh, a British physicist, in 1885 [57]. He described an analytical model for waves propagation on the surface of an isotropic solid. This kind of waves are now called Rayleigh waves. SAWs are used in different applications such as telecommunications, as RF filters, non-destructive testing analysis and biosensors [58]. The integration of SAW devices with microfluidics is relatively recent and it offers several advantages [59]:

- *Simple, compact, inexpensive devices and accessories*: SAW devices have been used extensively in various compact commercial electronic systems, demonstrating the possibility to be simply reproduced for mass production and on-chip integration even in microfluidics.
- *High biocompatibility*: the acoustic power intensity and frequency used in many SAW-based microfluidic devices are both in a range similar to those used in ultrasonic imaging. These properties can be tailored to grant biocompatibility.
- *Fast fluidic actuation and large forces*: microfluidic technologies have difficulty generating fast fluidic actuation or large forces on particles. Small feature sizes typically prevent flow velocities from being high enough to yield high Reynolds numbers. High-frequency acoustic waves, however, provide a good solution for fluid pumping avoiding the use of mechanical or electrical pumps [60].
- *Versatility*: SAW technologies enable biological or chemical detection, fluidic control (fluid mixing, translation) and particle manipulation (focusing, patterning, separation, sorting, concentration, and re-orientation). SAW devices can manipulate microparticles, regardless of their shape, electrical, magnetic, or optical properties; they are capable of manipulating objects with a variety of dimensions (from μm to hundreds of nm); and they are able of manipulating a single particle or groups.
- *Non-contact*: manipulation of particles is contact-free, avoiding any kind of contaminations.

- *On-chip integration*: SAW-based microfluidic devices can be integrated with other components, such as SAW-based sensors to build complex systems.

When compared with bulk acoustic wave (BAW) microfluidics, SAW microfluidics shows its advantages and limitations. BAWs technologies are mature, more studied and provide a higher throughput. SAW technologies have better control for excitation frequencies in a wider range and utilize higher excitation frequencies (from 1MHz up to few GHz). This feature gives SAW devices the possibility to handle smaller particles (down to hundreds of nm) with greater precision than BAW systems. SAW technologies do not require fluid channels to be made of materials with high acoustic reflection, because standing surface waves are generated by the interaction of waves from opposite directions, opening to the use of cheaper polymers for channel fabrication. Finally, SAW devices are more efficient because the acoustic energy is confined at the surface of the substrate avoiding losses [59].

The best-known form of SAWs, Raleigh-SAWs, is composed of a longitudinal and a vertically polarized shear component [61]. Rayleigh-SAW strongly couples with media in contact with the wave propagation surface, enabling the sensing of mass perturbation and elastic properties of a medium introduced on the wave's propagation path. Other SAW modes exist in elastic materials of different compositions. For example, Love-SAWs are guided shear-horizontal waves propagating in a thin layer on top of a substrate.

2.4.1 Traveling surface acoustic waves microfluidics

Traveling surface acoustic waves (TSAWs) are generated by a single IDT on the piezoelectric substrate. The application of an electric field on the surface, enables a mechanical stress to be propagated. When a TSAW gets in contact with a liquid, the viscosity of the liquid increases, relative to the substrate, causing part of the SAW to refract into the liquid as a longitudinal wave. Because of this acoustic refraction, the mode of SAW changes to a form called "leaky SAW" or "pseudo-

SAW". The refracted waves move in a direction tilted of an angle ϑ_R with respect to the vertical direction:

$$\vartheta_R = \arcsin\left(\frac{c_F}{c_S}\right) \tag{2.9}$$

where c_F is the velocity of the acoustic waves in the fluid and c_S is the velocity of the acoustic waves in the piezoelectric substrate. The refracted longitudinal waves generate a force in their propagation direction and induce flow within the confined liquid. The boundaries of the channel reflect the actuated liquid and lead to internal streaming. Such a non-linear phenomenon that transforms the SAW attenuation into a steady fluid flow is called SAW-induced acoustic streaming [59].

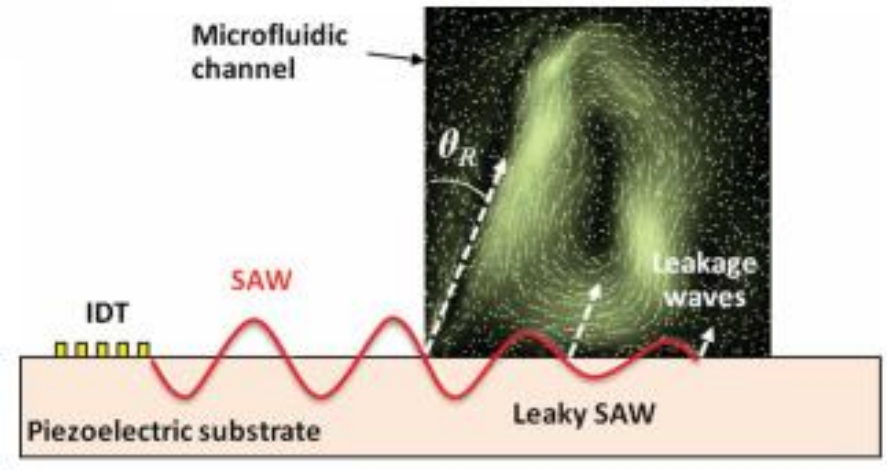

Figure 2.14: SAW induced acoustic streaming [59].

A high-frequency acoustic wave propagating through a liquid loses its energy through viscous damping, induces acoustic streaming flow (ASF) in the fluid, and imparts an acoustic radiation force (ARF) to suspended particles. In the work of Destgeer and Jin Sung [62], polystyrene particles influenced by the TSAW-based ASF or ARF may be distinguished based on the value of a κ-factor:

$$\kappa_f = \frac{\pi d}{\lambda_f} \tag{2.10}$$

where d is the diameter of the particles and λ_f is the sound wavelength in the fluid. If $\kappa_f < 1$, the acoustic radiation force dominates over the drag force induced by acoustic streaming. If $\kappa_f > 1$, particles are not influenced by the ARF, but they are

affected by the ASF vortices [62]. The authors specify that this evaluation can be done only for polystyrene (PS) particles in water, other materials should be furtherly investigated to find other values for the parameter to discriminate between different behaviours.

2.4.2 Standing surface acoustic waves microfluidics

The basic principles that govern the interference of all waves give rise to the formation of SSAWs. If two or more identical IDTs fabricated on a piezoelectric material generates two travelling SAWs propagating toward each other, the interference will result in a one-dimensional SSAW field [59]. SAWs provide the formation of a pressure field in the fluid, with a pattern of pressure nodes, points of zero pressure, and antinodes, points of maximum amplitude of the wave. The pattern is developed following the SAW wavelength, then the distance between two neighbouring nodes is equal to half of a SAW wavelength. It is conventional to divide the acoustic radiation forces into two types, namely, primary forces, which are experienced by single particles, and secondary forces, which are responsible for particle-particle interactions. Dispersed particles suspended in the fluid interact with the pressure field being displaced by the primary acoustic radiation force (PRF). This force is proportional to the volume of particles, then PRF depends on the cubic power of particles radius. Therefore, small changes in particles dimensions can induce huge variations in the magnitude of the force. The force depends also on the acoustic contrast factor ϕ, which is computed through the density and the compressibility of particles and fluid. This factor is a discriminant of the direction of motion of particles: if ϕ is positive, the particles are moved towards pressure node, while, if ϕ is negative, the particles are moved towards pressure antinodes. Primary acoustic radiation force has two components: one axial and one transversal. The axial component pushes the particles towards the nodes or antinodes, while the transverse component tends to keep the particles together [63]. Secondary radiation forces can be observed in case of high concentration of particles. These forces result from the scattered field between neighbouring particles. Usually, the effect of this force is very weak. Only when the distances

between particles become very small, this force can be considered for particles aggregation [14].

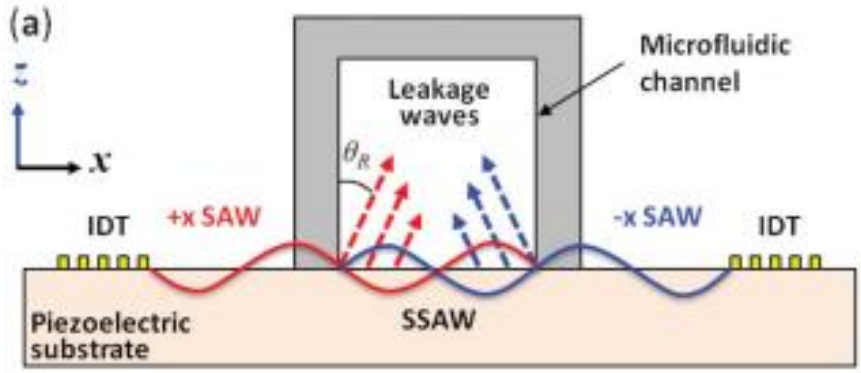

Figure 2.15: Illustration of SSAW generation. Leakage waves propagates following the direction given by the Rayleigh angle [59].

2.4.3 Love wave surface acoustic waves

This kind of waves are not strictly related to particles manipulation in microfluidics. Love waves are presented being another possibility of actuation of piezoelectric materials for biological analysis (exploited in biosensors).

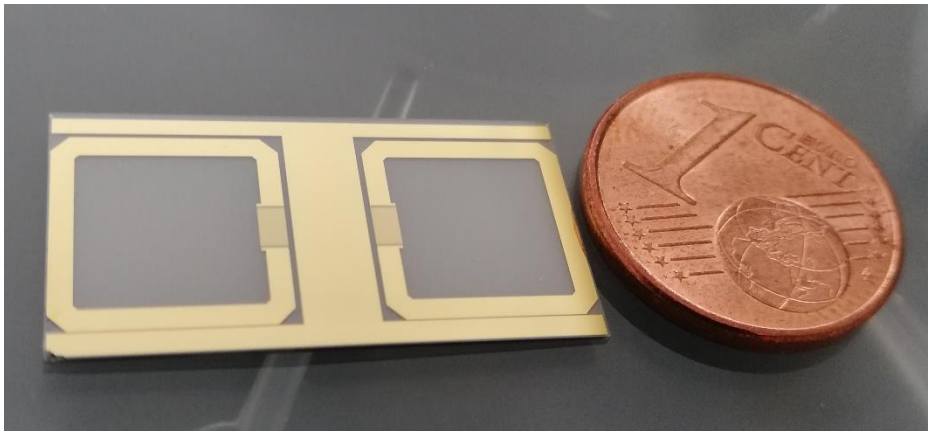

Figure 2.16: Photo of a 400MHz chip biosensor [new design of work 58].

Love wave surface acoustic waves (LW-SAW) are shear waves propagating on the surface a substrate which can support their propagation. The basic configuration supporting the propagation of Love waves consists of a guiding layer (typically, quartz or SU-8 are used) which is deposited on a piezoelectric material for waves generation. A necessary condition for obtaining a bound shear mode in the top layer

is that the bulk shear velocity ($v_S = \sqrt{G/\rho}$ where G is the shear modulus of an isotropic material and ρ is the density) of the guiding layer is lower than that of the substrate [64].

Love waves can be used in biosensors development [58]. These devices generate Love waves through an input IDT exploiting the piezoelectric effect. At the opposite side, another IDT is used as reading system for waves collection. Before being recollected, the waves interact with a biological sample in the middle region, usually a metallic layer specifically functionalised. This interaction can provide changes in resonance signal, which can be compared and elaborated to find the mass collected by the sensor [65].

2.4.4 Comparison between TSAW and SSAW

A comparison between TSAWs and SSAWs should consider the effects generated: acoustic streaming and acoustic radiation force can be defined. The acoustic streaming is exploited with TSAW devices: it enables the possibility to move the fluid in a direction or generate controlled vortexes for fluid mixing. In case of SSAW systems, acoustic streaming is usually seen as a limit for particle manipulation due to the generation of interferences with the acoustic radiation force. Both the technologies can be considered particles manipulation: SSAWs move them towards the pressure nodes, while TSAWs, not having fixed pressure nodes, move the particles along the direction of waves propagation. The force acting on particles with standing waves is greater than the force generated by traveling waves. The main dependency changing the forces magnitude is related to the particle radius, r [66]:

$$F_{TSAW} \propto (kr)^3 \tag{2.11}$$

$$F_{TSAW} \propto (kr)^6 \tag{2.12}$$

where $k = 2\pi/\lambda_f$ is the wavenumber. Then, considering the same particles dimension, TSAWs must have a greater frequency (to reduce the wavelength and increase the wavenumber) to be comparable with the acoustic radiation force related to SSAWs. Another comparison can be done on channel design related to the application. Being particles moved towards pressure nodes with SSAWs, the

maximum displacement they can undergo is λ/4 (from an antinode to a node). Moreover, channel dimensions must be tuned to fit the wavelength and IDTs must be aligned with the channel walls to achieve the right directionality. Conversely, with TSAWs, since there are no pressure nodes particles move away from the acoustic source and they can be displaced over the entire width of the channel. The choice between the two solutions should be done depending on the specific application, considering advantages and disadvantages of both.

2.5 SAW-based microfluidic applications

In this section, several applications exploiting both TSAWs and SSAWs are reported. Reference [59] is suggested as a good review in surface acoustic waves technologies and their applications.

2.5.1 TSAWs applications

Traveling surface acoustic waves are exploited in both open and confined microfluidic geometries to accomplish several requirements such as fluid mixing, fluid translation, jetting and atomization, particle/cell concentration, droplet and cell sorting, and re-orientation of nanoobjects.

2.5.1.1 Fluid mixing

Mixing is a fundamental operation related to fluids and can become critical considering microfluidics. Since the flow, for straight channels, is laminar at the microscale, mixing occurs only by diffusion. Diffusion mixing is a slow operation, not suitable for some applications, therefore researchers have looked to SAW-induced streaming for its ability to mix fluids quickly by generating chaotic advection.

As reported by Sritharan et al. [67] fluid mixing can be operated in small droplets exploiting the acoustic streaming induced by SAW leaky waves (see Section 2.4.1). Shilton et al. [68] generated a TSAW to induce liquid recirculation inside a droplet. Their results demonstrate the fast mixing of dyed water and dyed glycerine solution.

Considering free-surface droplets, other phenomena can occur, for example, by increasing the input acoustic power above a certain threshold, droplet translation, jetting or evaporation. Developing a closed reservoir for droplet mixing, Frommelt et al. [69] investigated the possibility to tune the interaction between two IDT-generated surface acoustic waves to achieve different mixing modes. Their experiments show that by modulating the power frequency of the second wave source, keeping constant the power of the other transducer, different mixing is obtained. The study of Lim et al. [70] introduced for the first time a dome-shaped chamber-based SAW (DC-SAW) device. Two different fluids are injected through two separated inlets and flow into the chamber. A focused IDT generates a SAW which travels to the chamber where acoustic mixing takes place. Increasing the applied voltage and decreasing the flow rate led to a higher mixing efficiency. To maximize the mixing efficiency, the contact angle of the chamber was properly selected.

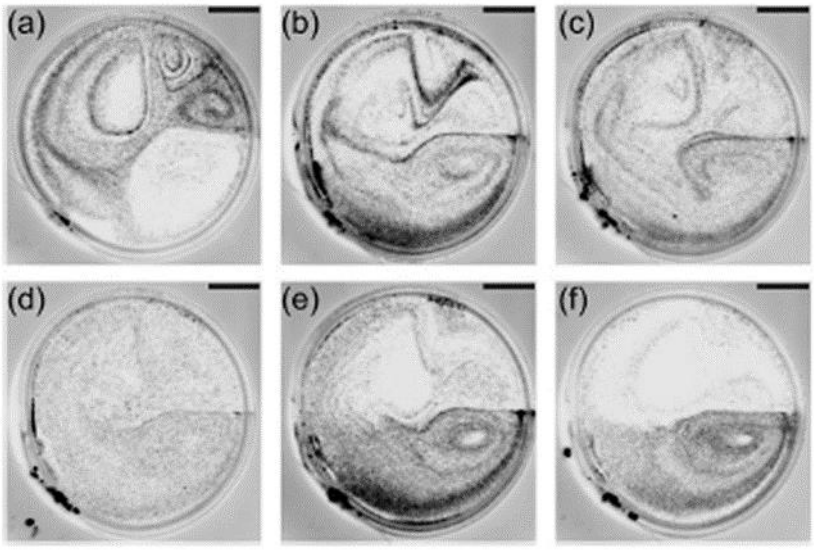

Figure 2.17: Top view of the mixing status of dual-jet experiments after 105.6s. The power of IDT II is constant in (a), and modulated at frequencies 0.042, 0.083, 0.17, 0.34, 0.68Hz respectively for (b), (c), (d), (e) and (f) [69].

Of course, the same mixing effects can be replicated in microchannel with different shapes. One example is the work of Westerhausen et al. [71] who exploit the mixing effect induced by SAWs to produce therapeutic nanoparticles. Two fluids, coming from separated inlets, are mixed in a Y-shaped microchannel. The perturbation of the fluids causes the formation of nanoparticles with precise dimensions.

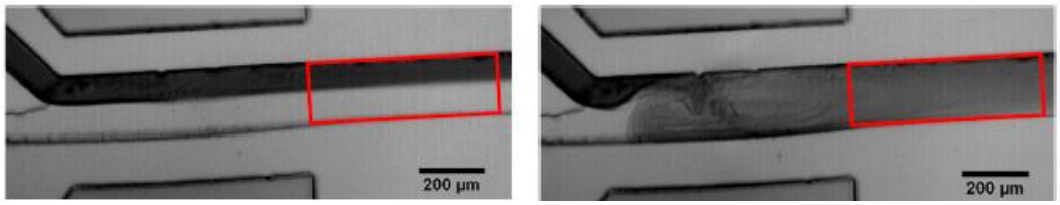

Figure 2.18: Micrographs of the mixing process. No SAW applied (on the left), SAW applied (on the right) [71].

2.5.1.2 Fluid translation in open space

When a liquid droplet is placed within the propagation path of TSAWs, leaky SAW will be diffracted into the droplet at the Rayleigh angle. If the SAW has sufficiently intermediate amplitude, the leaky acoustic energy generates an acoustic force on the droplet along the SAW propagation path, causing the droplet to deform into an axi-symmetrical conical shape and translate across the substrate. Moreover, as electrical actuation of IDTs can be programmed, droplet translation can be automated. Through the automated control of multiple droplets, merging, mixing, splitting, and chemical or biochemical reactions can be performed in so-called "programmable bio-processors".

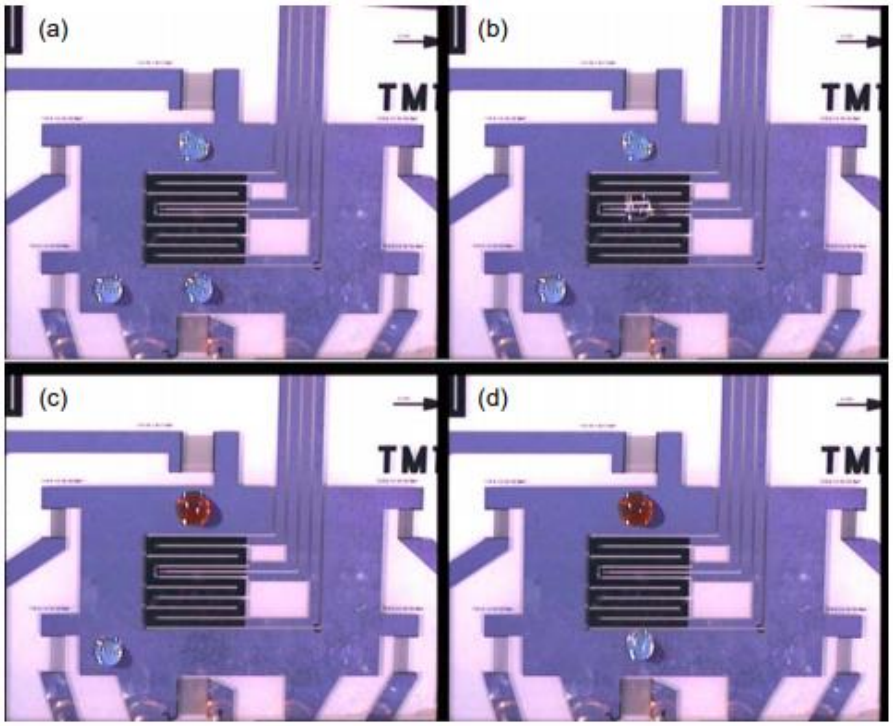

Figure 2.19: A SAW driven microfluidic processor. The snapshots are in sequence to follow droplets translation and chemical reactions [72].

Wixforth [72] experimentally demonstrated this phenomenon by moving independently in any desired direction three droplets made of different fluids and merging them to perform chemical reactions. A further development considered is the functionalization (make surface hydrophobic or hydrophilic to tune the interactions) of the device surface to create specific paths for droplets.

2.5.1.3 Fluid jetting

A fluid jet is commonly defined as a coherent stream of fluid projected into a surrounding medium. For a fluid to undergo jetting phenomena, it must possess sufficient inertia to overcome the restoring capillary forces acting on the interface of the fluid and surrounding media. Micro-scale jetting can be accomplished by exposing small fluid volumes to TSAWs (with the SAW power higher than that used for droplet translation).

Tan et al. [73] investigated the effect of SAWs on droplets by changing the actuation parameters of IDTs to generate the waves. They characterize jetting length as a function of the driving force and also predict the velocity of the jet, verifying their results with experimental data.

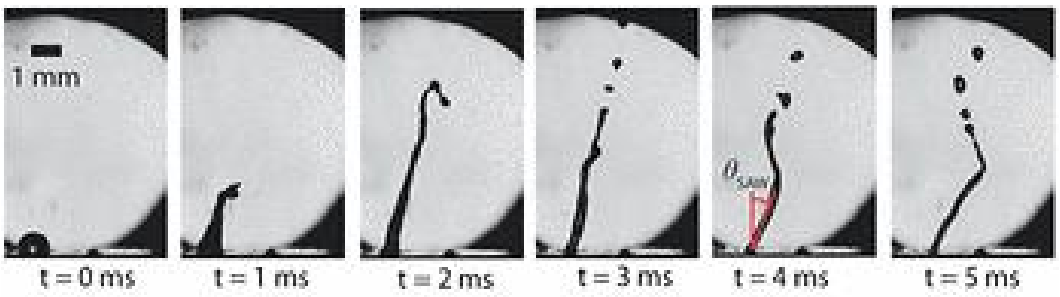

Figure 2.20: Fluid jetting at the Rayleigh angle as a consequence of propagating SAW irradiation [73].

2.5.1.4 Particle concentration

Concentrating particle/cell suspensions is a basic but critical operation in many applications in chemistry and biomedicine. At the macro-scale, particles can be easily concentrated using centrifugation. At the micro-scale, however, concentrating cells or particles can be difficult. As volume decreases, surface forces acting on the particles dominate over body forces. Lack of significant body forces makes standard centrifugation impractical, so researchers have explored SAW-

induced acoustic streaming to concentrate cells and particles for low-volume systems.

Li et al. [74] demonstrated the concentration of 1µm polystyrene (PS) particles in a droplet. To obtain the effect, SAWs are generated through IDTs deposed on a piezoelectric substrate. The waves are generated with a so-called "breaking symmetry configuration" in a way to generate bulk recirculation in the droplet. The fluid motion recalls the effect exploited for centrifugation.

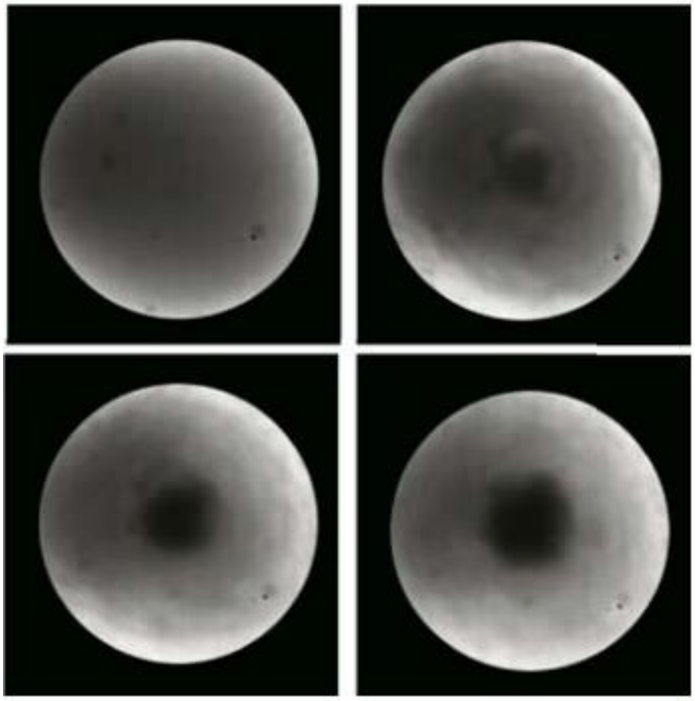

Figure 2.21: Bright-field images acquired at 60 fps, showing the rapid concentration of the PS particles [74].

Bourkin et al. [75] presented an acoustically actuated microchip for the detection of infected red blood cells (RBCs) for malaria diagnosis. The device consists in a slanted-finger interdigitated electrode (SFIDT) deposed on a piezoelectric substrate. A drop of blood is placed in a defined position, with one portion of the drop directly exposed to the SAW to induce a rotational motion of the fluid leading to separation between infected and non-infected cells. Considering the differences in density between infected and good RBCs and fluid, the device can concentrate RBCs in the middle of the drop, while the infected RBCs are enriched at the periphery. The separation can be clearly seen in Figure 2.22.

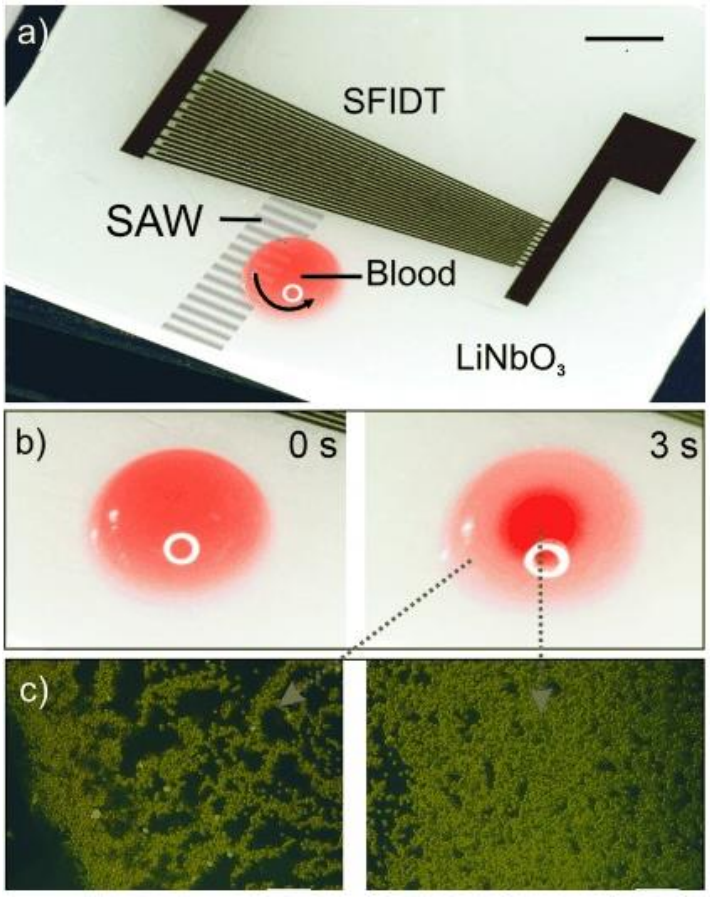

Figure 2.22: (a) Photograph of the device. (b) Droplet of blood before and after the SAW interaction. (c) Fluorescent micrograph of the infected RBCs (left) and non-infected RBCs (right) [75].

2.5.1.5 Particle sorting

Recently, several groups have shown that SAW-induced effects (acoustic streaming and acoustic radiation forces) can sort droplets, particles or cells. Franke et al. [76], [77] developed a device for particle sorting. The device used to accomplish this task consists of a branched PDMS channel and an IDT positioned adjacent to the channel that generates TSAWs propagating across the channel width. Particles or cells are injected into the main channel and hydrodynamically focused in its centre before reaching the region of TSAW exposure. When the IDT is off, the droplets or cells travel through the upper outlet branch because of its larger cross-sectional area and correspondingly lower hydrodynamic resistance (Figure 2.23 (a) and (c)). When the IDT is activated, the resulting TSAWs generate acoustic streaming in the channel fluid and push the fluid, which carries the contained droplets or cells,

towards the lower outlet branch (Figure 2.23 (b) and (d)). In this way, the device harnesses SAW-induced acoustic streaming to sort droplets or cells into two outlets.

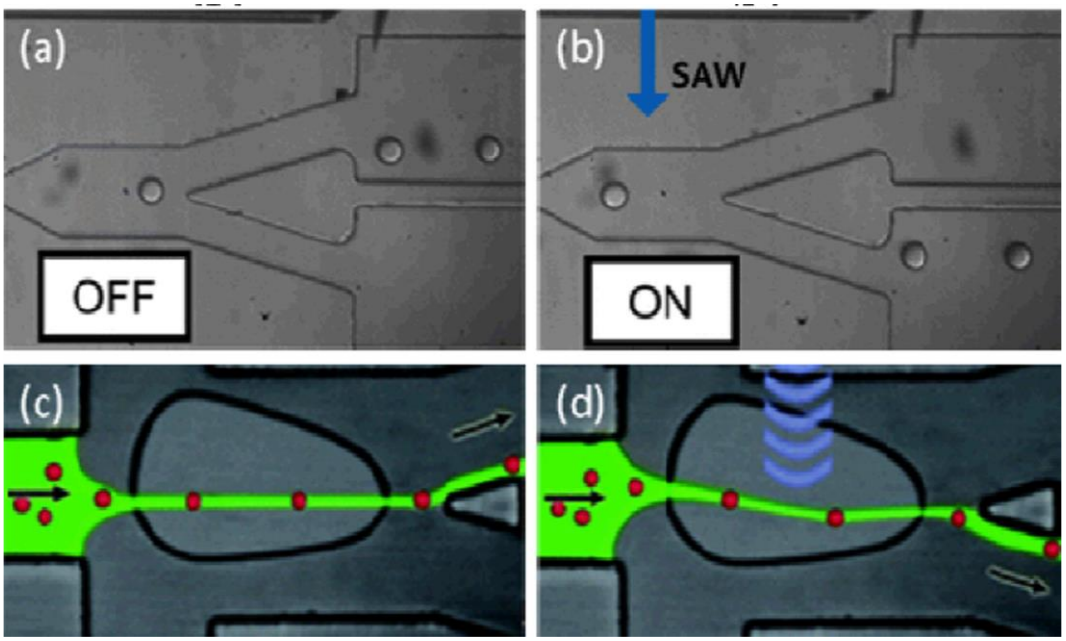

Figure 2.23: Schematic illustration of the SAW-based mechanism for droplet or cell sorting [76], [77].

An interesting work was done by Ma et al. [78], who proposed a detachable system to achieve particles separation through TSAWs. Components in biomedical analysis tools that have direct contact with biological samples, are ideally discarded after use to prevent cross-contamination. However, a conventional acoustofluidic device is typically a monolithic integration that permanently bonds acoustic transducers with microfluidic channels. Their idea was to propose a detachable acoustofluidic system comprised of a disposable channel device and a reusable acoustic transducer for non-contact continuous particle separation via TSAWs. A microstructured pillar is used to couple acoustic waves into the fluid channel for noncontact particle manipulation. The main advantage of this detachable system is that the disposable part can be discarded after use, while the SAW transducer is reusable, it is an efficient way to reduce the costs and waste of materials.

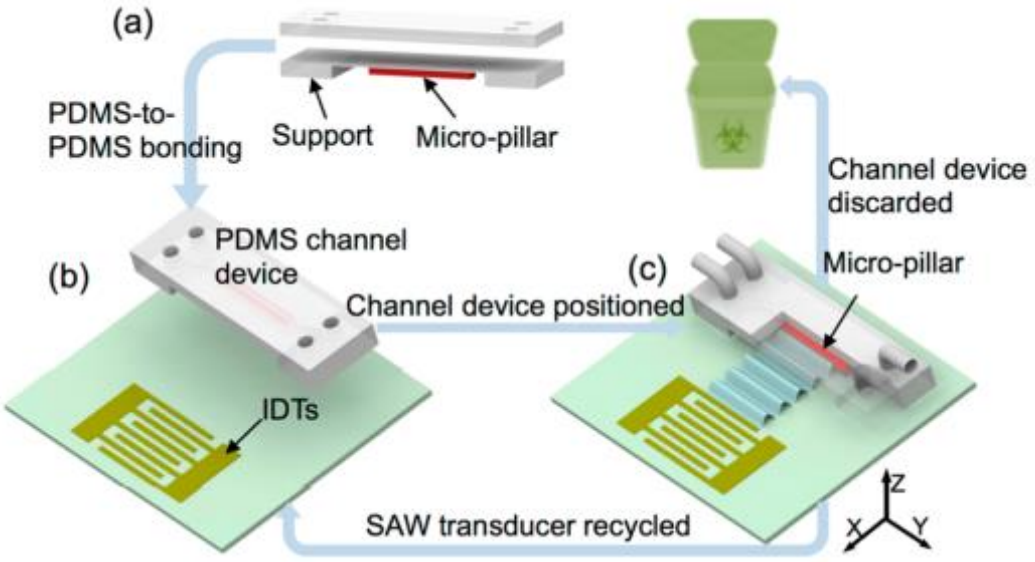

Figure 2.24: Scheme of the cyclic use of the system. (a) PDMS support with micropillar and PDMS channel. (b, c) Bonding and positioning of the two PDMS structures. The disposable structure is placed on the substrate with the SAW transducer [78].

2.5.2 SSAWs applications

Instead of exploiting the acoustic streaming, SSAW-based devices use the acoustic radiation forces acting on particles via the surrounding fluid. Standing SAWs can be used to focus a flow stream of particles into a single line, separate a flow stream of particles based on particle properties, actuate a single particle or cell moving with a flow stream, pattern a group of particles in stagnant fluid, manipulate a single particle/cell/organism in stagnant fluid and align micro/nano materials.

2.5.2.1 Particle focusing

Focusing of particles is an important feature to be achieved in microfluidics considering the possibility to study the properties of particles. One example is cytometry, defined as the measurement of the characteristics of cells. Variables that can be measured include cell size, cell number (counting), cell morphology and the presence of proteins on their surface. SSAWs are selected as a biocompatible method to focus particles and cells without needing complex or bulky structures to exploit hydrodynamic effects. Chen et al. [79] demonstrated a sheath-less microfluidic cytometer which integrates a SSAW-based microdevice capable of 3D particle/cell focusing with a laser-induced fluorescence (LIF) detection system. To

test particles, the system requires them to pass the detection point at the same velocity. By tuning some parameters such as flow rate and input power is possible to manipulate and focus particles of different sizes (smaller particle means lower acoustic radiation force). They demonstrated that fluorescently labelled human promyelocytic leukemia cells (HL-60) could be effectively focused and detected with this system.

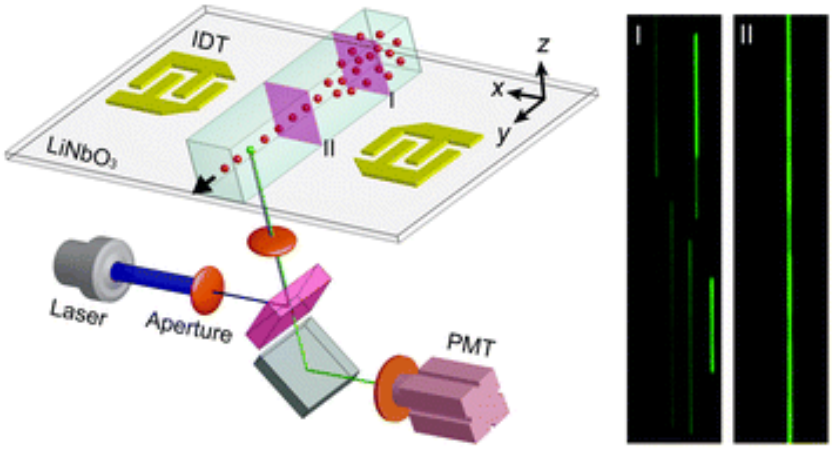

Figure 2.25: Schematic of the SSAW-based microfluidic cytometer. A microfluidic device is integrated with a LIF detection system. Fluorescent staking images of the particle flow patter without (I) and with (II) SSAWs [79].

Focusing of particles within the channel width satisfies the needs of some applications. Other applications require particles to be focused on a three-dimensional way (both in channel width and height). 3D focusing is especially important for flow cytometry applications, as fixing particle position along the channel height minimizes fluorescence variations caused by varying focal depths. Shi et al. [80] showed that SSAW can effectively achieve 3D focusing. Applying a SSAW to fluid in a microchannel, the researchers realized that a non-uniform acoustic field generates a primary acoustic radiation force in an orthogonal direction with respect to the flow plane. This force moves the particles towards the point of maximum acoustic kinetic energy. However, the acoustic radiation force acting in the z-direction is weaker than that acting in the device plane. Therefore, particles focus first along the channel width and then migrate to a focal point along the channel height.

2.5.2.2 Particle separation

A standing acoustic wave field exerts a primary acoustic radiation force whose magnitude and direction depend on particle size, density, and compressibility. Therefore, SSAW fields can differentiate particles or cells based on their physical properties.

Free-flow acoustophoresis is a good method for multiple fractionation. A solution of mixed particles beforehand focused is exposed to the acoustic force. The bigger particles move faster to the pressure nodes compared to smaller ones. As a result, the different particles are on different positions in the microfluidic channel. With as many outlets as size of particles, it is then possible to sort the particles in an easy way. To design efficient microfluidic devices, two parameters need to be taken care of: the width of the particle stream when it enters the acoustic zone compared to the channel width and the distance travelled by the particles in the acoustic zone. Guldiken et al. [81] present a microfluidic platform for sheath-less particle separation using standing surface acoustic waves. In this platform, particles are first lined up at the centre of the channel without introducing any external sheath flow. The particles are then entered into a second stage where particles are driven towards the off-center pressure nodes for size-based separation. The larger particles are exposed to more lateral displacement in the channel due to the acoustic force differences. Consequently, different-size particles are separated into multiple collection outlets.

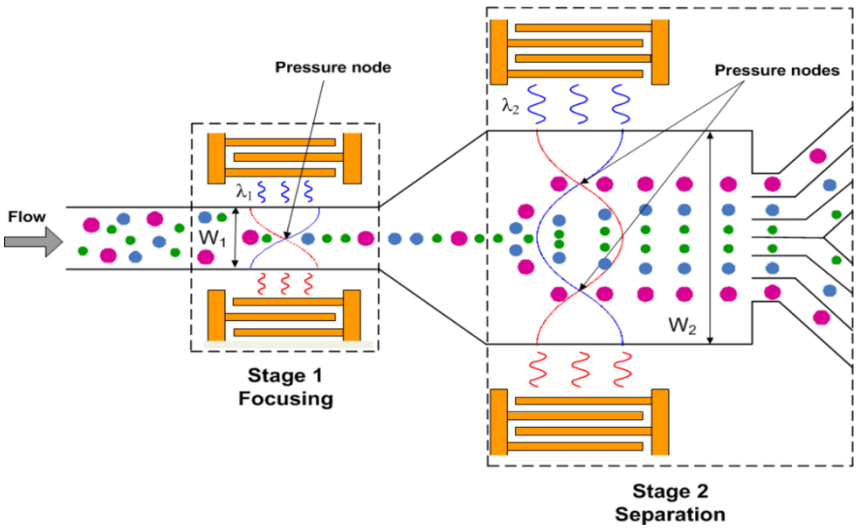

Figure 2.26: Conceptual view of the sheath-less particle separator using SSAWs. The first stage aligns the particles on the centre, while the second stage separates them according to size [81].

Besides size, differences in density and compressibility can be exploited to separate and sort particles. These two parameters are indeed involved in the calculation of the acoustic contrast factor of the particles. The separation process called binary acoustophoresis is based on the idea that two particles may have different acoustic contrast factors. Particles with positive acoustic factors are driven to the pressure nodes, while particles with a negative one, are moved to the pressure antinodes. For half-wavelength resonators, particles are separated between the central outlet and side outlets. Nam et al. [82] presented a method for density-based separation of monodisperse encapsulated cells using a standing surface acoustic wave in a microchannel. A mixture of beads of equal sizes but dissimilar densities was hydrodynamically focused at the entrance of the system and then actively driven toward the sidewalls by a SSAW. The lateral displacement of the beads is proportional to the density of the bead related to the number of encapsulated cells.

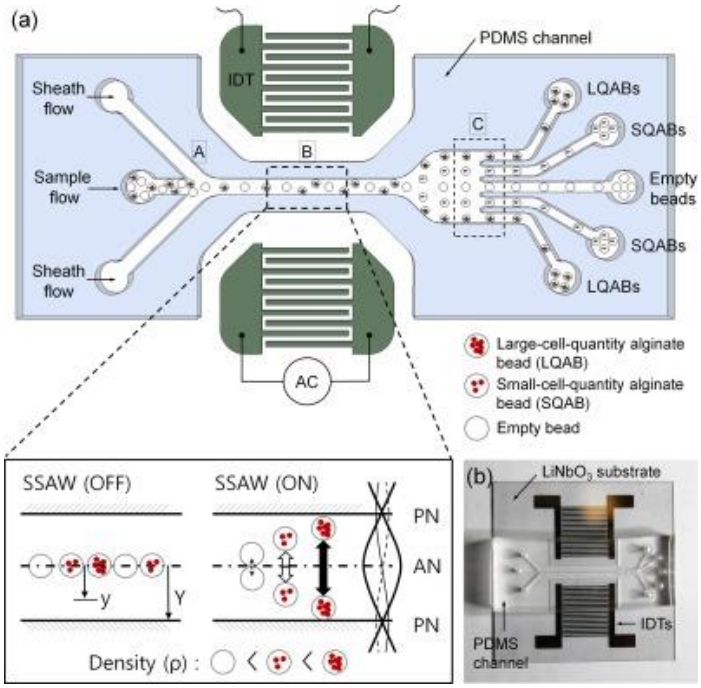

Figure 2.27: (a) Schematic illustration of the working principle of the device. (b) Photograph of the device [82].

By switching frequencies of acoustic waves and as a result, by tuning the magnitude of the primary acoustic radiation force, it is possible to obtain an alignment of different particles in different pressure nodes. An excellent control over the frequencies and the interval of time is required to get the best results. Changing

frequencies is also a good technique to sort similar particles to multiple outlets. Particles are driven to different pressure nodes according to the frequency applied. The channel design and the choice of frequencies need to be carefully chosen to optimize the set up. Adams and Soh [83] describe a tunable acoustophoretic separation architecture capable of sorting cells and particles based on a range of sizes, analogous to a band-pass filter (acoustic band-pass particle sorter, ABPS). The device can sort an arbitrary range of particle sizes between 3 and 10μm in diameter with high efficiency. The ABPS consists of two independently controlled, serially connected stages, each characterized by a channel width, a piezo actuation amplitude and frequency. A particle mixture of different sizes is introduced into the sides of the first stage alongside a central buffer flow. Due to the volume dependence of the acoustic radiation force, larger particles are focused faster than smaller particles. The selected particles are reintroduced into the sides of a second stage and subjected to another step of controlled focusing. By selecting appropriate operating parameters (flow rate, actuation amplitude and frequency), any range of particle sizes particle can be sorted into the band-pass outlet.

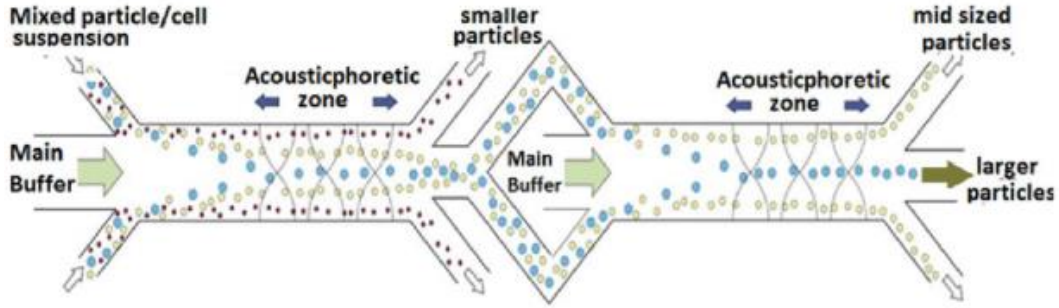

Figure 2.28: Schematic illustration of the ABPS functioning [83].

2.5.2.3 Cell trapping

To understand the function of single cells, it is very important to monitor the dynamic behaviour of a single cell in a living environment. Cell trapping is a fundamental step in single cell analysis [84]. Wu et al. [85] reported a simple and reliable method to generate multicellular spheroids, using acoustic method. Their device consisted of capillaries, a pair of interdigital transducers and a piezoelectric substrate. Once the RF signal was applied, a distributed acoustic field could be formed in the capillary. A pressure node array was generated. The suspended cells

in the capillary were pushed by the acoustic force to the pressure nodes and assembled into spheroids which can be extracted and singularly analysed.

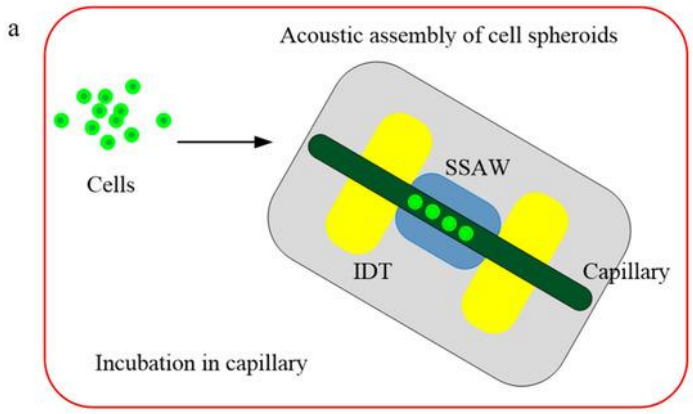

Figure 2.29: Schematic illustration of the acoustic assembly cell spheroids [85].

Lu et al. [86] investigated topographical manipulation of microparticles and cells, using acoustic microstreaming. This technique was called acoustic topographical manipulation (ATM). Some particles became obstacles due to the existence of electrostatic and van der Waals interactions. A localized microstreaming around the obstacles would be formed upon the application of a standing acoustic wave field. The acoustic microstreaming force, as well as radiation forces, could trap the microparticles at the vicinity of the obstacles.

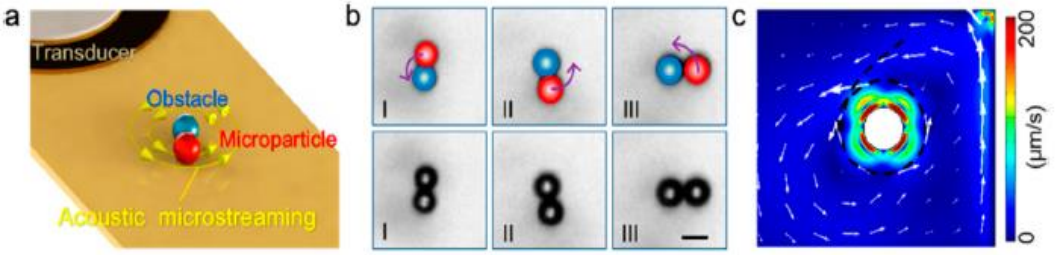

Figure 2.30: Schematic illustration of the ATM process. (a) Working principle, (b) description of motion of obstacles and microparticles, (c) simulated acoustic microstreaming velocities [86].

2.5.2.4 Manipulation of micro-objects

Another important process in biological samples analysis is micro-entities manipulation. The behaviour of specific species and cells interactions can be investigated. Ding et al. [87] demonstrated a standing surface acoustic wave based "acoustic tweezer" that can trap and manipulate single microparticles, cells, and

entire organisms (as *Caenorhabditis elegans*) in a single-layer microfluidic chip. The acoustic tweezer uses the wide resonance band of chirped interdigital transducers to achieve real-time control of a standing surface acoustic wave field, which enables flexible manipulation. The power density required by the acoustic device is significantly lower than its optical counterparts (10,000,000 times less than optical tweezers and 100 times less than optoelectronic tweezers), which makes the technique more biocompatible and amenable to miniaturization. Cell viability tests were conducted to verify the tweezer compatibility with biological objects. With its advantages in biocompatibility, miniaturization, and versatility, the acoustic tweezer presented can become a powerful tool. As demonstrated by Shi et al. [88] acoustic tweezers can be developed in 1D or 2D configurations for particle manipulation in specific patterns following the pressure field. The differences can be obtained designing specific IDTs positioning to generate the wanted standing SAWs for particles manipulation.

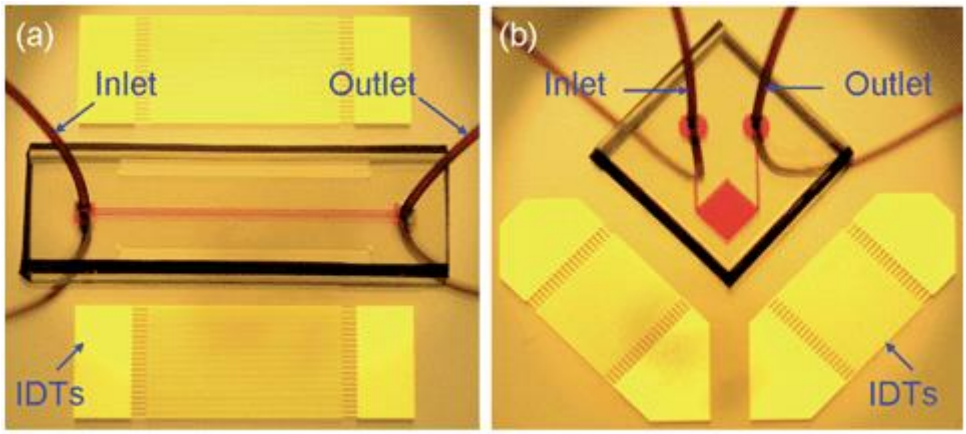

Figure 2.31: Optical images of the "acoustic tweezers" devices used in (a) 1D and (b) 2D patterning experiments [88].

2.5.3 Limits and future trends

As described in the brief review of the previous sections, acoustofluidics can be considered as a valid solution for several applications. However, this technology is still showing some limitations which prevent acoustofluidics to be a valid substitute for commercial solutions. One important limit is related to the size of the manipulated particles. Acoustic methods have proven their utility in contactless

manipulation of microscale objects mainly relying on the acoustic radiation effect, though the influence of acoustic streaming has typically prevented manipulation at smaller length scales. The acoustic streaming induced drag force is proportional to the radius of the particles, while the acoustic radiation force scales with its cube. Thus, decreasing the size of the particles, the drag force becomes dominant over the acoustic radiation force, making particles manipulation difficult to be controlled. To increase the effect of the acoustic radiation force, one solution can be the increase of the frequency of acoustic waves. SAW devices can work at high frequencies and can be considered for nanoparticles separation. Wu et al. [89] reported the separation of polystyrene nanoparticles with different sizes (500 and 100nm) using tilted angle SSAWs. The separation was achieved choosing a frequency of 33.13MHz. Another solution can be the use of acoustic trapping for separating sub-micrometric particles. Hammarström et al. [90] reported a method for acoustic trapping of sub-micrometric particles in glass capillaries using secondary acoustic forces. By using preloaded larger particles (seed particles of 10μm) to initiate clustering, trapping of sub-micrometric particles (110nm) is greatly improved and can be accomplished at lower concentrations. As a potential application for this method, they demonstrated capture and enrichment of Escherichia Coli. Collins et al. [91] explicitly take advantage of the strong acoustic streaming in the vicinity of a highly focused, high frequency SAW beam emanating from a series of focused interdigital transducers patterned on a piezoelectric lithium niobate substrate and actuated with a 633 MHz sinusoidal signal. This streaming-induced manipulation of nanoscale particles is maximized with the formation of micro-vortices that extend the width of the microfluidic channel even with the imposition of a lateral flow. They demonstrated manipulation of particles of 100nm size.

The throughput of acoustofluidic devices is another limitation. To be considered as a valid alternative to other commercial techniques, the separation throughput must be comparable with the other solutions (for example electrophoresis). Ren et al. [92] reported a high-throughput cell sorting method based on SSAWs. They used a pair of focused interdigital transducers to generate SSAW with high resolution and high energy efficiency. As a result, the sorting throughput is improved significantly

from conventional acoustic-based cell sorting methods. They demonstrated the successful sorting of 10μm polystyrene particles with a minimum actuation time of 72μs, which translates to a potential sorting rate of more than 13800 events per second. Without using a cell-detection unit, they were able to demonstrate an actual sorting throughput of 3300 events per second.

One followed trend in microfluidics is the integration of different technologies together in a single chip to fulfil different requests [5]. It is important to design specific connections between different integrated stages. Felton et al. [93] report a novel, negligible-cost and open-source process for the rapid prototyping of complex microfluidic devices in PDMS using 3D-printed interconnecting microchannel scaffolds. These single-extrusion scaffolds are designed with interconnecting ends and used to quickly configure complex microfluidic systems before being embedded in PDMS to produce an imprint of the microfluidic configuration. The scaffolds are printed using common material extrusion (MEX) 3D printers. Researchers, following this integration trend, are studying the use of piezoelectric materials thin films for acoustic wave actuation. Thin films can be deposited on different substrate as silicon, glass, metals or polymers. Deposition of thin films can occur only on selected areas of the substrate where the generation of waves is required. Luo et al. [94] created a flexible and transparent polymeric device for SAW technology exploiting the deposition of 4μm thin films of ZnO for surface acoustic waves generation.

3D printing has made widespread impact across science, engineering, and industry by producing materials with complex architectures that would be difficult or impossible to create using conventional fabrication methods. In microfluidics, 3D printing can be considered as an alternative solution to microfabrication. For some applications, there is interest in active materials that can respond to external stimuli by undergoing reversible shape changes. These can be achieved through 4D printing, which combines 3D printing with active materials to produce stimuli-responsive materials with complex architectures that can change shape over a fourth dimension (time or temperature). 4D printed liquid crystal elastomers (LCEs) show fully reversible shape changes and have been implemented in the development of

soft, temperature responsive actuators [95]. These materials can be considered as possible substitutes to piezoelectric materials.

2.6 Summary

In this chapter acoustofluidics and all the issues related to this field have been introduced. An introduction to microfluidics and the behaviour of fluids at the microscale through the definition of dimensionless numbers was given. The manipulation of particles was presented considering the biocompatibility of this technology. Piezoelectricity was defined to explain how acoustic waves can be generated and used in acoustofluidics. Then, the devices exploiting acoustic waves (both BAW and SAW devices) were described focusing on the soft lithographic technique and its advantages in terms of simplicity and reproducibility to produce SAW-based systems. Finally, a better description on traveling and standing SAWs was provided, highlighting the differences between the two possibilities, and reporting several applications exploiting SAW-based devices.

All the considerations done in this chapter are useful to give a complete overview on acoustofluidics and the applications for which this field is exploited. In chapter 4, piezoelectricity, surface acoustic waves generation and their interaction within a microchannel are exploited to make numerical simulations on a SSAW-based device for particles manipulation. Also, different positionings of IDTs are considered in the analysis to investigate the effects of waves propagation and interaction on the surface of a lithium niobate substrate. Also, maskless photolithography is performed to obtain an SU-8 mold on silicon wafer to be exploited in a soft lithographic process to produce a simple PDMS microchannel, previously designed.

3 Theoretical background

In this chapter, the theoretical formulation of the acoustofluidic problem is reported. The governing equations for fluid mechanics are presented. Solid and piezoelectric constitutive laws are reported with a focus on Rayleigh waves and their transmission to fluids. The described equations and conditions are the same exploited by the numerical analysis software to compute the solutions to the problem solved in Chapter 4. Finally, the acoustic effects such as the acoustic radiation force and the acoustic streaming are described.

3.1 Fluid mechanics

A fluid is a substance in liquid or gaseous phase. The distinction between a solid and a fluid is the capability of a substance to sustain shear stresses. While a solid can sustain shear stresses with a deformation, a fluid deforms in a continuous manner under the action of small shear stress. In solids the stress is proportional to the deformation, while in fluids the stress is proportional to the velocity of deformation.

Fluids can be modelled as a continuum or at molecular level. In microfluidics, a fluid can be treated as a continuum, neglecting its molecular structure. This assumption can be justified considering the characteristic volumes of fluid considered (in the order of few micrometres). Small volume elements containing several molecules can be defined. They are smaller than the whole volume of fluid but bigger than intermolecular distances (sub-nanometric values). Physical properties of fluids such as density, pressure or temperature are well-defined within these volumes, varying continuously depending on the volume.

To describe the governing equations of fluid mechanics, the Eulerian approach of the continuum field is used. The spatial coordinates $\boldsymbol{r}$ are fixed in space and the evolution of fields in time at these fixed coordinates $\boldsymbol{r}$ is observed [20].

In the next sections, the governing equations of fluid dynamics are presented. An arbitrarily shaped region of fluid Ω with its surface $\partial\Omega$ is considered. The fluid is considered as Newtonian and compressible with its density ρ varying in space and

time. Then, two flow solutions of interest in microfluidic applications are highlighted: the Stokes flow, for low flow velocity, and the Poiseuille flow, considering a pressure driven, steady-state flow. These solutions are described as simplification of the Navier-Stokes equation (described in Section 3.1.2).

3.1.1 The continuity equation

The first governing equation to be introduced is the continuity equation, which expresses the conservation of fluid mass. A compressible fluid is considered, such that the density ρ may vary as function of space and time. The equation states that the rate of change of mass in the volume Ω equals the mass flux through its surface:

$$\partial_t \rho = -\boldsymbol{\nabla} \cdot (\rho \boldsymbol{v}) \tag{3.1}$$

where ∂_t is the time derivative, $\boldsymbol{v}$ is the fluid velocity and $\boldsymbol{\nabla} \cdot$ is used to denote the divergence of a vectorial field. If the density is constant in space and time, the equation (3.1) is simplified to:

$$\boldsymbol{\nabla} \cdot \boldsymbol{v} = 0 \tag{3.2}$$

Fluids are considered as incompressible when the change of the density with pressure is negligible. However, for propagation of acoustic waves, fluid compressibility is fundamental, then, dealing with acoustofluidics, the Equation (3.1) should be considered.

3.1.2 The Navier-Stokes equation

The second governing equations are the Navier–Stokes equations, which are partial differential equations describing the motion of viscous fluids. These equations express the conservation of momentum and mass for Newtonian fluids (fluids in which the viscous stresses are linearly related to the local strain rate). They are found by applying the Newton's second law to fluid motion, taking into account that stresses in a fluid are composed by a diffusing viscous term (viscous flow) and a pressure term. In contrast to the mass, which can only change by advection through the surface of the domain, the momentum can change both by advection and by the action of external forces. These forces can be divided into body forces,

as gravitational or electrical, and contact forces, as pressure and viscosity. The solution of the equations is a flow velocity $\boldsymbol{v}$ which is a vector field (associating a vector to every point of the fluid domain at any time moment). For fluids is better to study velocity instead of position, even though integral curves of the velocity field are computed to visualize the streamlines, which are the trajectories of fluid particles along the fluid domain, of the field. The Navier-Stokes equations for a compressible fluid are:

$$\rho[\partial_t \boldsymbol{v} + (\boldsymbol{v} \cdot \boldsymbol{\nabla})\boldsymbol{v}] = -\boldsymbol{\nabla} p + \eta \boldsymbol{\nabla}^2 \boldsymbol{v} + \beta\eta \boldsymbol{\nabla}(\boldsymbol{\nabla} \cdot \boldsymbol{v}) + \boldsymbol{f_b} \qquad (3.3)$$

The terms on the left-hand side of the equations, are related to the inertial forces per unit volume (being ρ the density of the fluid). The expressions contained between the square brackets are the definition of the material derivative applied to the fluid velocity: $\partial_t \boldsymbol{v}$ states the variation in time of the velocity (time derivative, the definition of an acceleration), while $(\boldsymbol{v} \cdot \boldsymbol{\nabla})\boldsymbol{v}$ is the convective term. p is the pressure and $\boldsymbol{\nabla} p$ introduces the pressure forces acting on the fluid. η is the shear dynamic viscosity and β is the ratio between the dynamic viscosity and the dilatational viscosity. The dynamic viscosity expresses the resistance of the fluid to flow. It is caused by the cohesive intermolecular forces between adjacent layers of fluids when they slide one with respect to the other. The dilatational viscosity is related to the viscous forces generated by compression and dilatation. The two terms containing the viscosity, introducing the viscous forces, arise from the divergence of the deviatoric stresses. $\boldsymbol{f_b}$ is the sum of the external body forces acting on the fluid.

The Navier-Stokes equations are introduced because are fundamental to model and describe flowing fluids. The greatest limit of these equations is their complexity: non-linear terms are contained in the equations making the mathematical treatment very complicated. In Section 3.1.4, two particular solutions neglecting the non-linearities of the equations are reported to simplify the treatment of fluid dynamics.

3.1.3 The heat-transfer equation

The third and last governing equation to be presented, is the heat-transfer equation, built on the energy density flux and the conservation of energy. The thermodynamic

quantities for fluids are usually taken per unit mass, directly relating them to the molecules of the fluid. The heat-transfer equation states:

$$\rho T[\partial_t s + (\boldsymbol{v} \cdot \boldsymbol{\nabla})s] = \boldsymbol{\sigma}' : \boldsymbol{\nabla}\boldsymbol{v} + \boldsymbol{\nabla}(k\boldsymbol{\nabla}T) \tag{3.4}$$

where s is the entropy per unit mass, T is the temperature, $\boldsymbol{\sigma}'$ is the viscous stress tensor and k is the thermal conductivity of the fluid. The viscous stress tensor is formally similar to the elastic stress tensor, the difference is that elastic stresses are generated by deformations, while viscous stresses are caused by the rate of change of the deformation in time (the strain rate). In viscoelastic materials, the total stress tensor comprises both viscous and elastic components. The left-hand side of the equation is ρT times the material time derivative of the entropy per unit mass, hence expressing the total gain in heat density per unit time. The right-hand side represents the sources for heat gain: viscous friction and thermal conduction.

The heat-transfer equation was presented to show and describe all the three fundamental equations related to fluid dynamics. Nevertheless, the heat-transfer equation will not be used to model the acoustofluidic problem considered in Chapter 4.

3.1.4 Flow solutions

The non-linear term $\rho(\boldsymbol{v} \cdot \boldsymbol{\nabla})\boldsymbol{v}$, in the Navier-Stokes equation, is responsible for complicating the mathematical treatment of the equation. In the following sections, two different cases are reported, where the non-linear term can be neglected.

3.1.4.1 Stokes flow

The first case is the limit of low flow velocities, a limit highly relevant for microfluidic systems. Here, the non-linear term can be neglected as it is much smaller than the viscous term, and we enter the linear regime of the so-called Stokes flow. To obtain this condition, the Reynolds number Re must be small:

$$Re = \frac{\rho v L}{\eta} \ll 1 \tag{3.5}$$

considering water as fluid, with $\eta = 1.002\text{mPa} \cdot \text{s}$ [20], $\rho = 998\text{Kg/m}^3$, $v = 1\text{mm/s}$, $L \approx 10^{-4}\text{m}$. The same values are used for the numerical model presented

in Chapter 4. These quantities lead to a small value for the Reynolds number, then the non-linear Navier-Stokes equation reduces to the time-dependent, linear Stokes equation:

$$\rho \frac{\partial \boldsymbol{v}}{\partial t} = -\boldsymbol{\nabla} p + \eta \nabla^2 \boldsymbol{v} \qquad (\mathbf{3.6})$$

An example of Stokes flow relates to particle solutions. Let an external force move a spherical particle of radius r with velocity $\boldsymbol{v}_p$ through a fluid that itself moves with velocity $\boldsymbol{v}$ far from the particle. The viscous Stokes drag force acting on the particle is:

$$\boldsymbol{F}_{drag} = 6\pi\eta r(\boldsymbol{v} - \boldsymbol{v}_p) \qquad (3.7)$$

This force is a fundamental contribution dealing with particle manipulation in a flowing fluid. Specifically, considering the acoustophoretic phenomenon, one particle is mainly subjected to two forces: the acoustic radiation force (described in Section 3.3.1) generated by the pressure waves travelling within the fluid and the drag force caused by the flow velocity. In the numerical analyses presented in Chapter 4, the effect of the drag force on the manipulation of particles is highlighted by comparing the trajectories of the particles without simulating the fluid flow and by simulating different fluid velocities (see Section 4.4.4.2).

3.1.4.2 Poiseuille flow

A solution to the Navier–Stokes equation in the dynamic case, is a pressure-driven (through a pressure difference Δp between the two ends of the channel), steady-state flow in a straight channel of length *L*, also known as Poiseuille flow. This class of flow is important for the basic understanding of liquid handling in microfluidic systems. The channel is placed horizontally along the *x*-axis, so along the *z*-axis gravity is balanced by the hydrostatic pressure. Furthermore, the cross-section of the channel is constant along the *x*-axis, then the liquid in the channel is only affected by the force generated from the pressure drop along the *x*-axis. The velocity field is therefore assumed to have only an *x*-component, and this component depends only on the transverse coordinates *y* and *z*, such that $\boldsymbol{v} = v_x(y, z)\boldsymbol{e_x}$. This

implies $(\boldsymbol{v}\cdot\boldsymbol{\nabla})\boldsymbol{v} = (v_x\partial_x)v_x(y,z)\boldsymbol{e_x} = 0$, and the non-linear Navier–Stokes equation becomes the linear Stokes equation.

The no-slip boundary condition is applied for the fluid flow on the walls of the channel: the velocity of the fluid in contact with the walls is equal to their velocity, which typically is zero. A justification of this condition is that at fluid-solid interface, the force of attraction between the fluid particles and solid particles is greater than that between the fluid particles (adhesion forces overcomes fluid cohesion forces). Then, on all the points of the solid surface, the velocity of the fluid equals the one of the walls (equal to zero). Therefore, the no-slip condition is correlated to the viscous effects generated at the fluid-solid interface. This condition does not always hold in reality: in case of low pressure or for the description of an inviscid flow, when the effect of the boundary layer (a layer of fluid in the immediate vicinity of a boundary surface where the effects of viscosity are significant) is neglected.

The steady-state Navier-Stokes equation for the Poiseuille flow becomes:

$$0 = -\boldsymbol{\nabla}p + \eta\nabla^2[v_x(y,z)e_x] \tag{3.8}$$

The resulting velocity field can be determined analytically for a limited number of cross-section shapes. In case of rectangular cross-sectional channels, the velocity profile is parabolic with the maximum value in the centre of the channel and zero velocity on the walls (due to the no-slip condition).

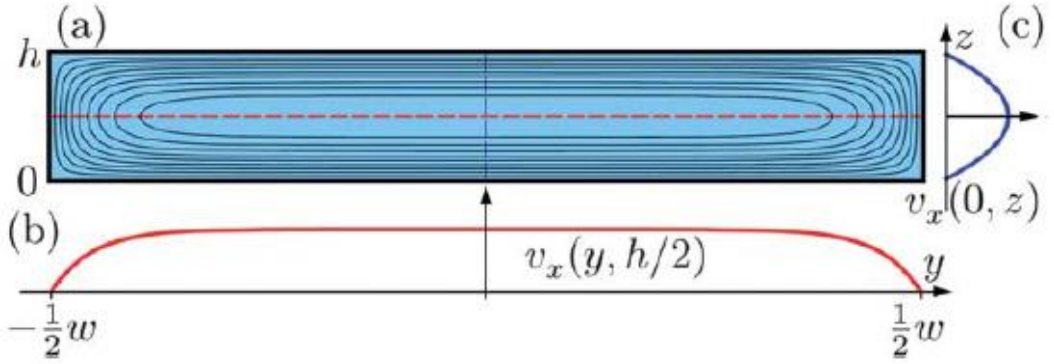

Figure 3.1: (a) Contour lines for the velocity field for a Poiseuille-flow in a rectangular channel. (b) A plot of velocity along the long centerline. (c) A plot of velocity along the short centerline [20].

3.2 Solid mechanics

Solid deformable bodies are the objects studied in the discipline called solid mechanics. These bodies are considered as linear elasto-dynamic solids, which can be described through stress, strain and displacement fields [96]. Differently than fluids, solids can sustain shear deformations, therefore their behaviour and description should be different with respect to fluid substances.

The reference frame considered to deal with solid mechanics is composed by three mutually perpendicular directions (x_1, x_2, x_3). The spatial coordinates of a material point (massless point of the continuum body) in the reference frame can be defined as:

$$\boldsymbol{x} = x_i \boldsymbol{e}_i \equiv \sum_{i=1}^{n} x_i e_i = x_1 \boldsymbol{e}_1 + x_2 \boldsymbol{e}_2 + x_3 \boldsymbol{e}_3 \tag{3.9}$$

where $\boldsymbol{e}_i$ are the unit base vectors corresponding to the directions composing the reference frame, used to define the direction and the versus, $i = 1, 2, 3$ is an index associated to every direction of the frame and n is the number of dimensions (equal to three in this case). The movement of a continuum body is described in terms of displacements of all points of coordinates $\boldsymbol{x}$ inside the body. The displacement is defined as the difference between the position of the material point in the current configuration ($\boldsymbol{x}$) and the same material point in the reference configuration ($\boldsymbol{X}$)**.** The displacement field $\boldsymbol{u}$ (dimensionally, a length) is considered as the vectorial function composed as the sum of the components of displacements (u_1, u_2, u_3) in all the directions of the reference frame:

$$\boldsymbol{u} = u_i \boldsymbol{e}_i \equiv \sum_{i=1}^{n} u_i \boldsymbol{e}_i \tag{3.10}$$

The displacement is assumed to be a continuous function of the position $\boldsymbol{x}$, varying with time t, $\boldsymbol{u}(\boldsymbol{x}, t)$.

The hypothesis of small strain and displacements is assumed, meaning that the displacements, shape and volume variations of the body are very small with respect to the body dimensions. In the analyses reported in Chapter 4, nanometric

displacements are obtained on the surface of a piezoelectric substrate with the smallest dimensions of 500μm (height) and the maximum value of displacement achieved is around 0.8μm on the surface of a PDMS microchannel with the smallest dimension of 100μm (height). Therefore, the use of the hypothesis is justified. For a given displacement field, with the hypothesis of small strain and displacements, the strain tensor can be defined:

$$S_{ij} = \frac{1}{2}\left(\frac{\partial u_i}{\partial x_j} + \frac{\partial u_j}{\partial x_i}\right) \quad or \quad \boldsymbol{S} = \frac{1}{2}[(\nabla \boldsymbol{u})^T + \nabla \boldsymbol{u}] \tag{3.11}$$

Strain is defined as the relative change in the position of points within a body that undergoes a deformation. The strain tensor, as all second-order tensors, is defined by nine functions of the position and of time, which reduce to six functions being the tensor symmetric. The diagonal strain terms S_{ii} are called longitudinal strains, describing the elongation or compression along the three directions, while the off-diagonal terms S_{ij} (with $i \neq j$) stand for shear strains, representing the sum of the variation of the angle between the two directions considered.

Volume forces and surface forces load the deformable body; their effect is felt in terms of reaction forces in correspondence of the constrained boundaries and of an internal field of forces per unit surface, which are called stresses. The stress field is defined by means of another second-order and symmetric tensor T_{ij}. This tensor represents the ith component of the force acting on one normal jth surface of an infinitesimal volume element of the body.

A constitutive law for a deformable material is a relation between the strain and the stress components. For small deformations, the strains are linearly proportional to the stresses applied to the solid. The linear elastic constitutive law is:

$$T_{ij} = c_{ijkl} S_{kl} \quad or \quad \boldsymbol{T} = \boldsymbol{c}:\boldsymbol{S} \tag{3.12}$$

where c_{ijkl} is a fourth-order tensor called stiffness tensor (or elasticity tensor) which is a property of the material depending on physical state variables as temperature, pressure and microstructure. The microstructural crystalline symmetry of a material defines the number of independent parameters needed to compute the coefficients filling the stiffness tensor: due to the intrinsic symmetries of the stress and strain

tensors, 21 elastic constants are needed to define anisotropic materials (triclinic symmetry), 13 for monoclinic crystalline symmetry, 9 for orthotropic materials, 5 for transversely isotropic materials (hexagonal crystalline symmetry), 3 for cubic crystalline structures and only 2 elastic constants are required for isotropic materials.

The equation of motion, without body forces, can be written:

$$\frac{\partial T_{ij}}{\partial x_j} = \rho \frac{\partial^2 u_i}{\partial^2 t} \quad \text{or} \quad \boldsymbol{\nabla} \cdot \boldsymbol{T} = \rho(\partial_t^2 \boldsymbol{u}) \tag{3.13}$$

As said before, the isotropic case is the simplest way to describe a material: the complete description of the stiffness tensor is obtained only exploiting two independent parameters, which are the Young's modulus E and the Poisson's ratio ν (which is the negative of the ratio between a strain component and the strain component in an orthogonal direction with respect to the other one). A second couple of material parameters, λ and μ (also called shear stiffness modulus and denoted by G), named Lamé constants can be used. Using them, the stress tensor is defined as:

$$T_{ij} = \lambda S_{kk} \delta_{ij} + 2\mu S_{ij} \quad or \quad \boldsymbol{T} = \lambda tr(\boldsymbol{S})\boldsymbol{I} + 2\mu \boldsymbol{S} \tag{3.14}$$

where δ_{ij} is the unit tensor or Kronecker delta (equal to 1 when $i = j$, equal to 0 when $i \neq j$), $tr(\boldsymbol{S})$ is the trace of the strain tensor, defined as the sum of the diagonal terms of the tensor, and $\boldsymbol{I}$ is the second order identity tensor. Then, in the isotropic case, the equation of motion becomes:

$$\rho \frac{\partial^2 u_i}{\partial^2 t} = (\lambda + \mu) \frac{\partial u_i}{\partial x_j \partial x_i} + \mu \frac{\partial^2 u_i}{\partial^2 x_j} \quad or \quad \rho(\partial_t^2 \boldsymbol{u}) = (\lambda + \mu)\partial_i \Delta + \mu \nabla^2 \boldsymbol{u} \tag{3.15}$$

where Δ is the dilatation (volume strain). Combining the equations, can be seen the existence of two types of waves (satisfying the classical wave equation) with a longitudinal wave speed c_L and a transverse wave speed c_T. For an isotropic medium, they are found to be:

$$c_L = \sqrt{\frac{\lambda + 2\mu}{\rho}}, \qquad c_T = \sqrt{\frac{\mu}{\rho}} \tag{3.16}$$

3.2.1 Rayleigh waves

Rayleigh waves are a type of surface waves described as a combination of longitudinal motion and transverse motion confined to the surface of an elastic medium, penetrating only to about one wavelength in depth [61]. The reference frame in Figure 3.2 is used to describe the propagation of Rayleigh waves: the *x*-direction is taken as the propagation direction, while the *z*-direction is taken positive towards the depth of the medium. This type of waves is exploited in SAW-based devices, therefore it is introduced and briefly described.

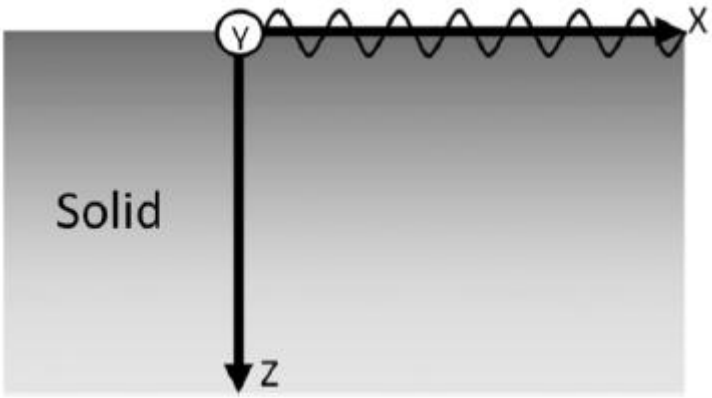

Figure 3.2: A schematic showing the propagation of a surface wave along the xy plane of a half space [61].

In reference [61], the complete calculation of the displacements along *x* and *z*-directions is reported, starting from the Equation (3.15). Here, only the real part of the formulation of the displacements is reported. Knowing that the solutions for the surface wave equations for the two polarizations will have a common wave number, we look for solutions propagating as harmonic waves along the *x*-axis with wavenumber k and variations in the *z*-direction to be determined by the boundary conditions. The solutions for the displacements are named as u_R (*x*-direction) and w_R (*z*-direction):

$$u_R = Akf_{u(z)}sin\,(\omega t - kx) \tag{3.17}$$

$$w_R = A\gamma_L f_{w(z)}cos\,(\omega t - kx) \tag{3.18}$$

where A is a constant, while $f_{u(z)}$ and $f_{w(z)}$ are decay functions which describe the rate at which the displacement amplitudes along the direction of propagation change with depth (z-dependent) [61]:

$$f_{u(z)} = e^{-\gamma_L z} - \frac{2\gamma_L \gamma_T}{(\gamma_T^2 + k^2)} e^{-\gamma_T z} \tag{3.19}$$

$$f_{w(z)} = e^{-\gamma_L z} - \frac{2k^2}{(\gamma_T^2 + k^2)} e^{-\gamma_T z} \tag{3.20}$$

where $\gamma_L^2 = k^2 - k_L^2$ is called longitudinal Rayleigh combination and $\gamma_T^2 = k^2 - k_T^2$ is called transverse Rayleigh combination, with k_L and k_T being the longitudinal and the transversal wavenumbers. Considering Equation (3.17), the displacement in the x-direction decreases rapidly as the depth (z) increases. At a certain depth the displacement in the x-direction passes through zero, and changes polarity. On the other hand, the movement perpendicular to the surface increases slightly before reaching a maximum and then decreases but does not change polarity. Displacements u_R and w_R, are functions of sine and cosine respectively (as reported in Equations (3.17) and (3.18) and found in reference [61]), hence the motion of particles is rotational about the y-axis [61].

A simple approximation for the speed of Rayleigh waves c_R, expressing it solely in terms of Poisson's ratio ν, is quoted by Victorov [61]:

$$\frac{c_R}{c_T} = \frac{0.87 + 1.12\nu}{1 + \nu} \tag{3.21}$$

Thus, as the Poisson's ratio varies between 0 and 0.5, c_R varies between $0.87c_T$ and $0.96c_T$.

3.2.2 Leaky Rayleigh waves

A pure Rayleigh wave (with a completely free surface) is of less interest in microfluidics than a surface bounded by a fluid into which the surface wave will deliver energy. This will lead to an exponentially decaying wave propagating along the fluid–solid interface. The wave is converted into a "leaky" Rayleigh wave.

The components of a Rayleigh wave, as described before, can be divided into one normal and one tangential components and arranged into the following form [61], called characteristic equation (from which Equation (3.17) and (3.18) arise):

$$4k^2\gamma_L\gamma_T - (k^2 + \gamma_T^2)^2 = 0 \tag{3.22}$$

Since the surface is in contact with a fluid, the surface is no more free. By including the continuity of normal stresses into the above equation, a new characteristic equation for Rayleigh waves is generated (compared to Equation (3.22)):

$$4k^2\gamma_L\gamma_T - (k^2 + \gamma_T^2)^2 = i\frac{\rho_F}{\rho_R}\frac{\gamma_L k_T^4}{\sqrt{k_L^2 - k^2}} \tag{3.23}$$

where ρ_F and ρ_R are the densities of the fluid and of the solid medium, respectively. If the condition $c_F < c_R$, where c_F is the speed of waves in the fluid and c_R is the speed of the Rayleigh wave, is satisfied, the equation results in a complex root that corresponds to a system of three waves. One wave is found in the fluid while two waves are found in the solid. A complex root for the equation means that the interaction of a Rayleigh wave with a fluid medium causes a loss in energy for the waves. The energy is radiated at a specific angle θ (called Rayleigh angle, see Figure 3.3) into the fluid medium, with respect to the normal direction to the solid surface:

$$sin\,\theta = \frac{c_F}{c_R} \tag{3.24}$$

This energy loss, caused by the interaction with a fluid, attenuates the propagation of the Rayleigh waves. A complete description of the attenuation phenomena related to leaky Rayleigh waves can be found in [98]. The attenuation phenomenon is measured through an attenuation coefficient (used to quantify different media according to how strongly a transmitted ultrasound amplitude decreases). The attenuation coefficient for a leaky Rayleigh wave travelling along a solid–fluid interface is given by:

$$\alpha_L = \frac{\rho_F c_F}{\rho_R c_R \lambda_R} \tag{3.23}$$

where λ_R is the Rayleigh wavelength. The coefficient defines the energy loss resulting from the transmission of a bulk wave into a fluid over a distance *x* as being $e^{-\alpha x}$ [61]. This attenuation coefficient is related to the propagation of compression waves in the fluid, associated to the normal component of the Rayleigh waves. However, there are also frictional losses from the transverse motion of the surface, with an associated attenuation coefficient:

$$\alpha_S = \frac{\left(\rho_F \eta \frac{\omega^2}{2}\right)^{\frac{1}{2}}}{4\pi^2 \rho_R c_R^2} \tag{3.24}$$

where η is the viscosity of the medium and ω is the angular frequency of the leaky Rayleigh wave. The frictional component of actuation is typically smaller compared to the longitudinal contribution [61].

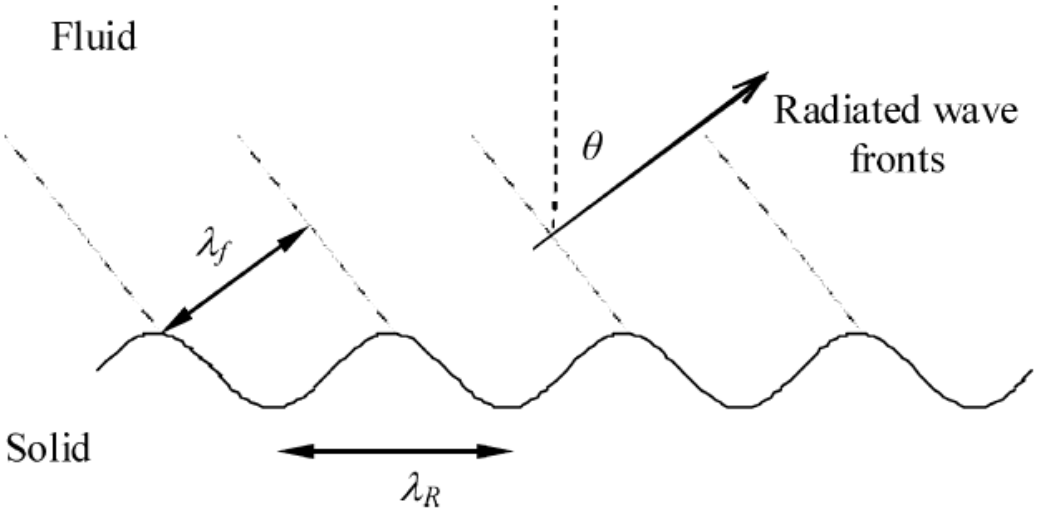

Figure 3.3: A schematic showing a SAW radiating into a fluid [62].

Modelling a SAW-based microfluidic system is important to take into account all these considerations about the kind of waves involved and their behaviour. In Table 4.1, which contains all the material parameters considered to model the materials involved in the numerical analyses performed, the values of the attenuation coefficients applied to PDMS and water are reported. These coefficients can be associated to the materials when modelled as acoustic media, providing the propagation of acoustic pressure waves and the generation of a standing pressure

field. The coefficient is contained in the formulation of the wave (modifying the definition of the wavenumber) to take into account transmission losses in a fluid. Being the microchannel dimensions in the order of few hundreds of micrometres, the attenuation is practically not effective, therefore no relevant effects are generated by modelling the fluids as wave attenuating media.

3.2.3 Piezoelectricity

The description done, has been based on isotropic non-piezoelectric materials. Most materials used for waves generation and propagation in SAW-based devices are piezoelectric. The Rayleigh wave still exist for any given direction of propagation, but the characteristics will differ based on the orientation (due to the anisotropy related to the crystalline material structure). All the three components of the displacement field are involved considering waves propagating in a piezoelectric medium (there are two different transverse modes as well as the longitudinal mode). $LiNbO_3$ (lithium niobate) is often used, and it has a typical Rayleigh wave speed between 3500 m/s and 4000 m/s depending upon orientation [61].

When a piezoelectric material is subjected to a small perturbation caused by a small electric field or mechanical stress, can be assumed to be linear. To model a piezoelectric material, the coupling between solid mechanics and electrostatics is needed. This coupling is explicated in the piezoelectric materials constitutive law:

$$T_{ij} = c_{ijkl}^{E} S_{kl} - e_{kij} E_k \tag{3.25}$$

$$D_i = e_{ijk} S_{jk} + \varepsilon_{ij}^{S} E_j \tag{3.26}$$

where E_k is the electric field, D_i is the electric displacement, ε_{ij} is the permittivity tensor and e_{ijk} is the piezoelectric coupling tensor (third-order tensor) that links the elastic and electric fields and appears in both the formulations to describe the direct and the converse piezoelectric effects. The superscripts E and S indicate respectively that the stiffness tensor (c_{ijkl}^{E}) is defined for a constant electric field in the first equation, and the permittivity tensor is defined for constant strains in the second equation. The electric field can be expressed using a quasi-static approximation:

$$E_i = -\frac{\partial \Phi}{\partial x_i} \tag{3.27}$$

where Φ is the electric potential. The equation of motion can be found:

$$\rho \frac{\partial^2 u_i}{\partial^2 t} = e_{kij} \frac{\partial^2 \Phi}{\partial x_i \partial x_k} + c^E_{ijkl} \frac{\partial^2 u_k}{\partial x_j \partial x_l} \tag{3.28}$$

The electric potential appears in the equation as a source term for the generation of acoustic waves (by applying a time-dependent electric potential on IDTs deposited above the surface of a piezoelectric material).

The converse piezoelectric effect is fundamental for the description of surface acoustic waves-based devices. Therefore, the coupling between solid mechanics and electrostatics has been introduced to report the fundamental equations governing the piezoelectric effect, exploited in the numerical analyses reported in Chapter 4.

3.3 Acoustics

The last contribution to be considered for a complete description of the acoustophoretic problem is acoustics, a branch of physics which deals with the study of mechanical waves in solids, liquids and gases (sound is one topic related to acoustics). In the analysis described in Chapter 4, acoustics is exploited to compute the pressure distribution within the fluid domain caused by the transmission of SAWs from a piezoelectric substrate.

The linear acoustic wave equation can be derived exploiting the first order perturbation theory. The derivation is based on a set of coupled, non-linear partial differential equations: the thermodynamic equation of state expressing the pressure p in terms of the density ρ, the kinematic continuity equation for ρ (equation (3.1)), and the dynamic Navier–Stokes equation for the velocity $\boldsymbol{v}$ (equation (3.3)). The perturbation theory is useful to find an approximated solution because the acoustic wave can be seen as a small perturbation of density, pressure, and velocity fields. An isothermal problem is studied, neglecting all the external fields. Considering a quiescent liquid ($\boldsymbol{v}_0 = 0$), which before the presence of any acoustic wave has

constant density ρ_0 and pressure p_0, the acoustic wave constitutes a small perturbation in the fields of density, pressure, and velocity:

$$\rho = \rho_0 + \rho_1 \tag{3.29}$$

$$p = p_0 + c_F^2 \rho_1 \tag{3.30}$$

$$\boldsymbol{v} = \boldsymbol{v}_1 \tag{3.31}$$

Assuming the harmonic time dependence for all the fields:

$$\rho_1(\boldsymbol{r}, t) = \rho_1(\boldsymbol{r}) e^{-i\omega t} \tag{3.32}$$

$$p_1(\boldsymbol{r}, t) = c_F^2 \rho_1(\boldsymbol{r}) e^{-i\omega t} \tag{3.33}$$

$$\boldsymbol{v}_1(\boldsymbol{r}, t) = \boldsymbol{v}_1(\boldsymbol{r}) e^{-i\omega t} \tag{3.34}$$

The harmonic time dependence is represented by the exponential term, where $\omega = 2\pi f$ with f being the actuation frequency. The real part describes the physical meaning of these fields. The harmonic field is governed by the Helmholtz equation (a time-independent form of the wave equation) for damped waves:

$$\nabla^2 p_1 = -k^2 p_1 \tag{3.35}$$

where k, the complex wavenumber, is defined as:

$$k = (1 + i\Gamma) k_0 = (1 + i\Gamma) \frac{\omega}{c_F} \tag{3.36}$$

$$\Gamma = \frac{(1 + \beta)\eta\omega}{2\rho_0 c_F^2} \tag{3.37}$$

where k_0 is the wavenumber, Γ is the viscous damping factor, η is the dynamic viscosity and β is the viscosity ratio (described in Section 3.1.2).

As the Navier–Stokes equation is non-linear, the first-order fields calculated cannot be considered an accurate solution. A more precise description may be obtained by continuing the mathematical expansion to the second order approximation. Normally, the second-order fields would be negligible compared to the first-order fields. However, if time-average contributions are considered, the first order fields are not useful. In contrast, the time average effect of the product between two first

order fields proportional to cos(ωt) (arising from the complex exponential) is a non-zero value. A complete second-order study can be found in reference [97]. Physically, the non-zero velocity $\langle \mathbf{v}_2 \rangle$, where the angle brackets are used to consider the time average value of the quantity inside them over a full oscillation, represents the acoustic streaming, where the bulk fluid is moving steadily in time due to the absorption of energy and momentum from the acoustic wave, while the non-zero pressure $\langle p_2 \rangle$ gives rise to the acoustic radiation force coming from the scattering of acoustic waves on particles and causing their acoustophoretic motion.

3.3.1 Acoustic radiation force

The acoustic radiation force (ARF) is a phenomenon arising from the interaction of acoustic waves with an obstacle placed along their propagation direction. A small particle, with radius $r \ll \lambda$ (which is the wavelength of the pressure waves), density ρ_p and compressibility κ_p acts as a point-scatterer of acoustic waves, which can be treated by first-order scattering theory [98]. Acoustophoresis, which is the motion of particles induced by acoustic radiation forces, is generated by this scattering phenomenon. The expression of the acoustic radiation force for a small spherical particle in an inviscid fluid is:

$$\boldsymbol{F}^{rad} = \frac{4\pi}{3} r^3 \boldsymbol{\nabla} \left[\frac{1}{2} Re(f_1) \kappa_0 \langle p^2 \rangle - \frac{3}{4} Re(f_2) \rho_0 \langle \boldsymbol{v}^2 \rangle \right] \tag{3.38}$$

where f_1 and f_2 are the monopole and dipole scattering coefficients of the particles, respectively:

$$f_1(\tilde{\kappa}) = 1 - \tilde{\kappa}, \qquad with\ \tilde{\kappa} = 1 - \frac{\kappa_p}{\kappa_0} \tag{3.39}$$

$$f_2(\tilde{\rho}) = \frac{2(\tilde{\rho} - 1)}{2\tilde{\rho} + 1}, \qquad with\ \tilde{\rho} = \frac{\rho_p}{\rho_0} \tag{3.40}$$

with ρ_p and ρ_0 being the density of the particle and of the fluid, respectively, while κ_p and κ_0 stand for the compressibility of the particle and of the fluid, respectively. The scattering theory used to describe the pressure field scattered by particles and to find the formulation of the scattering coefficient is described by Bruus in reference [98]. In first-order scattering theory, f_1 is the coefficient associated to the

monopole scattering potential caused by a stationary sphere in the incoming density wave, while f_2 is the coefficient of the dipole scattering potential caused by an incompressible sphere moving with its velocity in the incoming velocity wave.

An important parameter to be considered when dealing with acoustophoresis is the acoustic contrast factor ϕ, obtained by Bruus [98] computing the acoustic radiation force from the scattering theory:

$$\phi(\tilde{\kappa}, \tilde{\rho}) = \frac{1}{3} f_1(\tilde{\kappa}) + \frac{1}{2} f_2(\tilde{\rho}) = \frac{1}{3}\left(\frac{5\tilde{\rho} - 2}{2\tilde{\rho} + 1}\right) - \tilde{\kappa} \tag{3.41}$$

The acoustic contrast factor can assume positive or negative values depending on the density ratio ($\tilde{\rho}$) and the compressibility ratio ($\tilde{\kappa}$). Particles with positive ϕ move towards the pressure nodes, while particles with negative ϕ concentrate in the pressure antinodes.

The inviscid assumption can be considered a good approximation when $r \ll \delta$, where δ is the size of the boundary layer around the particle, computed as:

$$\delta = \sqrt{\frac{2\eta}{\rho_0 \omega}} \tag{3.42}$$

For the numerical analysis reported in Chapter 4, the size of the boundary layer is smaller with respect to the chosen particle radius (the ratio is 1/50), then the application of this approximation is justified. For distances within a few times δ, large velocity gradients may occur, and viscosity cannot be neglected slightly modifying the force. The f_1 coefficient is unchanged, while the f_2 coefficient is modified:

$$f_2(\tilde{\rho}, \tilde{\delta}) = \frac{2\left[1 - \gamma(\tilde{\delta})\right](\tilde{\rho} - 1)}{2\tilde{\rho} + 1 - 3\gamma(\tilde{\delta})} \tag{3.43}$$

$$\gamma(\tilde{\delta}) = -\frac{3}{2}\left[1 + i(1 + \tilde{\delta})\right]\tilde{\delta}, \qquad with\ \tilde{\delta} = \frac{\delta}{r} \tag{3.44}$$

where $\tilde{\delta}$ is the penetration depth. In the inviscid case, $\tilde{\delta} = 0$, and the equation of f_2 returns as (3.40).

3.3.1.1 Secondary forces

When multiple particles in a suspension are exposed to a standing wave field, they will not only experience the primary acoustic force, but also the secondary forces caused by secondary waves scattered by other particles. The interparticle forces are sometimes called Bjerknes forces and are used to describe the ARF acting on deformable particles (like bubbles) [15]. A simplified expression is:

$$F^{sec} = 4\pi r^6 \left\{ \frac{(\rho_p - \rho_0)^2 (3\,cos^2\,\theta - 1)}{6\rho_0 d^4} v^2(x) - \frac{\omega^2 \rho_0 \left(\kappa_p - \kappa_0\right)^2}{9d^2} p^2(x) \right\} \quad (3.45)$$

where d is the distance between the particles and θ is the angle between the centre line of the particles and the direction of propagation of the incident acoustic wave. A negative value of force means an attractive interparticle force and a positive sign means a repulsive force. The left side of the equation depends on the particle velocity amplitude $v(x)$ and the right side depends on the acoustic pressure amplitude $p(x)$. When particles are concentrated in the direction of the acoustic wave propagation ($\theta = 0°$) the velocity-dependent term is repulsive, and likewise attractive when the particles are perpendicular ($\theta = 90°$) to the incident wave propagation. The pressure-dependent term is not affected by particles orientation at all and is always attractive. The influence of the secondary forces is usually very weak, due to the distance term in the denominator, which means that it is only effective when the interparticle distance is very small [14].

To complete the description of the acoustic radiation forces, also the secondary forces were described in this section, even though they are neglected in the numerical analyses performed. Secondary forces can be implemented in the analyses while simulating deformable particles (the ARFs can modify their shape) and when the interactions between particles produce non-negligible effects.

3.3.2 Acoustic streaming

The second effect generated by the propagation of pressure waves within a fluid is called acoustic streaming. This effect can be regarded as any flow generated by the force arising from the presence of a gradient in the time-averaged acoustic momentum flux in a fluid (a less explicit definition considers the acoustic streaming

as a fluid flow generated by the attenuation of an acoustic wave). The acoustic steaming can be classified in three types of phenomena, related to the scale at which they operate: inner boundary layer streaming, outer boundary layer streaming and Eckart streaming [30].

The boundary layer driven acoustic streaming is induced by the viscous dissipation of acoustic energy into the boundary layer of a fluid along any solid boundary. The dissipation into the boundary layer is large in comparison to bulk dissipation because of the steep velocity gradient, caused by the no-slip boundary condition between solid and fluid, that is formed perpendicularly to the solid boundary as the acoustic wave propagates parallel to it. In the case of a standing wave which is parallel to the surface, the viscous dissipation results in a steady momentum flux. Due to the spatially fixed pressure nodes and antinodes, this results in a steady boundary layer vorticity termed inner boundary layer streaming or "Schlichting streaming". The powerful inner boundary layer streaming flow generates counter rotating streaming vortices within the bulk of the fluid named outer boundary layer streaming or "Rayleigh streaming" [30].

Eckart streaming is the flow formed by the dissipation of acoustic energy into the bulk of a fluid. As an acoustic wave propagates through a fluid, a portion of the acoustic energy is absorbed by the fluid at a rate that is proportional to the square of its frequency. The loss of acoustic energy results in a steady momentum flux, forming a jet of fluid inside the acoustic beam in the direction of acoustic propagation. For the case of a fluid jet formed within the confinement of a microfluidic chamber, vorticity will typically be generated. Eckart streaming will only take place in microfluidics devices when high frequency ultrasound is propagated along a dimension on the order of millimetres [30].

The acoustic streaming effect is usually considered as a limitation dealing with acoustophoresis, because the generation of vortexes within the fluid can deplete the particle manipulation by ARFs. The Eckart streaming could be relevant when exploiting millimetric size channels, as in smaller domains the space is not enough to produce the effect. Nevertheless, the boundary layer acoustic streaming can influence the manipulation of particles being only related to the viscous dissipations

generated by the interaction of the pressure field at the fluid-solid interface of microchannels.

Also the acoustic streaming will not be modelled in the numerical analyses, and this choice is justified in the next chapter.

4 Numerical analyses and experiments

In this chapter, the numerical analyses performed on SSAW-based microfluidic devices are presented. The basic configuration of the device and the properties of the simulated materials are presented in the introduction (Section 4.1). The reference paper [99], due to the results obtained simulating a SSAW-based device two-dimensional cross section, was used as a starting point to take a clue of the numerical process to be adopted to solve this specific problem. The physics interfaces exploited in the software COMSOL Multiphysics, used for the simulations, are described in Section 4.2. Then, in Sections 4.3, 4.4 and 4.5, the analysis and the results are presented and discussed.

A two-dimensional (2D) cross section of the device is investigated, both with frequency and time domain simulations. Some variations have been considered regarding the simulations, comparing to the paper solution [99]: the geometry of the device was slightly changed, and the boundary conditions applied are different to achieve better results and show the dependency of the phenomenon on these features. A sensitivity analysis for the pressure field distribution modifying the geometrical features of the microchannel (width and height of the fluid domain) and the boundary conditions applied to the PDMS structure is presented. After that, a three-dimensional (3D) analysis of the device is described. To further investigate the behaviour of surface acoustic waves on the surface of anisotropic piezoelectric materials, different positions and geometries of the interdigital transducers (IDTs) deposed on the substrate, are presented. Finally, acoustic trapping is simulated within a static squared water “pool” exploiting the interaction of four travelling waves merging where the PDMS structure is positioned. The last section of the chapter describes the fabrication of a simple PDMS microchannel using soft lithography.

4.1 Introduction

A device exploiting standing surface acoustic waves (SSAWs) is considered to study acoustophoresis. A straight microchannel (constituted by a single inlet and a

single outlet), made of PDMS, is bonded to a lithium niobate piezoelectric substrate. Two gold IDTs (as long as the length of the device) are patterned on the surface of the substrate at the opposite sides of the PDMS channel (as in Figure 4.1). Due to the converse piezoelectric effect, strains are generated in the piezoelectric material by applying an electrical AC signal to the electrodes, to develop two traveling surface waves. The constructive interference between the two counter-propagating TSAWs results in a standing acoustic field within the microchannel. Polystyrene (PS) microparticles dispersed in the fluid are exposed to the acoustic field being subjected to the acoustic radiation force moving them towards the pressure nodes. Real device dimensions are in the order of tens of millimetres (to improve handling) but typically the simulations are performed on reduced-scale devices. Usually, this is done to reduce the computational time and memory required by the software to solve a complex multiphysic problem. Also, by reducing the dimensions, the finite element meshing of the model can be refined to avoid mesh-dependent effects influencing the results.

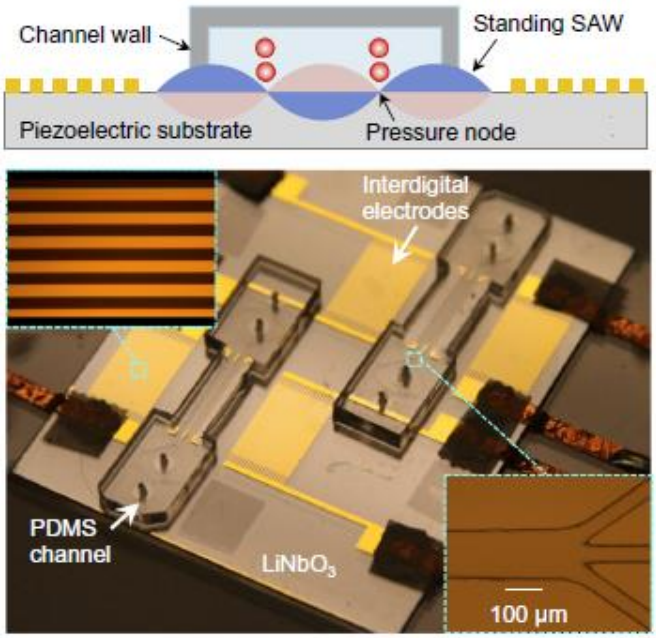

Figure 4.1: (Top) A scheme of the transversal cross section of a SSAW-based device and its working principle. (Bottom) A picture of a real SSAW-based device [99].

As reported by Travagliati et al. [100] also with experimental observations, if the height of the channel is smaller than the SAW wavelength in the fluid, the acoustic radiation force dominates over the acoustic streaming. Moreover, being the channel

height small, the acoustic attenuation is very limited. Because of these observations, acoustic streaming is negligible and not considered in the models. In the numerical analysis presented in this chapter, the height of the channel (25μm, taken from the reference [99], and 50μm, found in Section 4.3.4.5, are the values used in the 2D and 3D analysis respectively) is smaller than the SAW wavelength in the fluid (127μm), and therefore the acoustic streaming is not considered.

To reduce the computational effort and the time required for the analysis, a time-dependent analysis involving all the physics of the problem was not performed. To overcome this issue, it is possible to run an analysis in the frequency domain and consider it as the steady-state solution of harmonic time-dependent fields. First, the acoustic pressure field is computed solving a frequency domain analysis involving piezoelectricity (as combination of solid mechanics and electrostatics interfaces) and solid-acoustic interaction (as interaction between pressure acoustics and solid mechanics interfaces). Then, the velocity and pressure fields related to the fluid flow are computed solving a separate stationary analysis involving only the fluid domain. Finally, the trajectories of the particles are obtained through a time-dependent analysis under the effect of the acoustic radiation force, computed using the solution of the pressure field at the first step, and the fluid drag force, computed using the solution of the velocity field at the second step.

The software COMSOL Multiphysics, used to solve the numerical problems, provides a library of materials which can be selected and associated to the components of every analysis. The properties of the materials taken from this library has been checked and elaborated before being applied to the components in the analysis. Other properties, such as the acoustic attenuation coefficients for the fluids, have been taken from the references reported in Table 4.1, which contains all the material properties considered for the analysis. To calculate the pressure wave speed and the shear wave speed for polystyrene (to be specified in the acoustophoretic radiation force node of COMSOL), the following formulations have been used:

$$c_{p,p} = \sqrt{\frac{K + \frac{4}{3}G}{\rho}} \tag{4.1}$$

$$c_{s,p} = \sqrt{\frac{G}{\rho}} \tag{4.2}$$

where K is the bulk modulus (equal to 3000 MPa), G is the shear modulus (equal to 750MPa) and ρ is the density (reported in Table 4.1).

Lithium Niobate		
Density	ρ_{piezo}	4700 kg/m^3
Elasticity matrix	c_{ij}	Reported in section 4.2.2
Coupling matrix	e_{ij}	Reported in section 4.2.2
Dielectric matrix	ε_{ij}	Reported in section 4.2.2
PDMS		
Density	ρ_{PDMS}	970 kg/m^3
Longitudinal wave speed	c_{PDMs}	1076.5 m/s
Attenuation coefficient[1]	α_{PDMS}	8224 dB/m
Water		
Density	ρ_0	998 kg/m^3
Speed of sound	c_0	1500 m/s
Dynamic viscosity[2]	η	1.002 mPa·s
Bulk viscosity[2]	η_{bulk}	1.67 mPa·s
Attenuation coefficient[1]	α_0	36.64 dB/m
Young's modulus	E_0	750 kPa
Poisson's ratio	ν_0	0.49
Polystyrene (particles)		
Density	ρ_p	1050 kg/m^3
Diameter	d	4 μm, 8 μm
Pressure wave speed[3]	$c_{p,p}$	1952 m/s
Shear wave speed[3]	$c_{s,p}$	845 m/s

Table 4.1: Material properties associated to the components of the model. (1) Values taken from [99]. (2) Values taken from [20]. (3) Calculated values. If not specified, the properties used are taken from the library of COMSOL.

4.2 COMSOL Multiphysics – Physics interfaces

COMSOL Multiphysics [101] is a cross-platform finite-element analysis solver and multiphysics simulation software. It provides several interfaces to model different fields of physics. Moreover, these interfaces can be coupled to model multiphysic problems. In this section, the interfaces used to develop the acoustofluidic problem are described.

4.2.1 Solid mechanics interface

Solid mechanics interface is contained in the structural mechanics product of COMSOL and is selected to model objects with extension in all the directions. It solves the equation of motion for the model. The constitutive model is applied on the solid materials. The provided results are stresses, strains, and displacements.
Within the solid mechanics interface it is possible to associate to each component of the device the type of material to be modelled: to solve the acoustofluidic problem, PDMS is modelled as a linear elastic material, while lithium niobate is a piezoelectric material. To justify the choice of modelling the PDMS as a solid material, in Section 4.3 a comparison is provided between the solutions obtained modelling the PDMS structure as a linear elastic material or as a non-flowing fluid through the pressure acoustic interface (described in Section 4.2.3).

4.2.2 Piezoelectricity interface

The piezoelectricity interface combines the solid mechanics interface, through the piezoelectric material associated, with the electrostatic one. The electrostatic interface can be used to apply the oscillating voltage at the IDTs. It provides the electric field and electric displacements as results. The piezoelectricity interface allows to model the direct and the converse piezoelectric effects (in the acoustofluidic problem studied, it is exploited to generate SAWs).
Piezoelectric materials are sold with different cuts referring to the direction along which the single crystalline ingot of the material is cut. Being anisotropic materials, it is important to choose the right orientation of the crystalline structure to achieve the expected results. For SAW propagation, one typical piezoelectric material used

is the Y cut Z propagating lithium niobate. Considering a rectangular plate made of a piezoelectric material, the first letter stands for the direction of cut, such as the axis normal to the larger surface of the plate. The second letter refers to the direction of the longest dimension of the rectangular plate. Thus, YZ means that Y is the axis normal to the surface, while the Z axis refers to the direction of propagation. The usual convention specifies Z (or x_3 axis) to be the direction normal to the substrate. Then, in the COMSOL materials library the piezoelectric materials are reported with this cut.

The elasticity, coupling and permittivity matrices used to solve the problem are:

$$c_{ij} = \begin{bmatrix} 2.431 & 0.749 & 0.749 & 0 & 0 & 0 \\ 0.749 & 2.029 & 0.529 & 0 & 0.089 & 0 \\ 0.749 & 0.529 & 2.029 & 0 & -0.089 & 0 \\ 0 & 0 & 0 & 0.749 & 0 & 0.089 \\ 0 & 0.089 & -0.089 & 0 & 0.599 & 0 \\ 0 & 0 & 0 & 0.089 & 0 & 0.599 \end{bmatrix} [\cdot 10^{11}\mathrm{Pa}]$$

$$e_{ij} = \begin{bmatrix} 1.309 & 0.194 & 0.194 & 0 & 0 & 0 \\ 0 & 0 & 0 & -2.534 & 0 & 3.695 \\ 0 & -2.538 & 2.538 & 0 & 3.695 & 0 \end{bmatrix} [\mathrm{C/m^2}]$$

$$\varepsilon_{ij} = \begin{bmatrix} 29.16 & 0 & 0 \\ 0 & 43.6 & 0 \\ 0 & 0 & 43.6 \end{bmatrix}$$

The values contained in the matrices were distributed to fit the material to the modelled geometry. In this way, the surface acoustic waves generated can propagate along the *x*-direction. This is valid both for the 2D model and the 3D one.

4.2.3 Pressure acoustic interface

The pressure acoustic interface is used to compute the pressure developed by the propagation of acoustic waves in a fluid domain. This interface presents the

possibility to choose between a frequency domain interface or a time domain one. In the first developed model, both water and PDMS were associated to this interface. The choice to simulate the PDMS as an absorptive non-flowing fluid was justified by the work done by Ni et al. [102]. They compared different descriptions of the PDMS structure of the microchannel to state which effect is caused by simulating PDMS as a solid elastic material. Their numerical simulations clearly show that the presence of shear waves in the solid material generates acoustic streaming effects, mainly near the walls of the channel. In the models studied in this thesis, the acoustic streaming effect is neglected, therefore there should be no reason to simulate the PDMS structure as an elastic solid. However, in Section 4.3, a comparison is provided to see how the results change by modelling PDMS with these two different solutions.

In the frequency domain analysis, the Helmholtz equation is solved for a specific frequency and all the fields vary harmonically. The Helmholtz equation can be written as:

$$\frac{1}{\rho_i^*}\nabla^2 p - \frac{\omega^2 p}{\rho_i c_i^2} = 0 \tag{4.3}$$

where p is the pressure and ρ_i^* is defined as:

$$\rho_i^* = \frac{\rho_i c_i^2}{\omega^2}\left(\frac{\omega}{c_i} - jln(10)\frac{\alpha_i}{20}\right)^2 \tag{4.4}$$

where ρ_i, c_i, ω and j are the density of the fluid, the speed of sound in the fluid, the angular frequency, and the imaginary unit, respectively. The attenuation coefficient is defined as α_i. The two equations are valid for both PDMS and water and the index i is used to state which of the two materials is considered.

The pressure acoustic interface can be selected also to solve time-dependent analysis where the pressure wave equation is solved:

$$\frac{1}{\rho_i c_i^2}\frac{\partial^2 p}{\partial t^2} + \nabla \cdot \left(-\frac{\nabla p}{\rho_i}\right) = 0 \tag{4.5}$$

The interface between the fluid and the piezoelectric material is modelled with an acoustic-structure boundary condition. The mechanical motion of the actuated

piezoelectric substrate induces acoustic waves in the fluid domain. To transfer the acoustic pressure waves an acceleration boundary condition is applied at the interface as:

$$\boldsymbol{n} \cdot \left(-\frac{\nabla p}{\rho_i^*} \right) = a_n \tag{4.6}$$

where $\boldsymbol{n}$ is the unit normal vector to the interface and a_n is the normal acceleration. In COMSOL Multiphysics, pressure acoustics, solid mechanics and electrostatic interfaces are linked by the acoustic-piezoelectric interaction multiphysics interface.

4.2.4 Laminar flow interface

The laminar flow interface is associated to the fluid flowing in the channel. The governing equations of fluid mechanics have already been described in Chapter 3 (Equations (3.1) and (3.3)). The calculation of the Reynolds number, using Equation (3.5), provides a small value ($Re \approx 0.01$), meaning that the fluid can be considered as flowing in a laminar regime. The fluid is modelled as Newtonian and compressible in the analysis. This interface provides as result the velocity and pressure fields of a fluid flowing in a laminar regime. The velocity field is used to compute the drag force acting on particles through the particle tracing interface.

4.2.5 Particle tracing interface

The particle tracing interface for fluid flow is used to model the presence of particles in a fluid medium. Discrete particles and the continuous fluid phase wherein particles are dispersed are the two phases considered by the interface. This type of interface models diluted or dispersed flow but not dense suspensions.

In the sparse flow model, the two-way coupling is not considered: the continuous phase affects the motion of particles but not the contrary. The models presented in the following sections are computed considering this solution. The influence of the fluid on particles is governed by the second law of Newton:

$$m_p \frac{d}{dt}\left(\frac{d\boldsymbol{q}}{dt} \right) = \boldsymbol{F} \tag{4.7}$$

where $\boldsymbol{q}$ is the position of the particles, m_p is the particle mass and $\boldsymbol{F}$ is the term related to the forces acting on the particles. In the models presented, the forces acting on the particles are the acoustic radiation force (presented in Section 3.3.1) and the drag force (Equation (3.7)).

The compressibility of the fluid (κ_0) and of the particles (κ_p), which were not defined in Section 3.3.1 when the acoustic radiation force was presented, are computed as:

$$\kappa_0 = \frac{1}{\rho_0 c_0^2} \tag{4.8}$$

$$\kappa_p = \frac{1}{\rho_p \left(c_{p,p}^2 - \frac{4}{3} c_{s,p}^2 \right)} \tag{4.9}$$

where ρ_0 and ρ_p are the density of the fluid and of the particles, respectively. $c_{p,p}$ is the pressure wave speed of the particles while $c_{s,p}$ is the shear wave speed of the particles.

Being the size of the boundary layer ($\delta \approx 0.17\mu m$) negligible with respect to the radius of the particles (4 or 2μm), the viscous correction presented in Section 3.3.1 are not applied in the analysis.

The gravitational and the buoyant force (upward force exerted by a fluid that opposes the weight of an immersed body) are of the same magnitude and in opposite directions, so they equilibrate and are not considered in the models [81].

Finally, the interactions between particles are not considered. The particles can move everywhere in the fluid domain and also overlap without collisions.

4.3 Two-dimensional cross-section analyses

A two-dimensional cross-section of the device is simulated. The analysis can be considered as a starting point to understand and to manage the acoustophoretic problem from a 2D view. A frequency domain analysis is performed to find the acoustic pressure distribution in the fluid domain. Then, a time dependent analysis is carried out on the particles to investigate the action of the acoustic forces on them. In 2D analysis, the laminar flow interface is not needed because there is no flowing

fluid. The frequency domain analysis provides the results as steady-state solutions. To see the development of the acoustic field within the fluid domain and the propagation of the Rayleigh waves on the piezoelectric substrate, a time-dependent analysis is done

In the two-dimensional analysis performed, the PDMS channel has been modelled both as a non-flowing fluid and as a linear elastic solid. A comparison between the behaviours of the material and the interaction with the fluid domain is proposed in the results. Moreover, a sensitivity analysis changing the geometrical features of the channel (width and height) and the boundary conditions applied to the PDMS is done.

4.3.1 Geometry

The system (showed in Figure 4.2) is composed by a piezoelectric substrate (made of lithium niobate), a PDMS channel filled with water and two IDTs composed by 5 pairs of gold electrodes placed at the opposite sides of the channel. The properties of the used materials are reported in Table 4.1.

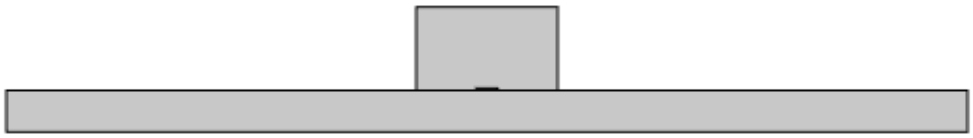

Figure 4.2: Two-dimensional cross-section of the system considered for the analysis.

In Table 4.2, the geometrical dimensions of the components are reported. Considering the analysis involving the simulation of the PDMS as an elastic solid, the height of the PDMS is reduced to investigate the effects of the boundary conditions. The distance between the first finger and the centre of the channel is 4270μm and is chosen to obtain a pressure node in the centre of the channel. Each electrode has a width of 70μm and the spacing between two successive electrodes is 70μm. With these measures, the pitch of the IDTs, which corresponds to the wavelength of the surface acoustic waves, is equal to 280μm.

	Lithium niobate	PDMS	Fluid channel
Width	11340μm	1650μm	280μm
Height	500μm	1000μm	25μm

Table 4.2: Geometrical dimensions of the components of the system.

The electrodes composing the IDTs are simply modelled as segments placed on the upper boundary of the piezoelectric substrate as shown in Figure 4.3.

Figure 4.3: Focus on the left-side IDT. The fingers are simulated as segments placed on the top boundary of the piezoelectric substrate.

4.3.2 Mesh

The mesh is made of triangular elements to generate an unstructured mesh. The maximum size of the elements composing the domains is 35μm (which is equal to $\frac{\lambda}{8}$) for the piezoelectric substrate, 8.75μm (corresponding to $\frac{\lambda}{32}$) for the PDMS structure and 4.375μm (which is equal to $\frac{\lambda}{64}$) for the fluid domain. The size of the elements was chosen to be a fraction of the wavelength to obtain results not influenced by the mesh (mesh-independent results).

4.3.3 Boundary conditions

4.3.3.1 Solid mechanics interface

The low-reflecting boundary condition was applied at the two lateral sides and at the bottom boundary of the piezoelectric substrate. This condition lets the waves move away from the model without reflections. As a default, it takes material data from the domain to create a perfect impedance match for pressure waves.

The low-reflecting boundary condition was chosen to avoid the generation of interferences between reflected and propagating waves. These interferences can spoil the solutions. This condition is justified also in real experiments where absorbing materials are placed laterally to the IDTs to avoid this kind of interferences between waves.

The top boundary of the piezoelectric substrate, not in contact with PDMS and the fluid, is stress free:

$$\boldsymbol{T} \cdot \boldsymbol{n} = 0 \tag{4.10}$$

where $\boldsymbol{n}$ is the normal unit vector.

The analysis done modelling the PDMS as a solid material was performed applying different boundary conditions on the top boundary of the PDMS. The conditions used are free boundary, fixed constraint, and low-reflecting boundary. The fixed constraint node adds a condition that makes the boundary completely fixed where the displacements are zero in all the directions.

4.3.3.2 Pressure acoustics interface

In the analysis considering PDMS as a non-flowing fluid, the default boundary condition of the interface is chosen for the external boundaries of the PDMS structure (not for the boundaries in contact with the substrate). This condition is called sound hard boundary condition which states that the normal fluid velocity at the wall is zero. This condition is used for a liquid that is interfacing with an infinitely hard wall and it is expressed as:

$$\boldsymbol{n} \cdot \left(-\frac{\nabla p}{\rho_i^*} \right) = 0 \tag{4.11}$$

ρ_i^* is defined in the Equation (4.4).

At the interface between the PDMS and the fluid domain, a continuity condition is applied between the acoustic pressure and its gradient that defines the acoustic velocity. The interface between the fluids and the substrate is modelled with an acoustic-structure boundary condition defined in the Equation (4.6).

In the case of solid PDMS, no conditions of the pressure acoustics interface are applied because all the boundaries are in touch with solids (piezoelectric substrate and PDMS) providing the application of the acoustic-solid boundary condition at all the boundaries of the fluid domain.

4.3.3.3 Electrostatics interface

The conditions of the electrostatics interface are associated to the fingers of the IDTs to apply the external electrical input to the piezoelectric material and generate mechanical strains through the converse piezoelectric effect. The fingers are alternatively charged and grounded (zero voltage applied) to provide a voltage difference. The electric voltage, applied on the blue fingers in Figure 4.2, is:

$$V = V_0 e^{i\omega t} \tag{4.12}$$

with $V_0 = 8V$. The harmonic dependence (given by the imaginary exponential term) is automatically added by COMSOL in a frequency domain analysis, while must be entirely specified in time domain analysis.

4.3.3.4 Particle tracing interface

Spherical polystyrene particles, with 8μm diameter, are released in the channel cross-section. The particles are released from a grid though a command provided by the interface. When $t = 0s$, the particles are released in their initial defined positions, then they start moving under the effect of the acoustophoretic radiation force (computed by this interface exploiting the pressure field previously computed). The time simulated is of 0.1s, enough for the particles to be displaced. On the walls of the channel, the condition applied is a freeze condition. It means that when a particle hits the walls, it remains attached to the boundary in the first touch position. This condition records the velocity of the particles in the time instant when they touch the walls and remain immobilized.

4.3.4 Analyses and results

4.3.4.1 Frequency domain analysis – Non-flowing fluid PDMS

A frequency domain analysis is performed between 11.5MHz and 12MHz searching for the frequency of actuation of the piezoelectric substrate. This range of frequencies was selected solving the Equation (3.19) and through the velocity of the Rayleigh waves computed, the frequency found was $f = 11.782\text{MHz}$. This value was obtained by assuming the approximation of an isotropic material. The value found from the analysis, corresponding to a precise and symmetric pattern for the pressure field in the fluid domain and the highest value for the pressure magnitude, is $f = 11.685\text{MHz}$.

The acoustic pressure plot, for the model considering the PDMS as a non-flowing fluid, is shown in Figure 4.4. The pressure field is precise and symmetric with a pressure node in the middle of the width of the channel. The magnitude of the acoustic pressure ranges between -0.6MPa and 0.6MPa (as can be seen from the colour legend in Figure 4.4).

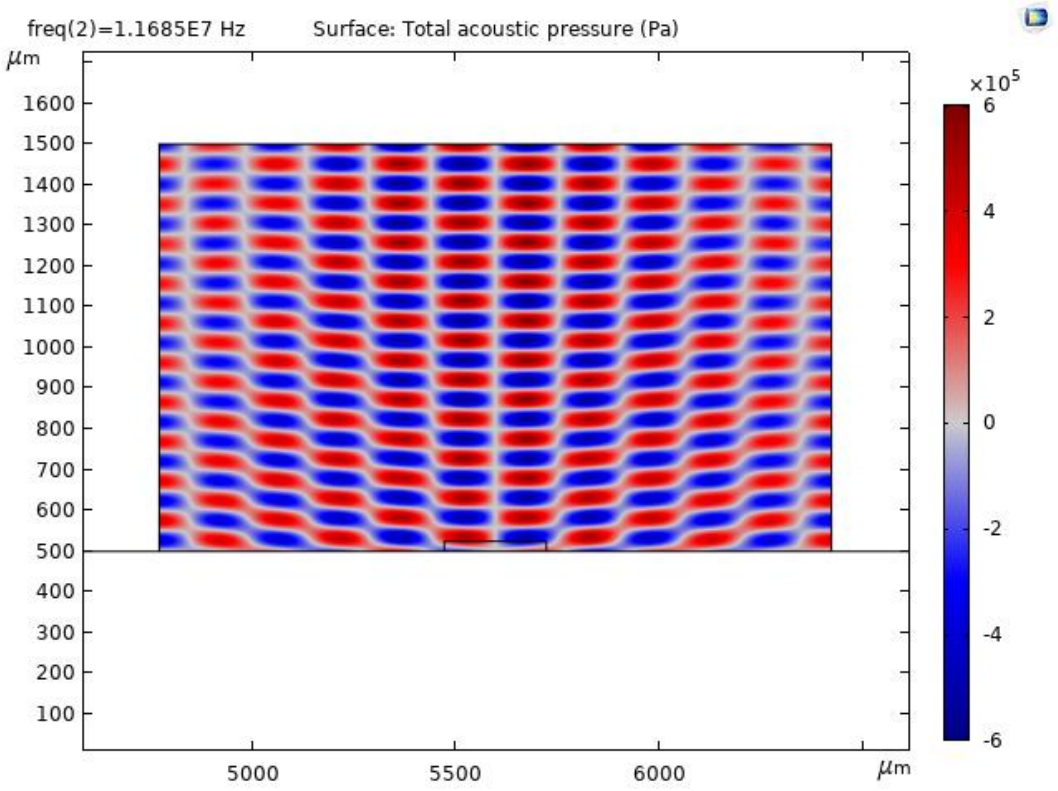

Figure 4.4: Acoustic pressure in the PDMS and fluid domain (non-flowing fluid PDMS).

Figure 4.5 shows a focus on the acoustic pressure distribution in the fluid channel. Also, the total sound pressure level is reported, clearly showing the presence of the pressure nodes. As expected, a pressure node is present in the middle of the channel. A horizontal pressure node (slightly tilted) can also be seen. Particles are expected to move towards these regions: the central vertical node and the horizontal ones.

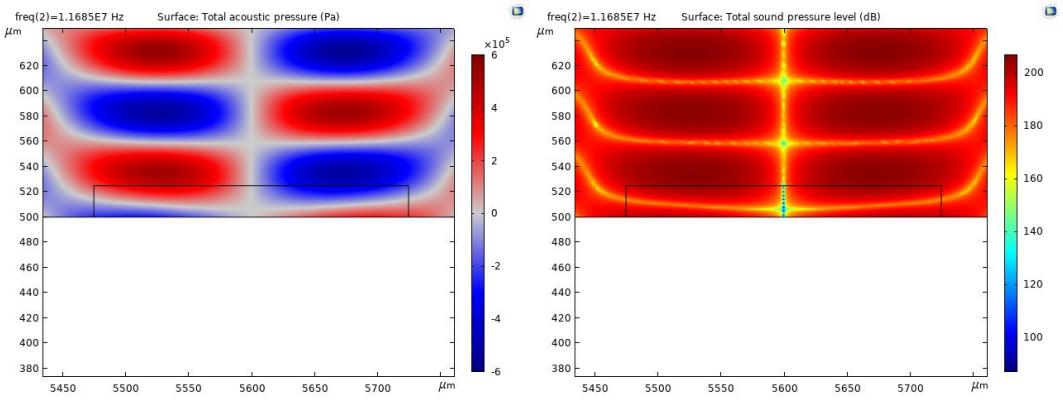

Figure 4.5: (Left) Focus on the acoustic pressure distribution. (Right) The total sound pressure level.

The displacements in the *y*-direction for the surface of the piezoelectric substrate are plotted in Figure 4.6. The surface waves can be seen in a steady-state condition. The maximum displacements obtained are in the order of 5nm.

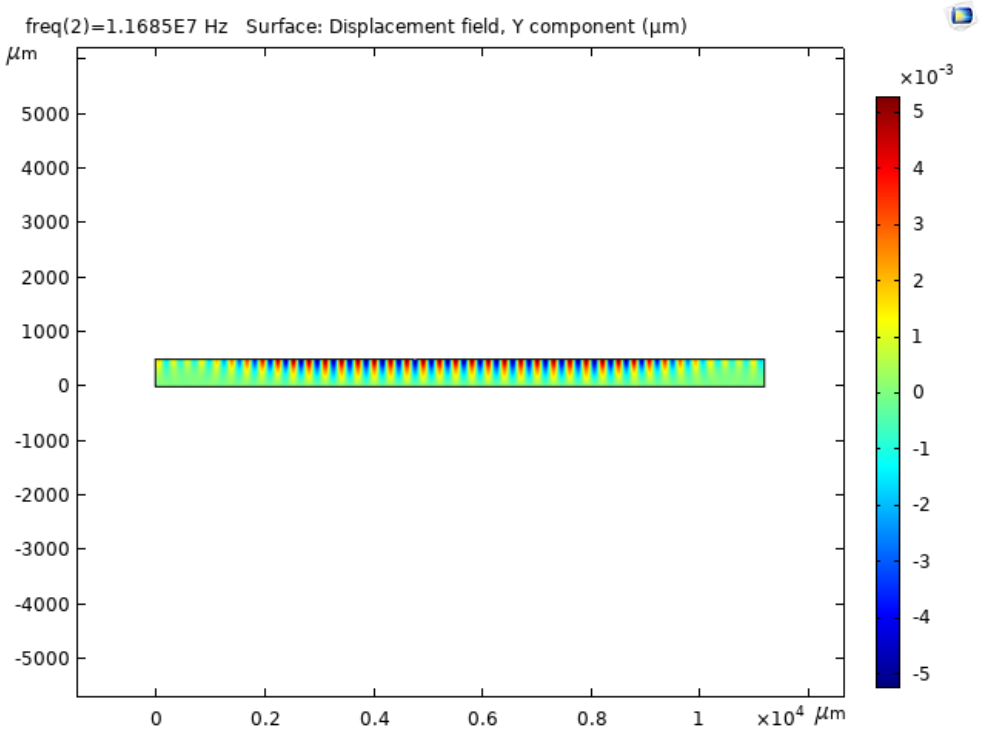

Figure 4.6: Y-displacements of the piezoelectric substrate.

A zoom showing the shape of the Rayleigh waves developed on the surface of the piezoelectric material is reported in Figure 4.7.

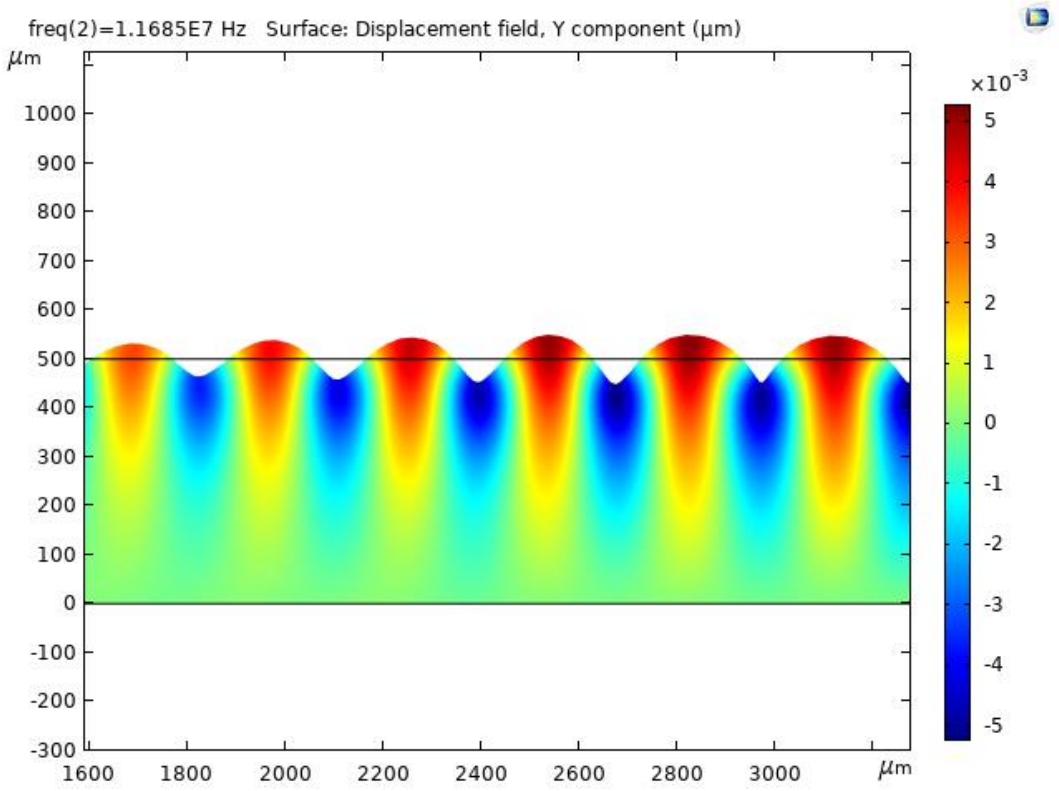

Figure 4.7: Zoom on the shape of the Rayleigh waves.

All the results obtained until this point were expected and are good compared to reference [99]. The standing waves are generated both on the surface of the piezoelectric substrate and within the PDMS microchannel with a precise and symmetric distribution. The magnitude of the pressure and the z-displacements are in the order of the one achieved in the reference paper.

Twenty particles are released from two horizontal rows in the cross-section of the channel. The trajectories of the particles after 0.5s are shown in Figure 4.8. As can be seen, the particles are moved towards the pressure nodes. The particles which started from the central position of the channel are moved up or down staying in the mid-width of the channel. Due to the distribution of pressure found, the other particles cannot be focused on the central vertical node, but a trapping effect is obtained in the two horizontal nodes. This effect can be recognised by the dense presence of trajectory lines in these two symmetric regions, meaning that the

particles continuously move along the nodes never escaping. The values reported in the lateral colour legend are the velocities of the particles in the *x*-direction in m/s and then the maximum velocity obtained is of 4mm/s (negative values are associated to the particles moving towards the negative values of the *x*-coordinate).

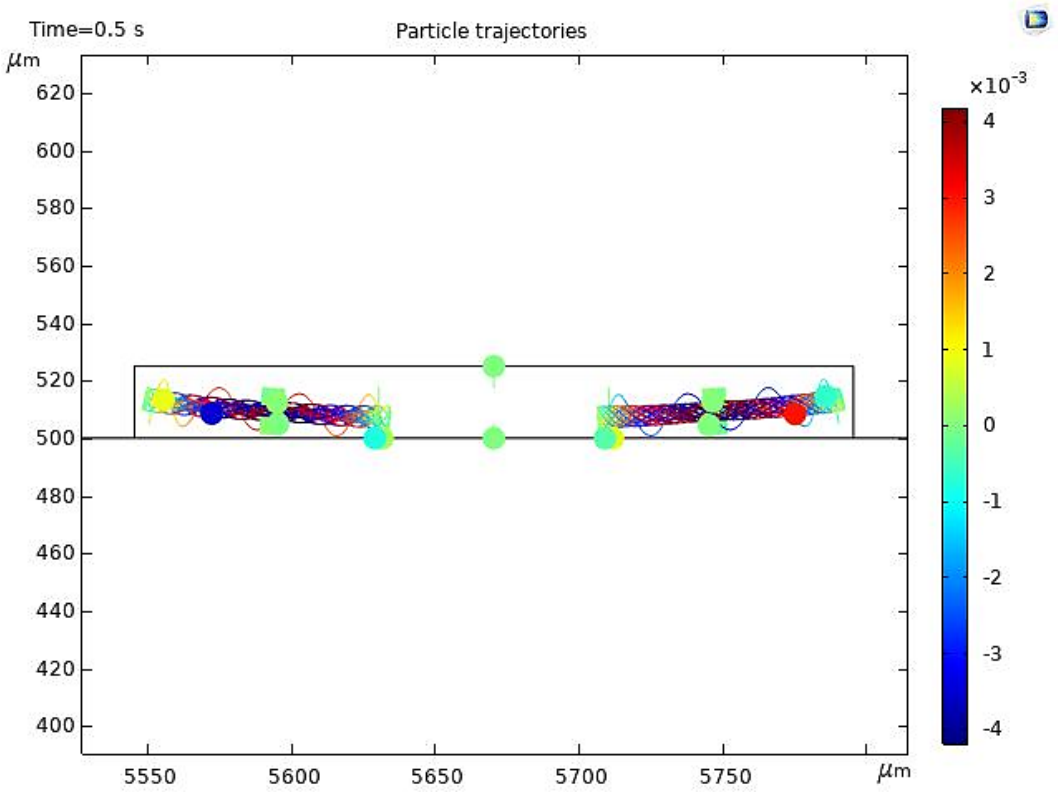

Figure 4.8: Particles trajectories and positions after 0.5s (non-flowing fluid PDMS).

4.3.4.2 Frequency domain analysis – Solid elastic PDMS

To investigate the difference of modelling the PDMS channel as an elastic solid material instead as a non-flowing fluid, the same frequency domain analysis, as the one of the previous section, was performed. In this way, the effect of the propagation of shear waves in the PDMS on the pressure field distribution into the fluid can be investigated. Again, the frequency which provides the best results is $f = 11.685\text{MHz}$. The low-reflecting boundary condition was associated to the upper boundary of the PDMS structure; therefore the height was reduced, being the waves completely transmitted and not reflected.

The pressure field obtained inside the fluid channel is reported in Figure 4.9. The presence of a central pressure node can be clearly seen, stating that the pressure pattern development is not influenced by the difference of the two models. The horizontal nodes seen in Figure 4.6 are not obtained in the second simulation. The magnitude of the acoustic pressure ranges between -0.127MPa and 0.119MPa, lower values compared with the previous results. This result can be associated to the model simulating the solid material: in this case the continuity condition between the two acoustic media (PDMS and fluid) is not set, being the two materials of a different type.

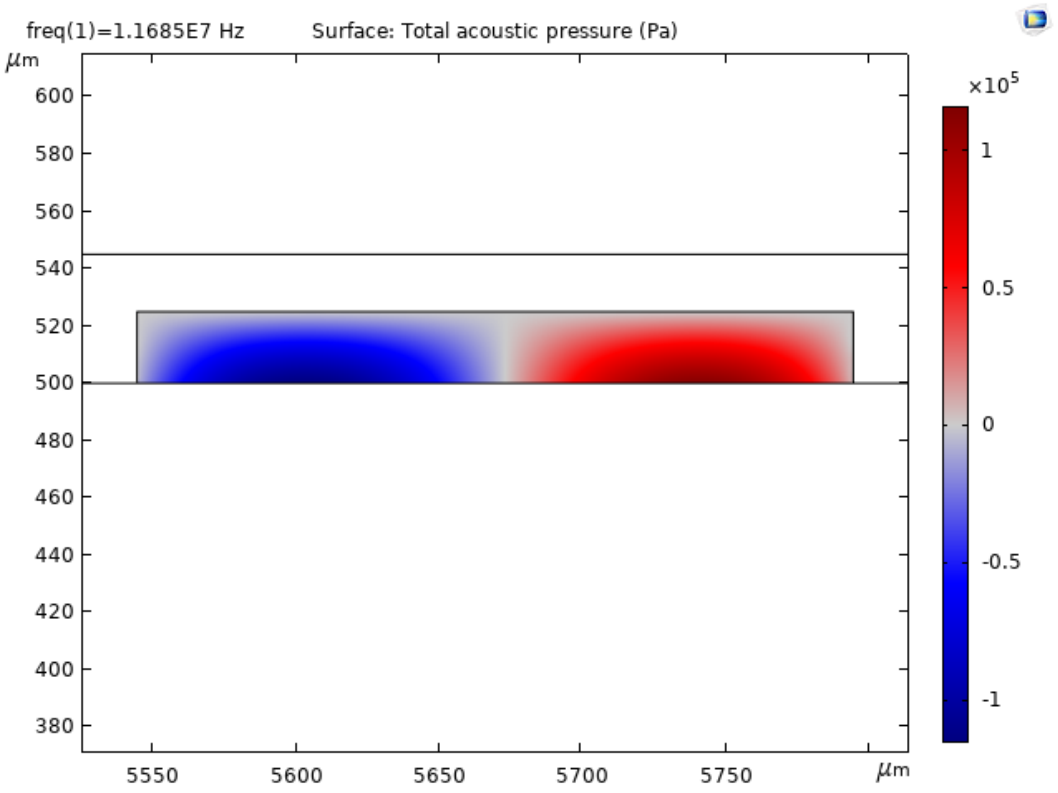

Figure 4.9: Acoustic pressure field in the fluid domain (solid PDMS).

A horizontal row of twenty-five particles is released. The trajectories of the particles are reported in Figure 4.10. The colour legend reports the *x*-component of the velocity of the particles after 0.1s. The particles are moved by the acoustic force following the dome shape of the pressure seen in Figure 4.9. Being the freeze boundary condition applied, when the particles come in contact with the walls, they are stopped in a fixed position and cannot move anymore. Thinking about the

possibility of extending their motion in time, while in contact with the walls, the particles can be moved by the acoustic force towards the pressure nodes. This phenomenon is difficult to be reproduced using COMSOL. The unique boundary condition which can be used to simulate this effect is the bouncing boundary condition which conservates the kinetic energy of the particles when touching the walls. Through this condition, the reflection of particles from the walls is too large in comparison with reality. Also, particles are supposed to transfer part of their energy by bumping the walls of the channel. For these reasons, the condition is not applied.

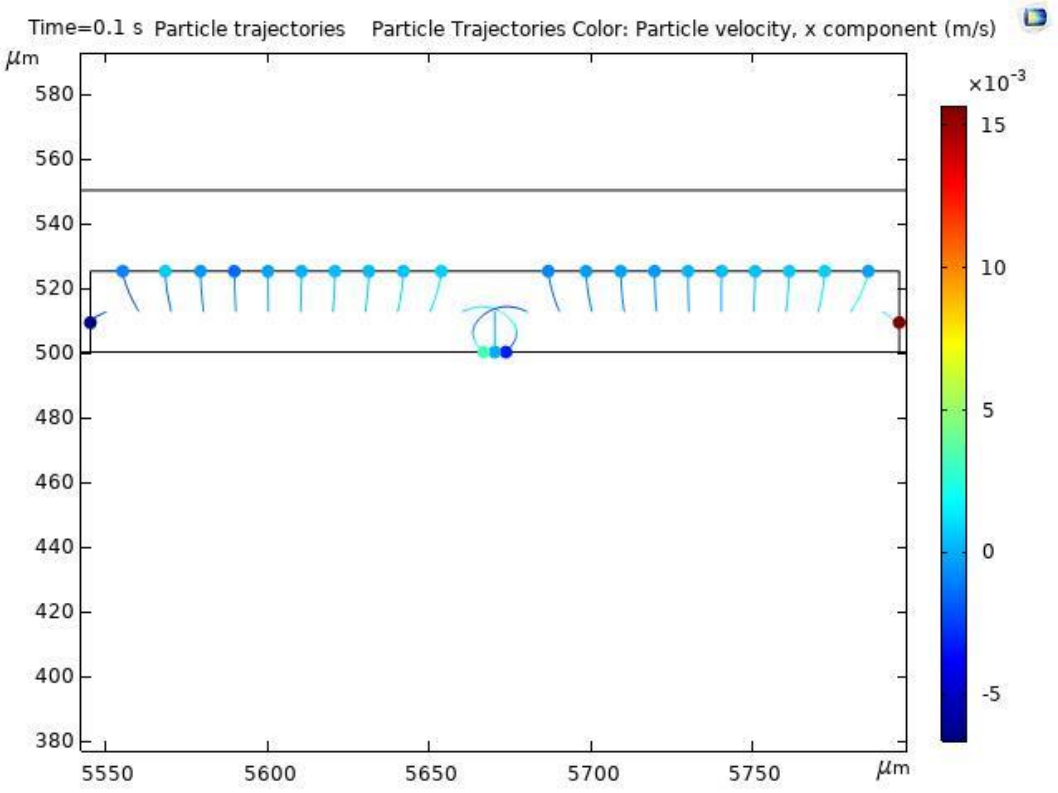

Figure 4.10: Particles trajectories and positions after 0.1s (solid PDMS).

At this point of the work, being the pattern of the pressure field more precise and not presenting the horizontal pressure nodes, the model with the solid elastic PDMS is chosen to be used for further investigations.

The frequency domain analysis provides results as steady-state condition of the problem. To simulate a phase shift of the electrical signal applied at the IDTs, the fluid domain and the PDMS channel are displaced with a parametric study

(changing the value of one geometrical parameter) simulating a delay between the waves. The displacements considered are sub-multiples of the wavelength $\left(\frac{\lambda}{4}, \frac{\lambda}{2}, \lambda\right)$ of the surface waves to correlate the displacement to a phase shift of the signal. The position of the pressure node is modified (see Figure 4.11): this effect can be used to switch the streamline of the particles during an experiment simply by changing the phase associated to the harmonic signal applied at the IDTs. From the results can be seen that the wavelength supposed to be obtained (280μm) is slightly different from the one of the simulations (around 300μm, confirmed in Section 4.3.4.5 by modifying the width of the channel), because displacing the system by λ, the central position of the node is not recovered.

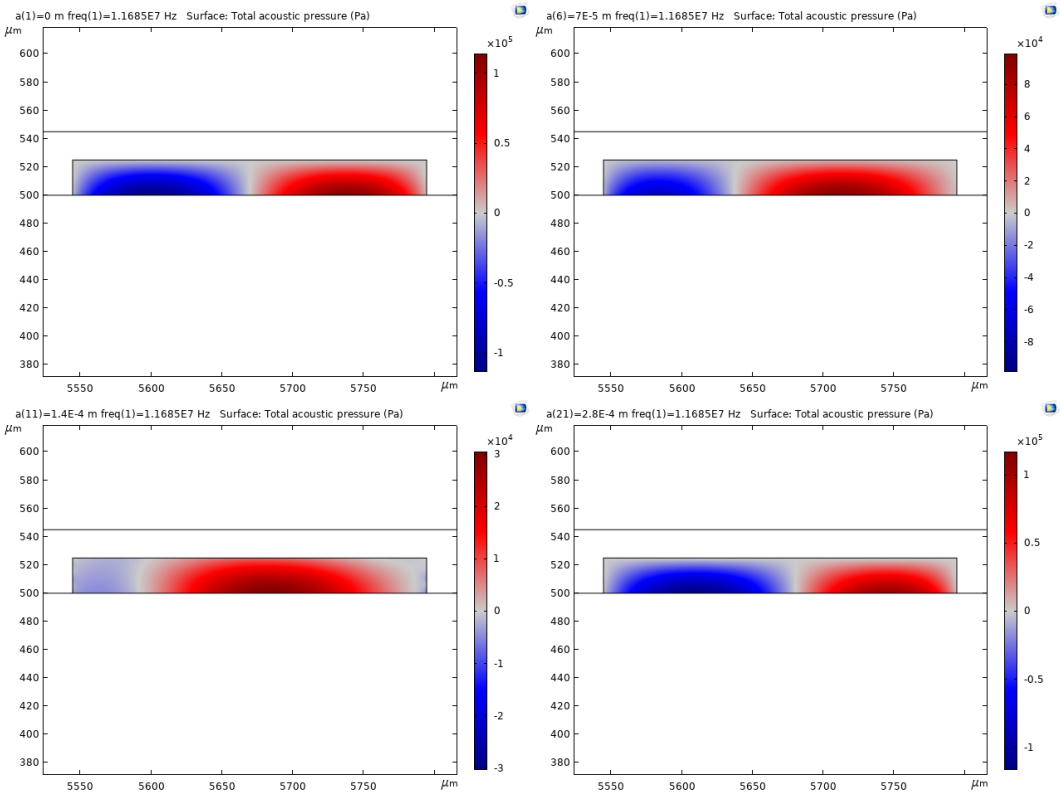

Figure 4.11: Effect of channel displacement to the pressure field. (Top-left) 0,(Top-right) 70,(Bottom-left) 140, (Bottom-right) 280μm displacements, respectively.

4.3.4.3 Time domain analysis

A time domain analysis is performed to see the generation and the development of the surface waves on the piezoelectric substrate and the pressure field inside the fluid domain. The setup is the same used for the frequency domain analysis (same

interfaces and boundary conditions). The voltage is applied, through the electrostatics interface, with a sinusoidal function of the time:

$$V = V_0 \sin(\omega t) \tag{4.13}$$

where $V_0 = 8V$, $\omega = 2\pi f$ and f is the actuation frequency (the same found in the frequency domain analysis). The time-step is chosen considering the frequency of actuation $\left(\Delta t = {}^{1}/_{2f}\right)$ to simulate each step as half of one period of actuation. With this time-step it is possible to see the generation and propagation of the surface waves on the substrate at each actuation step (Figure 4.12). The total simulated time is 10μs.

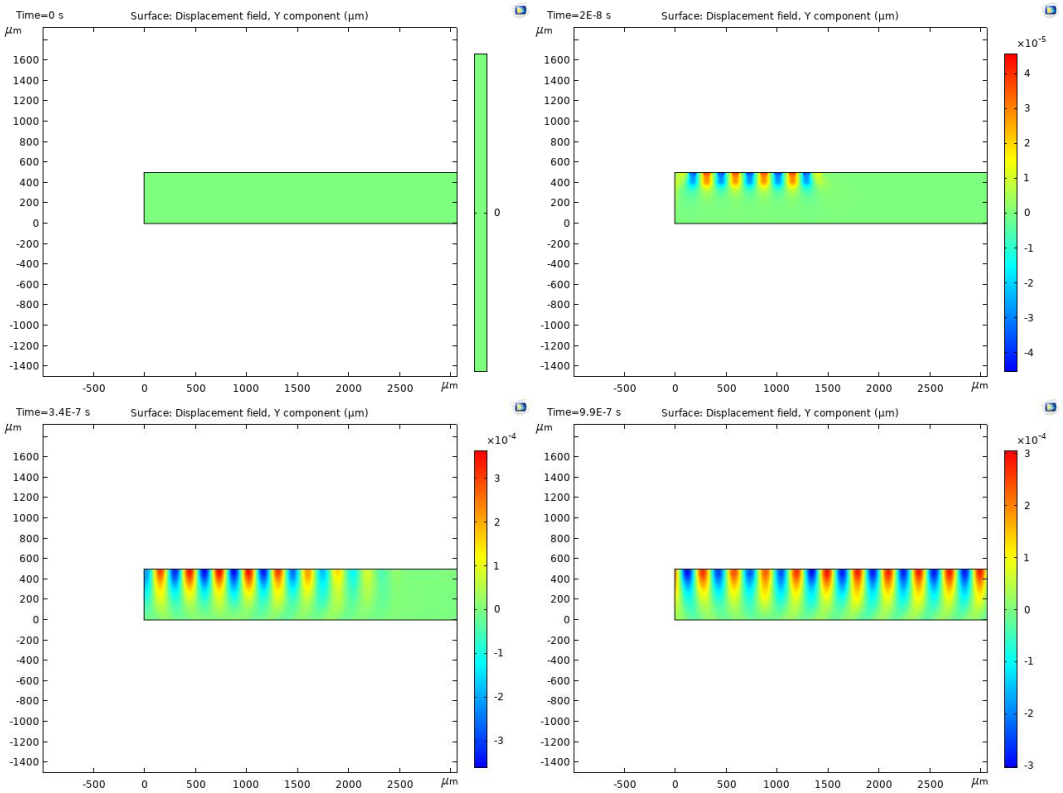

Figure 4.12: Generation and propagation of the surface waves generated by the left-side IDT. The time simulated in the bottom-right Y-displacement plot is 0.99μs.

In figure 4.13 the formation of the pressure field inside the fluid domain is reported. Successive time-steps are plotted to investigate the way in which the pressure field is developing as long as the surface waves come in contact with the channel. In the first image (top-left), the effect of the initial vibration of the piezoelectric substrate is plotted. In the top-right image, the propagation of the waves inside the fluid with

a tilted direction can be seen. This effect can be associated to the leaky-waves phenomenon for which the transmission of the waves from the substrate into the fluid happens with the formation of an angle between the vertical and the propagation directions (the Rayleigh angle, see Section 3.2.2). Then, the pressure field transforms ending up in the final symmetric patter with the central pressure node seen in the frequency-domain results.

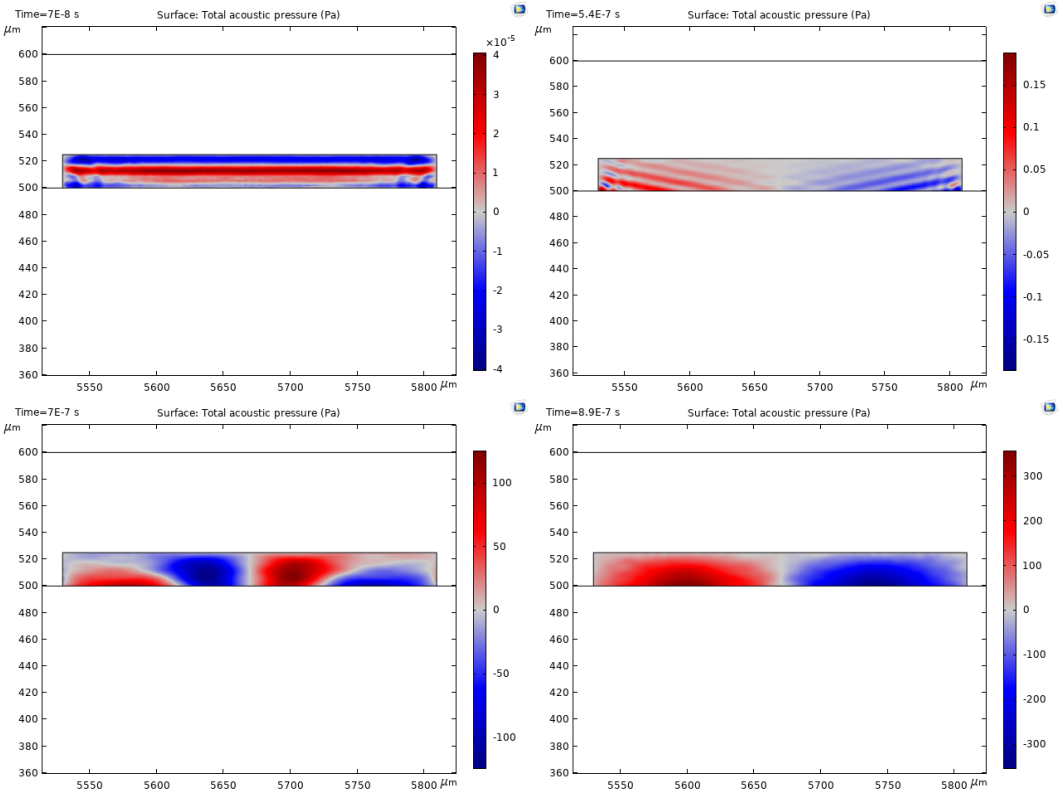

Figure 4.13: Pressure field development in the fluid domain.

At the time-step $t = 1\mu s$, the magnitude of the pressure found in the frequency domain analysis (0.12MPa) is obtained, then the steady state is achieved.

4.3.4.4 Pressure field sensitivity – PDMS boundary conditions

The sensitivity of the pressure field inside the fluid domain is investigated by changing the boundary conditions applied to the upper surface of the PDMS structure of the channel. The three conditions applied are the low-reflecting one, the free surface condition and the fixed constraint. Also, a simulation was performed without the PDMS, only modelling the fluid domain. In this analysis, the

importance of having the PDMS structure to develop a precise pattern for the pressure can be seen. The results are plotted in Figure 4.14.

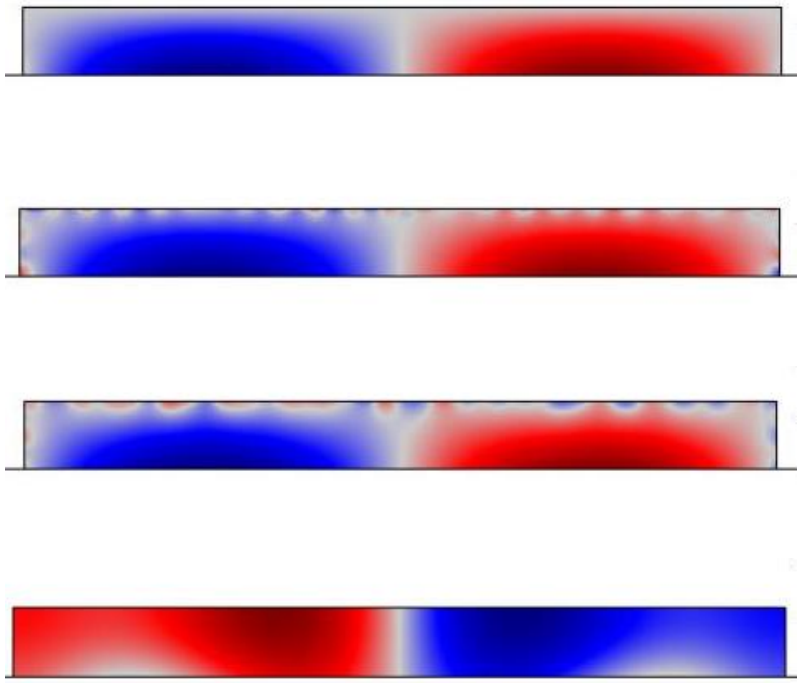

Figure 4.14: Comparison of the pressure field considering different boundary conditions for the upper boundary of the PDMS. Starting from the top: low-reflecting, free and fixed conditions. The field on the bottom is obtained without PDMS.

The first plot of Figure 4.14 is related to the use of the low-reflecting boundary condition which grants the transmission of all the waves through the boundaries where it is applied. It can be considered the same condition as having a thick PDMS structure, in a way in which the effect of the upper boundary of the PDMS on the fluid channel is neglected. As can be seen, the pressure field is precise and symmetric. This condition is the best to avoid the presence of any kind of disturbance in the solutions. It will be used also in the three-dimensional simulations of the device (Section 4.4). In both the cases of free surface and fixed boundary conditions, some disturbances appear in the solutions. This effect is generated because there is no transmission of the waves as in the first case (see Figure 4.15). In the second case (free surface), the surface is free to vibrate due to the propagation of the waves, therefore the waves are not controlled by a specific condition letting them to freely move and interact with the fluid. In the third case

(fixed boundary), the surface is fixed without the possibility to move in all the directions, then the waves can be reflected towards the channel and generate interferences with the pressure field. In Figure 4.15, the vertical displacements in the PDMS domain are reported considering the three boundary conditions applied for the time domain analysis. The simulated time is 60μs for the analysis of the low-reflecting boundary condition and the fixed boundary to see the propagation of the waves. In the analysis with the free surface condition applied, the simulated time was of 10μs to see the free propagation of the waves within the PDMS.

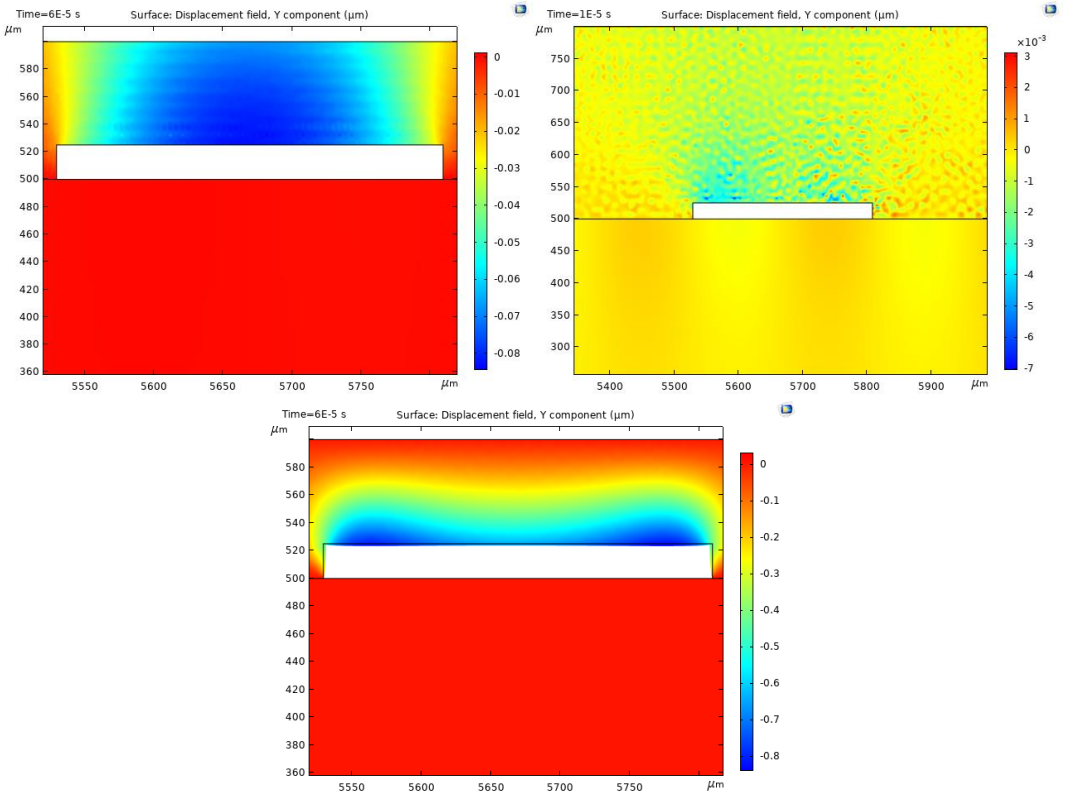

Figure 4.15: Y-displacement near the fluid domain considering different boundary conditions for the upper boundary of the PDMS. On top-left low-reflecting boundary (at 60μs), on top-right free surface (at 10μs), on the bottom fixed boundary (at 60μs).

4.3.4.5 Pressure field sensitivity – Geometrical features change

The sensitivity of the pressure field inside the fluid domain is also investigated by changing the geometrical features (width and height) of the channel. A parametric sweep was performed: the width ranges between 250μm and 400μm with steps of 5μm, while the height ranges between 25μm and 70μm with steps of 1μm. With this analysis, relevant modifications of the pressure field can be detected. The results

associated to the change in width are plotted in Figure 4.16. The pressure distribution is always symmetric with a pressure node in the mid-width. Up to 300μm, the pressure field shows the same distribution seen in the previous solutions. Above 300μm, two lateral nodes start to appear and can be clearly seen in the bottom-right plot of Figure 4.16, where the channel is 400μm wide. These results state that to obtain a single pressure node within the channel, the width should be selected as lower, at least equal, than the wavelength of the surface waves generated on the substrate. If three pressure nodes are needed, the width of the channel can be simply designed to be greater than the wavelength. In all the results, the pressure magnitude is not modified.

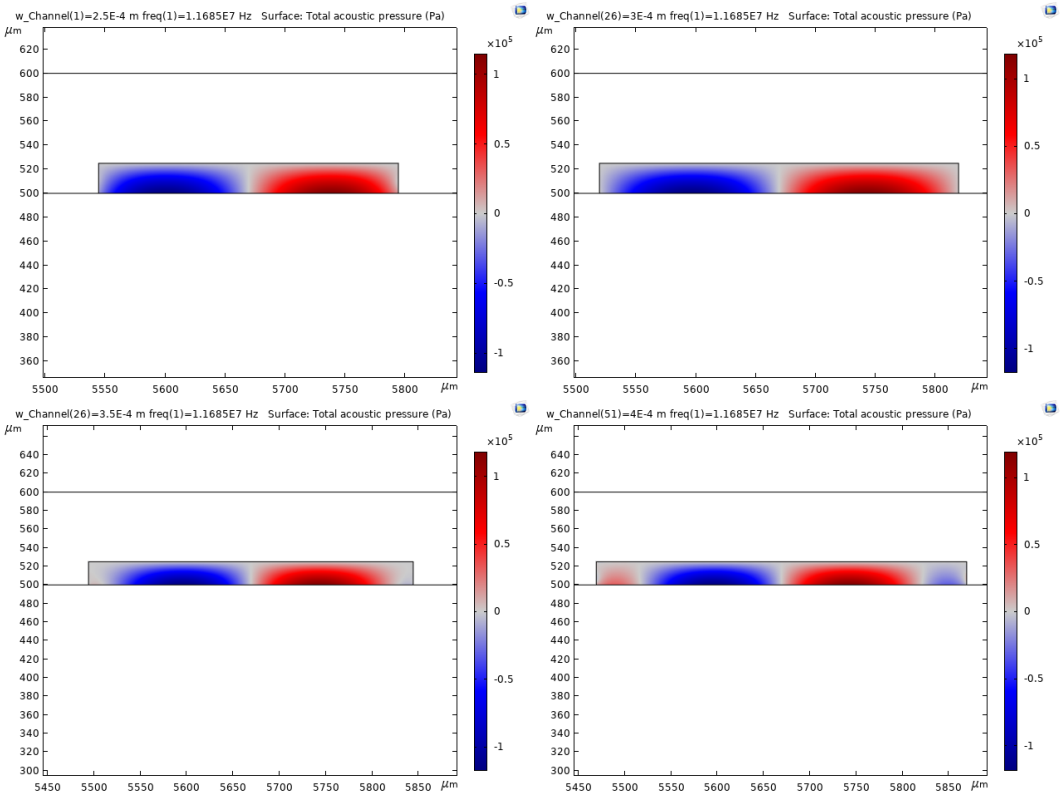

Figure 4.16: Width sweep for sensitivity analysis. On top-left the width is 25μm, on top-right 300μm, on bottom-left 350μm, on bottom-right 400μm.

The results associated to the change in height are plotted in Figure 4.17. The pressure field is symmetric with a central vertical node in all the results. In this case, by increasing the height of the channel, also the wavelength of the pressure waves within the fluid must be considered. Therefore, there should be a limit to the height to obtain the solution with the central node and the two antinodes (Figure 4.9). As

can be seen from the solutions, the distribution is stable up to 50μm. Above this value, the field is changing with the development of other lobes in the bottom corners of the channel, behaviour which can be associated to the formation of the pressure distribution through a tilted transmission with respect to the vertical direction (Rayleigh angle).

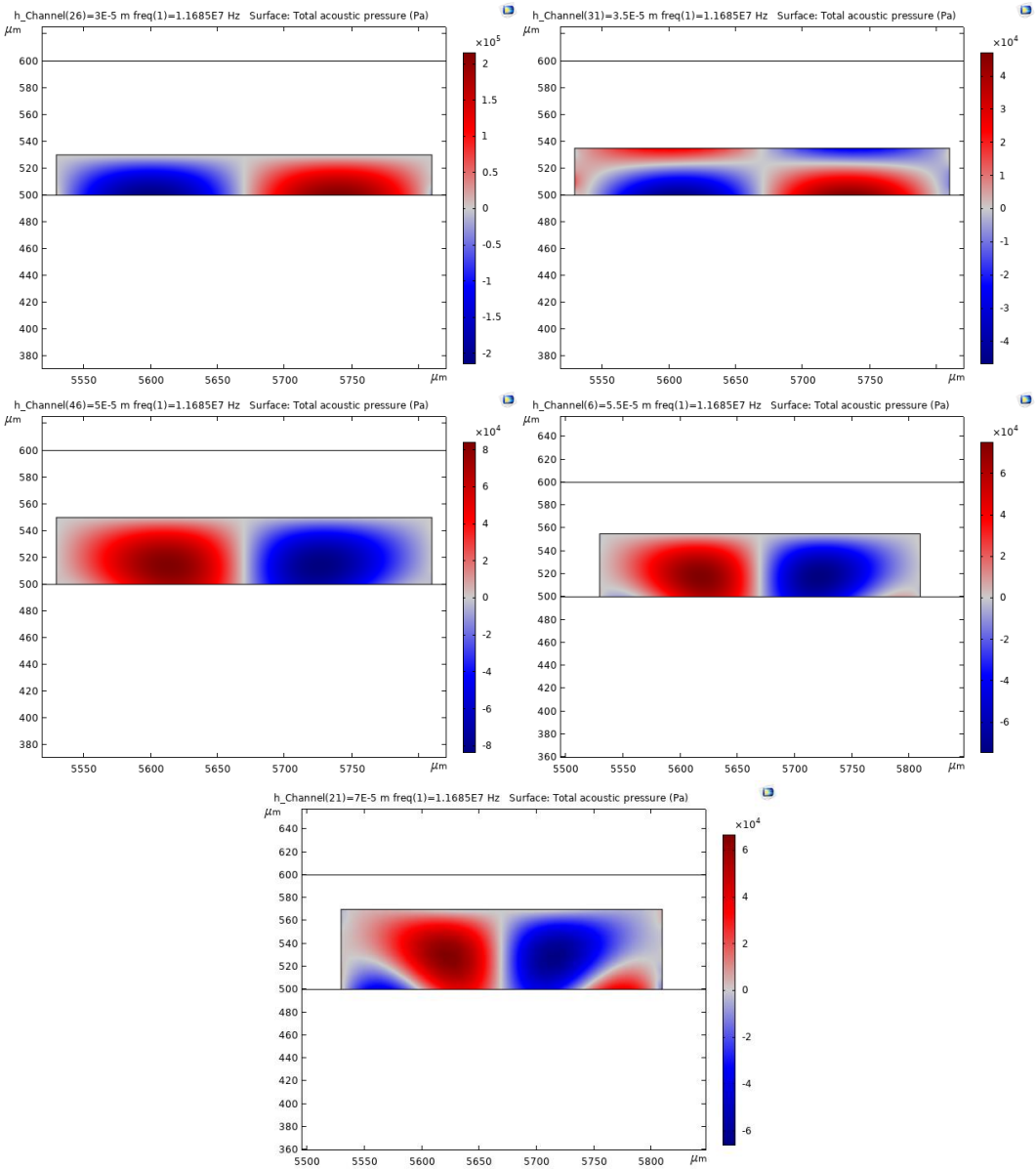

Figure 4.17: Height sweep for sensitivity analysis. (Top-left) The height is 30µm, (Top-right) 35µm, (Middle-left) 50µm, (Middle-right) 55µm, (Bottom) 70µm.

The only exception to this behaviour found is for the height of 35μm (top-right plot) where a different distribution is formed. This result can be associated to the development of lateral interactions between the fluid and the waves propagating in

the PDMS. This plot states the importance of the numerical analysis to design SAW-based devices to find particular solutions.

Considering the results of this section, for the three-dimensional analysis (Section 4.4), the channel will be modelled 280μm wide and 50μm high.

4.3.4.6 "Sandwich" SAW-based device

A different geometry was modelled, which is interesting for the results obtained but difficult to be fabricated as a real device. The structure is designed like a "sandwich" where two lithium niobate piezoelectric substrates are glued to a PDMS channel filled with water (Figure 4.18). The geometry is designed by using the configuration described in Section 4.3.1 and mirroring it on the other side to generate the "sandwich". On each substrate, two IDTs are positioned, in the same position of the previous configuration, therefore the actuation of the piezoelectric materials generates two SSAWs, one on the top substrate (at the bottom surface) and another on the bottom one (at the top surface). The distance between the two substrates and the channel is 10μm while the channel is 25μm high.

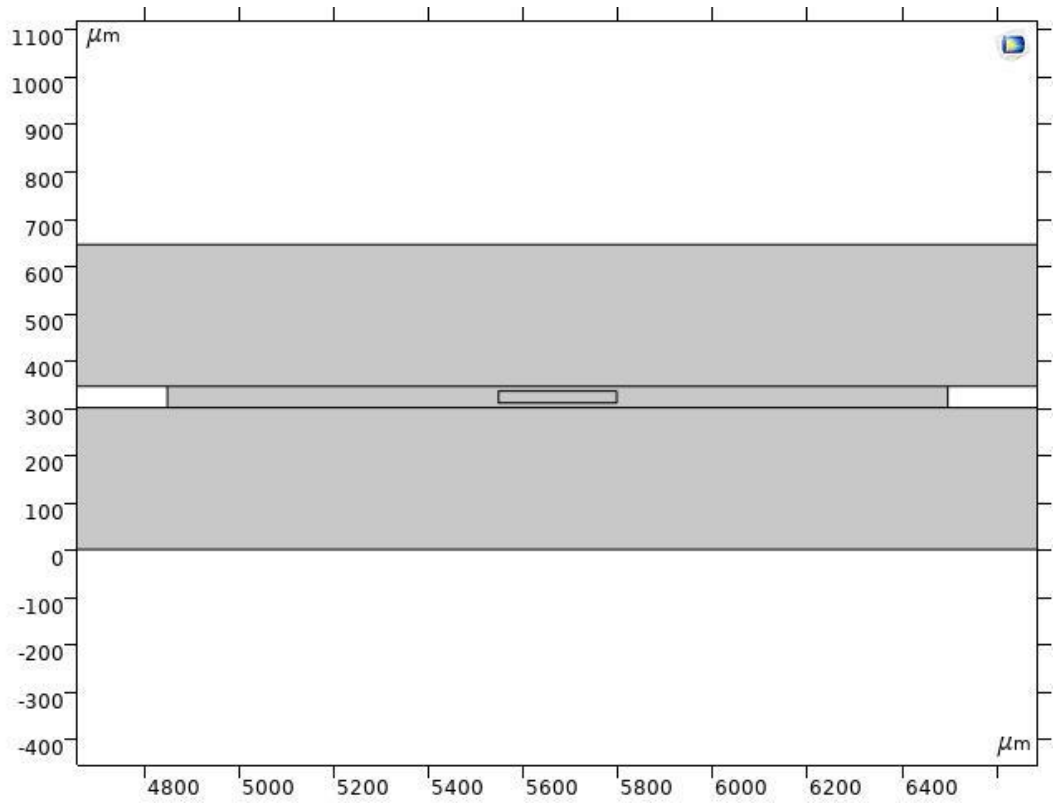

Figure 4.18: Focus on the PDMS channel of the "sandwich" structure.

In Figure 4.19, the pressure field in the fluid domain is plotted. The result is exactly what should be expected: the waves, propagating on the opposite piezoelectric materials, interact with the PDMS and the fluid providing an opposite contribution leading to the formation of a horizontal node in the mid-height of the channel. This kind of configuration can be used to control particles both in vertical and horizontal directions. The interaction between pressure waves and the distance between the piezoelectric substrate and the channel reduce the value of the acoustic pressure generated (up to 0.017MPa). The frequency detected to obtain this distribution (11.705MHz) is slightly different than the one found in the previous analyses.

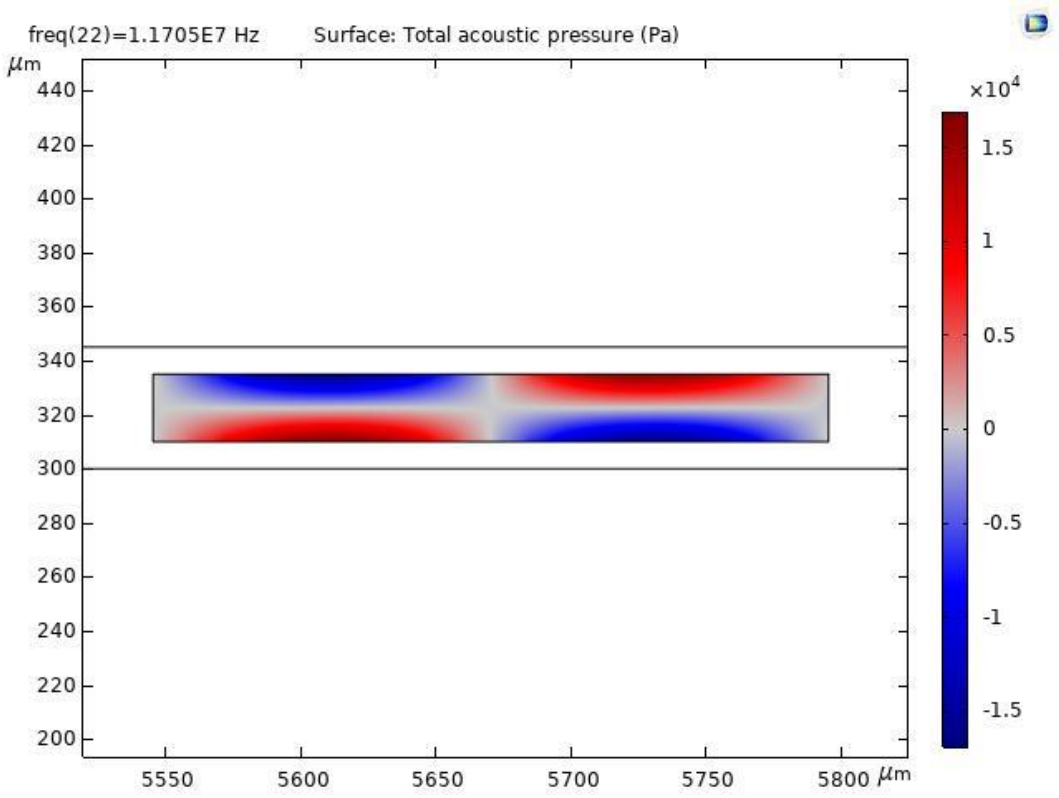

Figure 4.19: Acoustic pressure field for the "sandwich" configuration.

The trajectory and the position of particles after 0.1s are reported in Figure 4.20. The particles, starting from a horizontal row in the middle of the channel, are forced to move along the horizontal pressure node of the pressure field. The difference between this result and the one reported in Figure 4.9 is that for the configuration designed in this section the purpose is to control particles in both the directions, while in the other model the particles were intended to be moved towards the central

vertical node. Then, in this case the wanted effect is achieved. The colour legend reports the *x*-component of the velocity of the particles (with a maximum of 20mm/s).

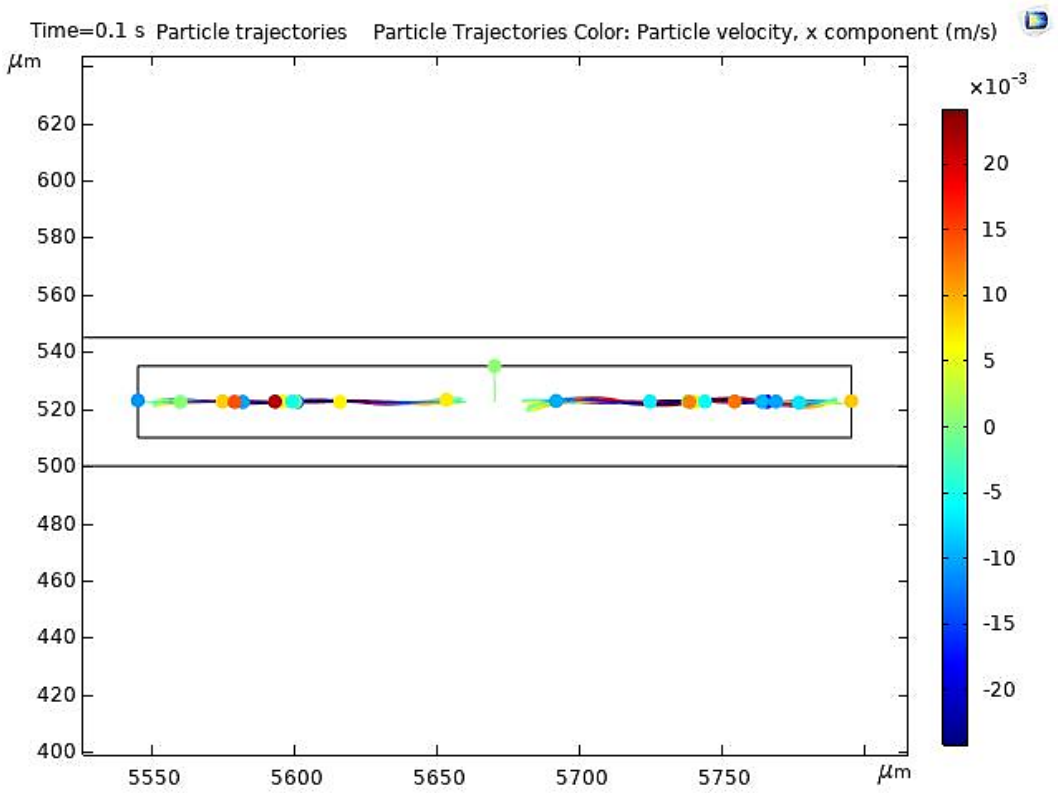

Figure 4.20: Particles trajectories and position after 0.1s in the "sandwich" configuration.

This result is useful to state that, managing the design of the devices and the interaction between the surface acoustic waves and the fluid, several effects can be achieved, stating the versatility associated to acoustofluidics.

4.4 Three-dimensional device analysis

The 2D analysis displays some limitations. For example, the fluid motion along the channel cannot be simulated with a two-dimensional domain, excluding the effect of the drag force on the particles. Also, the propagation of surface acoustic waves is not trivial considering a three-dimensional piezoelectric anisotropic material and the transmission of the waves inside the fluid domain is simplified with respect to a 3D model. Therefore, in order to validate the results obtained in the two-

dimensional analyses described before and to provide better solutions related to particle control, a three-dimensional frequency domain analysis is performed modelling a complete, though reduced in size, SAW-based device for particle focusing. To further investigate acoustophoresis, the analysis is conducted by changing the velocity of the fluid and the diameter of the particles: both the parameters are involved in the acoustophoretic phenomenon influencing the drag and the acoustic radiation force, respectively. Finally, the anisotropic behaviour of the lithium niobate substrate is studied by modifying the elasticity matrix to compare the anisotropic behaviour with the isotropic one.

4.4.1 Geometry

The geometry of the device is the same presented in Section 4.3.1, extruded in the *y*-direction for 2mm (Figure 4.21). This dimension is chosen to reduce the computational time needed by the software to solve the problem (around 15 minutes). In real devices the length of the devices can be of 10mm. In Section 4.4.3.1, the 2mm length selected is justified through the selection of proper boundary conditions. Also in this case, the length of the fingers composing the IDTs is equal to the length of the device and the fingers are modelled as no-thickness slender plates. Each IDT is composed by 10 couples of gold fingers.

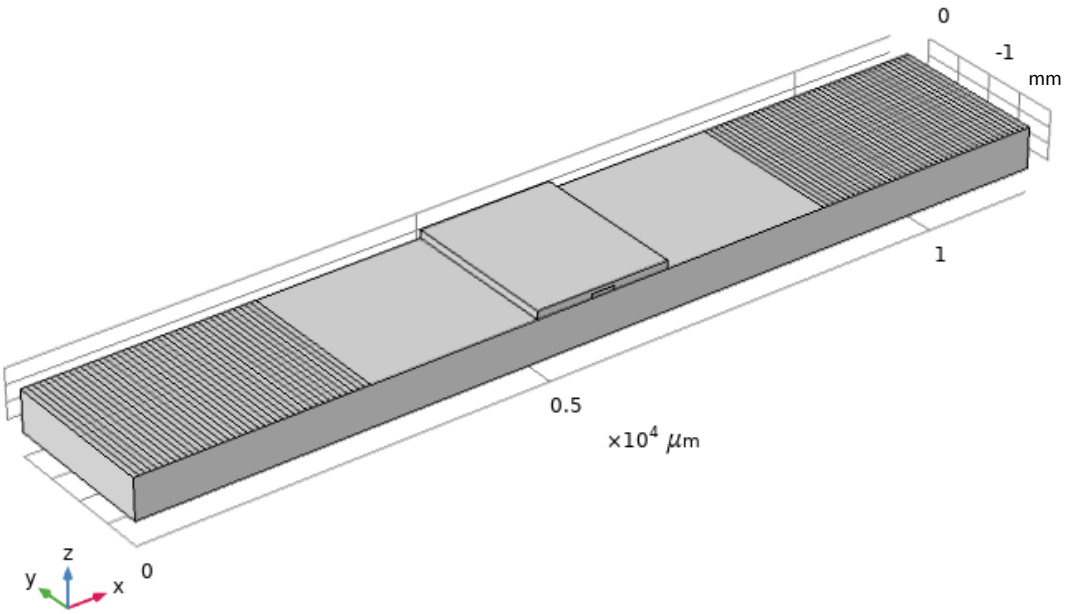

Figure 4.21: Three-dimensional model geometry.

Considering the solutions obtained in Section 4.3.4.2, for the three-dimensional model the PDMS is modelled as an elastic solid material with a height of 100μm. From the solutions of the sensitivity analysis reported in Section 4.3.4.5, the channel is chosen to be 280μm wide and 50μm high. The geometry of the lithium niobate substrate is the same reported in Table 4.2.

4.4.2 Mesh

A combination between a structured mesh (chosen to achieve better solutions in the domain for fluid velocity distribution) for the fluid domain and an unstructured mesh for the substrate and the PDMS is used (Figure 4.22). The maximum and minimum sizes of the elements composing the inlet face of the fluid channel are 17.5μm (corresponding to $\frac{\lambda}{16}$). A structured mesh is associated to this face and then the mesh is swept along the *y*-direction to reach the opposite side, the outlet of the channel. In this way hexahedral elements are generated within the fluid domain. For the substrate and the PDMS the maximum element dimension is 140μm (which is $\frac{\lambda}{2}$) while the minimum dimension is 35μm (which is $\frac{\lambda}{8}$). In this case the mesh is composed by tetrahedral elements. All the values chosen are fractions of the wavelength of the surface acoustic waves generated to adapt the solution to the mesh avoiding mesh-dependent effects.

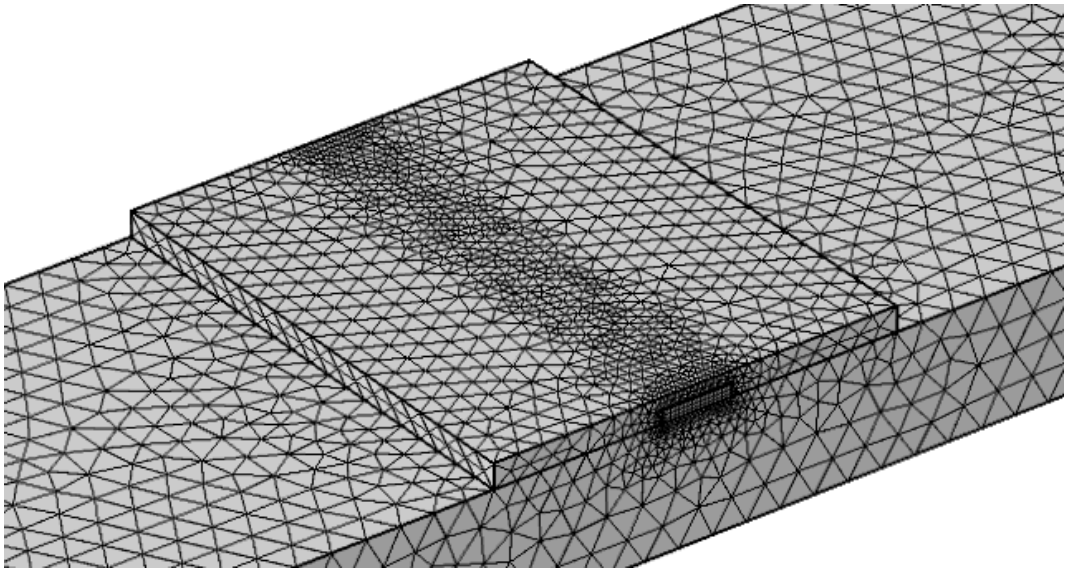

Figure 4.22: Mesh of the model. Focus on the central part of the device.

4.4.3 Boundary conditions

With respect to the two-dimensional model, in a three-dimensional one, all the boundaries must be associated to a specific condition. In this analysis, similar conditions as the cross-section model are applied, but a comparison is done by changing the boundary conditions associated to the lateral boundaries of the piezoelectric substrate to see the effects on waves propagation.

4.4.3.1 Solid mechanics interface

The solid mechanics interface is associated to the PDMS and the lithium niobate substrate. The low-reflecting boundary condition (described in Section 4.3.3.1) is applied on all the lateral boundaries and the bottom face of the substrate. The condition is selected to avoid the interferences which can be generated by the interaction between the propagating waves and the reflected ones. The upper face of the substrate, in all the parts which are not in contact with the PDMS and the fluid domain, is set as free surface. The upper surface of the PDMS is low-reflecting. The lateral faces of the PDMS along the *x*-direction are free while the two faces along the *y*-direction are low-reflecting to model the device to be longer than the simulated dimension (being the waves only transmitted). At the contact faces between the PDMS and the substrate, domain continuity is considered to provide the waves transmission.

Different boundary conditions were associated to the lateral boundaries of the PDMS and the piezoelectric material in the *y*-direction to model the device not being just 2mm long but longer, not to limit the effect of the waves in small spaces. The use of low-reflecting boundary conditions is a good solution to overcome this limit. Other investigated conditions are the symmetry one and the periodic condition of continuity. The symmetry condition is applied to a surface which should be considered by the model to be a plane of symmetry of the geometry. Then, by applying this condition to the lateral surfaces of the device, the latter is replicated in a symmetric way at the opposite side of the face selected. The periodic condition of continuity set the displacements for a destination face to be equal to the ones of a source face. This condition must be associated to two different

boundaries, cannot be applied on the same face to be selected both as source and destination. Then, the condition is applied on the opposite surfaces of the device in the *y*-direction to investigate the effects obtained.

4.4.3.2 Pressure acoustics interface

In three-dimensional analysis the PDMS is modelled as a solid elastic material, therefore no boundary conditions, associated to the pressure acoustic interface, are applied for the PDMS. The symmetry boundary condition is applied at the inlet and the outlet of the fluid domain, to simulate a more extended channel, with the same considerations discussed in the previous section. The walls of the channel are all in contact with solid materials (substrate and PDMS), then the acoustics-structure coupling condition is applied.

4.4.3.3 Electrostatics interface

The electrostatics interface is used to apply a voltage difference between the fingers composing the IDTs. The fingers are alternatively charged and grounded (the same as the two-dimensional analysis). The voltage applied is the same of the Equation (4.12) with $V_0 = 8V$. The harmonic dependence is automatically added by COMSOL in a frequency domain analysis.

4.4.3.4 Laminar flow interface

The laminar flow interface is added to the three-dimensional model to simulate the laminar fluid flowing through the channel. The fluid velocity is specified at the inlet and kept constant through the microchannel (obtained solving a stationary study for the fluid flow) with values of 1mm/s and 2mm/s. The two values of velocity are used to compare the effects of different drag forces on particle focusing phenomena: higher fluid velocity should move particles faster. The outlet, at the opposite side of the channel, is a zero-pressure outlet. At the lateral walls, at the top and at the bottom of the channel, the no-slip boundary condition is applied.

4.4.3.5 Particle tracing interface

Sixteen particles in a 4x4 grid are released from the inlet of the channel. The particles are made in polystyrene and have the same properties of the ones used in the 2D analysis. The velocity of the particles is the same of the fluid in every point

of the fluid domain contained in the microchannel, obtained solving the stationary study for the fluid flow. The walls of the channel and the outlet are associated to the freeze boundary condition (the same used for the previous analysis). To investigate the influence of acoustic and drag forces on particles, two values for the diameter are simulated: 4μm and 8μm.

4.4.4 Analyses and results

4.4.4.1 SAW-based device for particles focusing

A frequency domain analysis is performed considering the results obtained with the simulation of the cross-section to find the pressure field in the fluid domain. The frequency used is the one found previously, $f = 11.685\text{MHz}$. This analysis is done to build the standing waves on the piezoelectric substrate and the pressure distribution in the three-dimensional channel. Before solving the time domain analysis to see the trajectories of the particles, a stationary study is performed on the fluid to build the laminar flow.

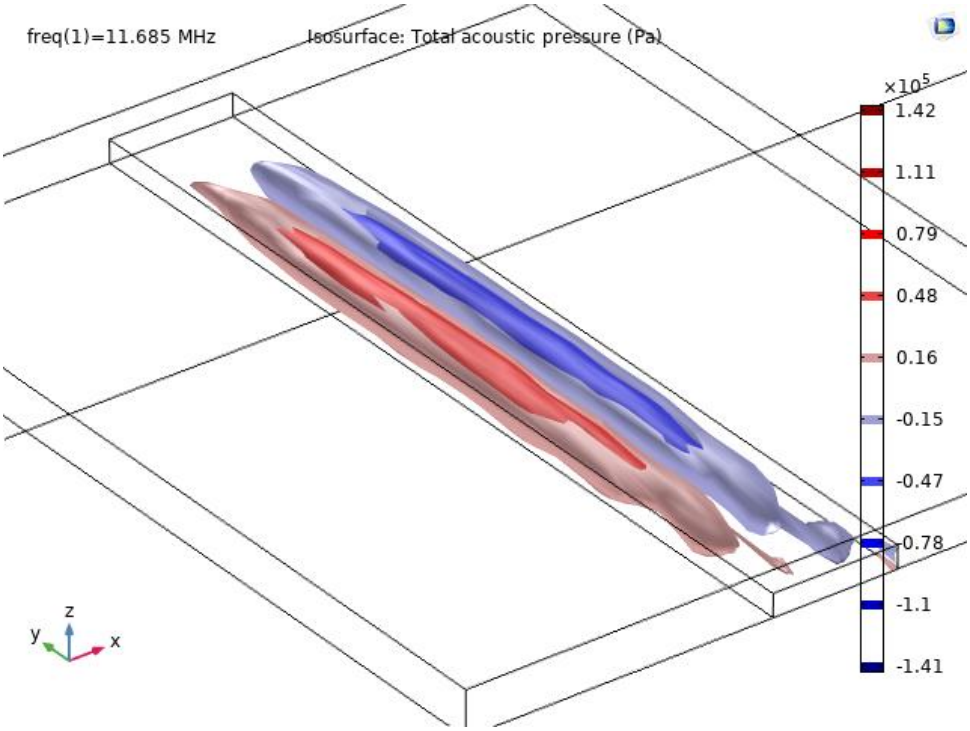

Figure 4.23: Total acoustic pressure iso-surface plot.

The iso-surface pressure distribution is plotted in Figure 4.23 with ten levels. This kind of plot is good to see the shape of the pressure field within the channel. In Figure 4.24, a series of cross-sectional planes showing the pressure field distribution is reported. The same shape seen from the cross-section sensitivity analysis is obtained (compare with Figure 4.17). The maximum value of pressure calculated (0.14MPa) is greater than the one computed in the 2D analysis (0.08MPa). The higher value can be associated to the total three-dimensional interactions between the components of the device with respect to the simple cross-sectional view. In both the images reported, the central pressure node can be recognised, then particles are expected to move towards this region of the channel.

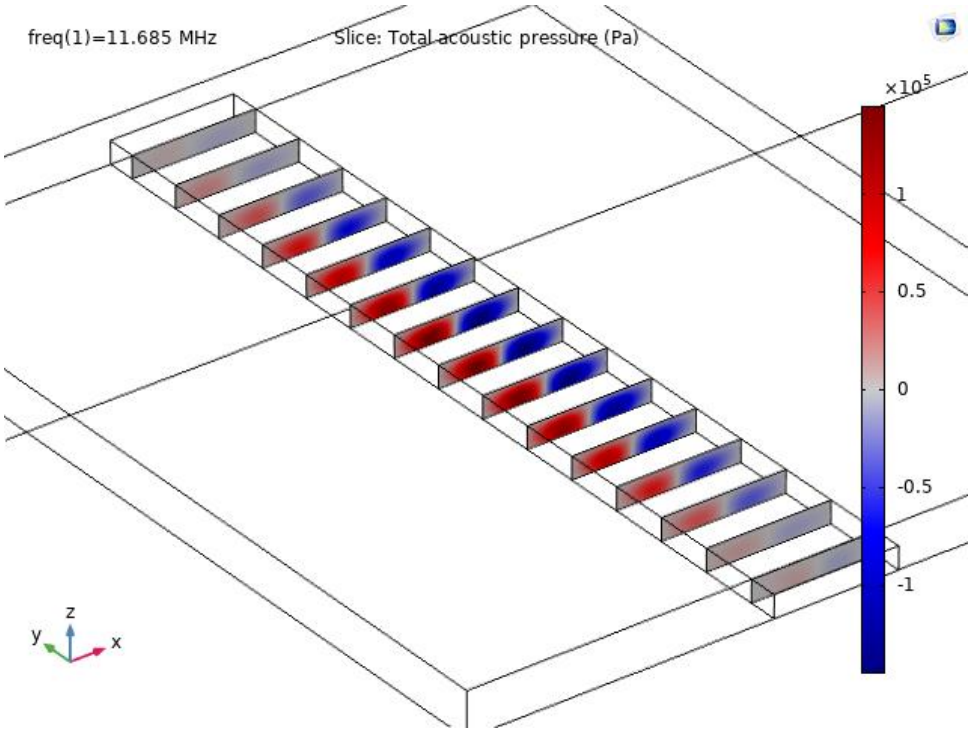

Figure 4.24: Cross-sectional slices of the pressure field to see the shape and the evolution of the field.

At the inlet and outlet regions, the acoustic pressure seems to be attenuated (reduction in the intensity of the colour). The effect is correlated to the shape of the standing SAWs developed on the surface of the piezoelectric substrate, applying the low-reflecting boundary condition on the lateral faces of the component (see Figure 4.25).

The z-displacements on the piezoelectric substrate are plotted in Figure 4.25. The values of the displacements are lower with respect to the two-dimensional analysis. The different result can be associated to the anisotropic nature of the piezoelectric material leading to more complex propagation and interactions of the waves in 3D than the simple cross-section. In Figure 4.25, also a magnification of the waves to see the shape is provided.

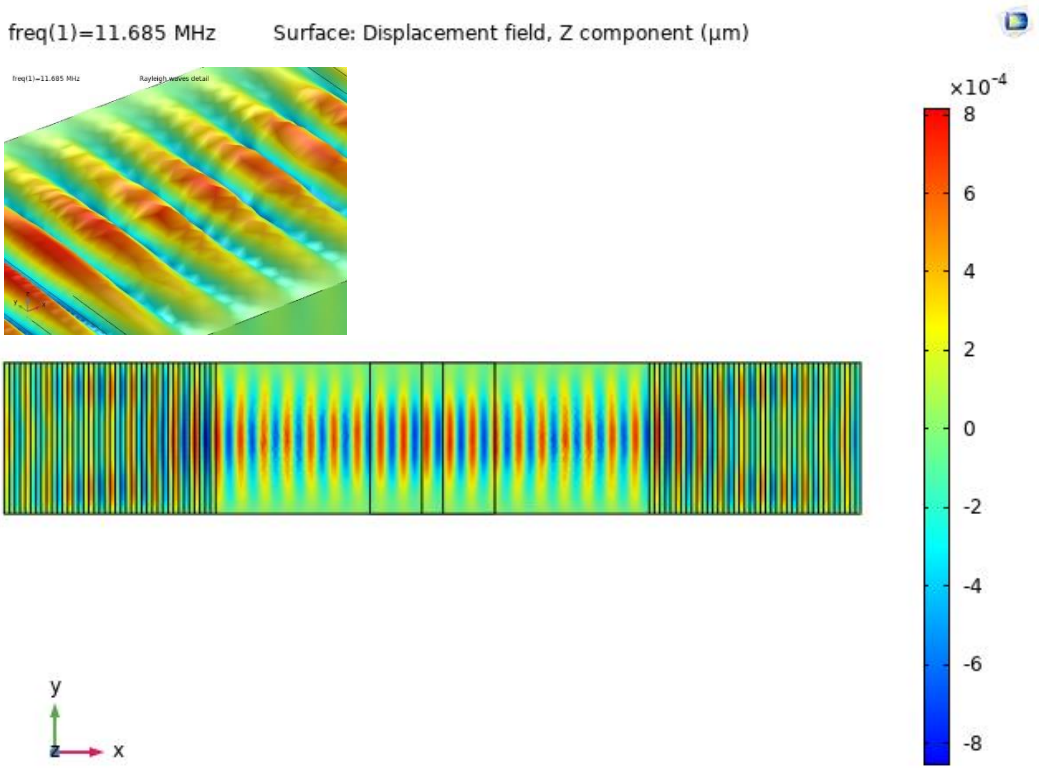

Figure 4.25: z-displacements on the piezoelectric substrate, a view of the top surface.

The fluid velocity plot is reported in Figure 4.26. The velocity magnitude is imposed at the inlet and the stationary study computes the complete velocity and pressure field. In this image, the velocity set at the inlet is 1mm/s. The shape of the velocity field, maximum of velocity in the centre of the channel and zero velocity near the walls, generates due to the no-slip boundary condition set at the walls (see Section 3.1.4.2). The regime is laminar (as specified by the interface name) according to the dimensions of the microchannel. Associating the solution of the velocity to the particles released into the fluid, the drag force can be computed.

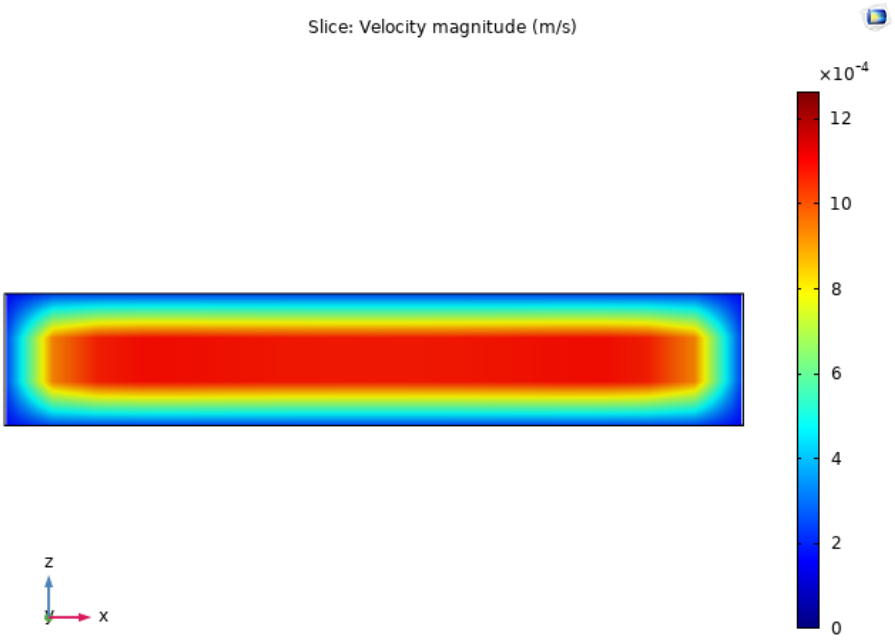

Figure 4.26: Fluid velocity in the channel.

Figure 4.27 reports the trajectories of the particles plotted together with the iso-surfaces of the acoustic pressure field. The red points plotted are the polystyrene particles, the black lines are the trajectories followed by the particles. In this image, the focusing on the central pressure node can be seen: the particles move around the pressure field being dragged by the flowing fluid. The horizontal component of the acoustophoretic radiation force pushes the particles towards the central pressure node. In the image, four particles stop their trajectories before reaching the outlet. This is due to the vertical component of the acoustic radiation force which pushes them in contact with the upper wall of the channel where particles are blocked by the freeze boundary condition.

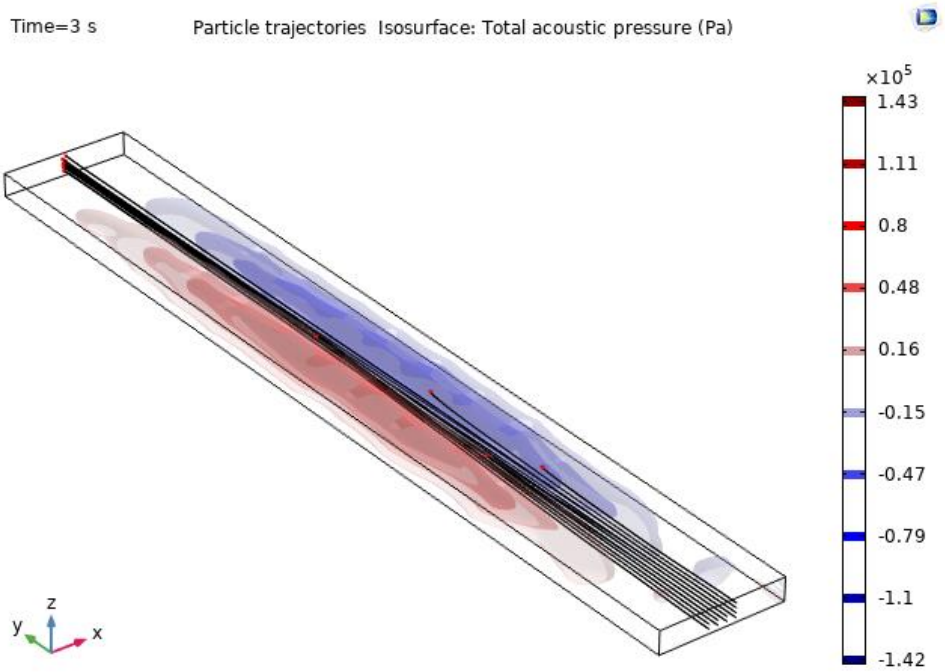

Figure 4.27: Particles trajectories plotted together with the acoustic pressure iso-surfaces.

The trajectories of the particles are shown in Figure 4.28. The *x*-component of the acoustic radiation force is reported in the colour legend. The acoustophoretic phenomenon can clearly be seen from the image: the particles are focused on the centre of the channel where the pressure node is located. The maximum value of the *x*-component of the acoustic radiation force is around 3pN. Four particles, far from the centre, are forced by the acoustic radiation force to come in contact with the upper wall of the channel where they freeze according to the condition applied. This effect is caused by the presence of the pressure antinodes pushing away the particles following the dome shape of the pressure distribution (as the trajectories obtained in the 2D analysis, see Figure 4.10). Differently than the two-dimensional analysis, the particles are moved towards the centre and can arrive to the outlet dragged by the flow of the fluid. A comparison is provided in the next section between different particle diameters and considering different velocities for the fluid flow to investigate the cooperation of the two forces involved.

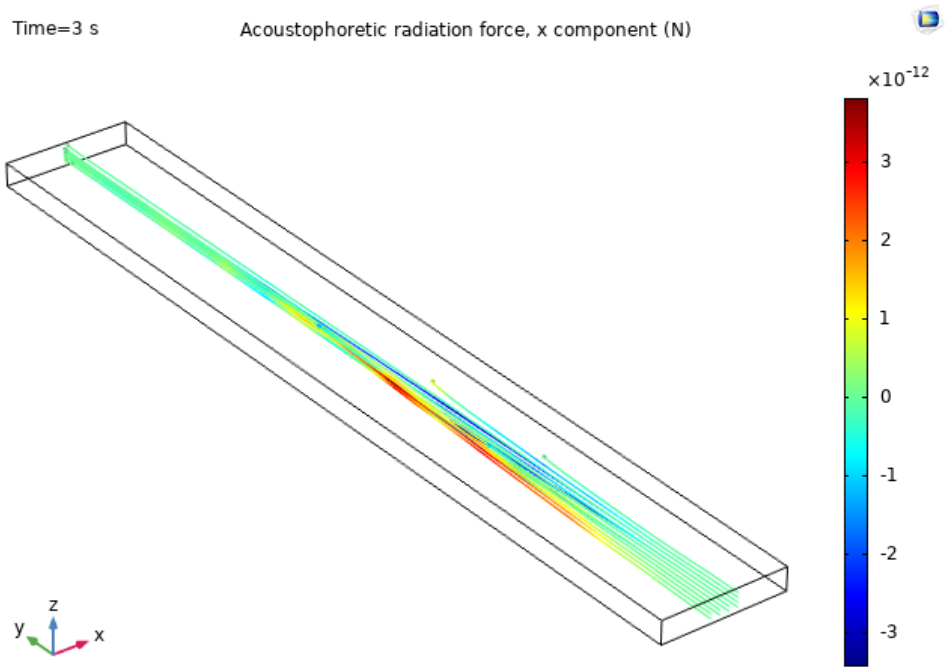

Figure 4.28: Particles trajectories at t=3s.

4.4.4.2 Particle diameters and fluid velocities

The particle focusing effect, achieved with the analysis described in the previous section, can be investigated by changing some properties correlated to the phenomenon. In this section, the same analysis considering two different diameters (4μm and 8μm) and two velocities for the fluid (2mm/s and 1mm/s) is performed to compare the solutions to see how the forces involved interact with the particles.

A view of the channel from the inlet is reported in Figure 4.29, comparing the horizontal displacements of the particles by changing their diameter. Being the acoustic radiation force proportional to the volume of particles, by reducing the diameter, the force should be reduced and then particles are expected to move less than in the case of higher diameter. This is the effect reported: with 4μm diameter, the particles are subjected to lower forces, and the focusing effect is reduced. The red and blue shades are the iso-surfaces of the acoustic pressure field. A longer channel can be simulated to see a complete focusing on the pressure node for the particles with lower diameter.

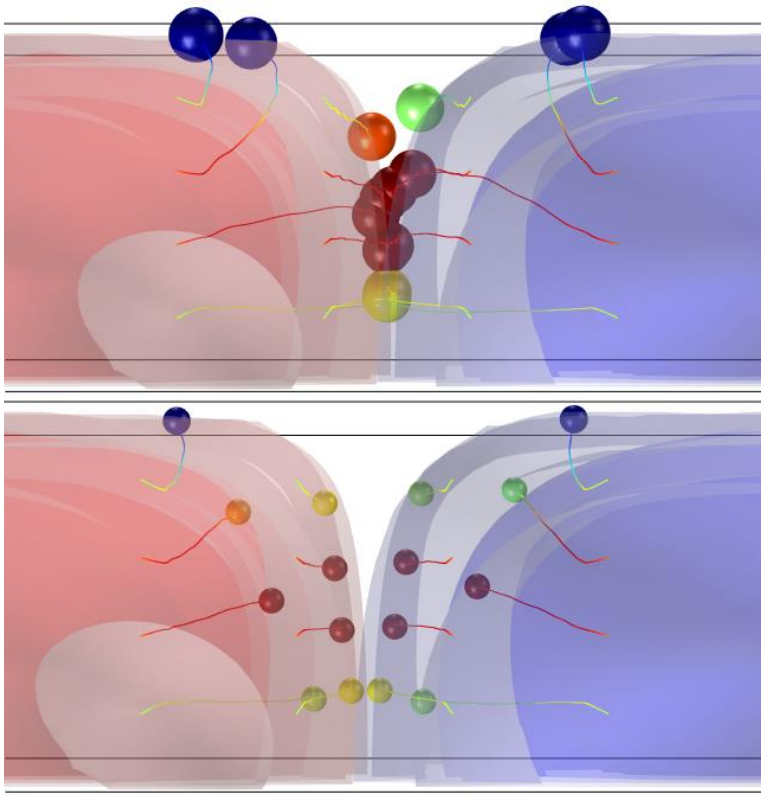

Figure 4.29: Particles trajectories seen from the inlet of the channel. (Top) 8μm particles and (Bottom) 4μm particles.

The *x*-component of the acoustophoretic radiation force with different particles are reported in the colour legend in Figure 4.30. As can be seen, the value of the acoustic force is around 3pN in case of 8μm diameter particles, while is around 0.8pN in case of 4μm diameter particles.

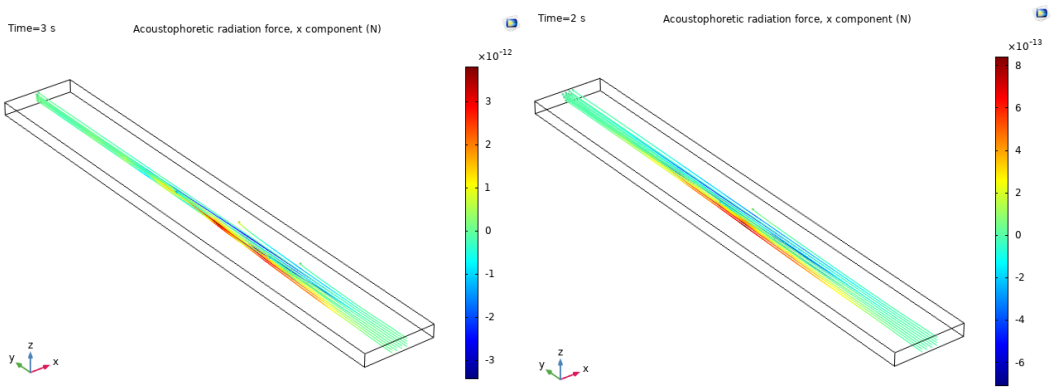

Figure 4.30: Comparison on the values of the acoustic radiation force on particles with different diameters. (Left) 8μm particles and (Right) 4μm particles.

Again, exploiting the inlet point of view, the trajectories of the particles subjected to different fluid velocities are plotted in Figure 4.31. In this case, the diameter of the particles is kept fixed to 8μm while two values of fluid velocity are set at the inlet of the channel. The velocities used are 1mm/s and 2mm/s. The acoustic radiation force should not be influenced by the velocity of the fluid while the drag force is increased transporting particles towards the outlet of the channel faster. From the images, the difference in the horizontal displacement of particles can be distinguished: the increased fluid velocity moves particles faster and then the focusing is not completed and three particles, instead then four, are frozen by the walls. Even though the effect is reduced, the focusing of particles towards the pressure node is still achieved in both the cases, denoting that the acoustophoretic phenomenon is effective in controlling particles motion and other conditions (such as the fluid velocity) can be modified to obtain different effects.

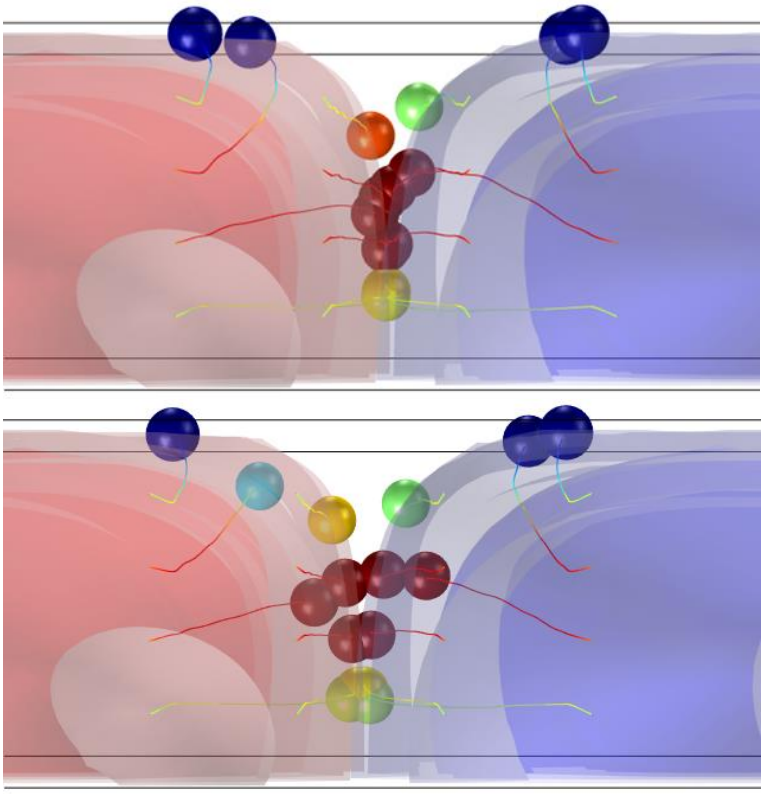

Figure 4.31: Particles trajectories seen from the inlet of the channel. (Top) 1mm/s fluid velocity is simulated, (Bottom) 2mm/s fluid velocity. The diameter of the particles is kept fixed as 8μm.

4.4.4.3 Varying boundary conditions on the substrate

To model the device with reduced dimensions than a real one and save time and power required for computation, different boundary conditions were considered and applied to the *y*-direction lateral faces of the piezoelectric substrate to simulate a larger device (not just the 2mm long one modelled). The boundary conditions used are the low-reflecting condition, the symmetry condition, and the periodic condition of continuity. The analysis is performed in the frequency domain with $f = 11.685\text{MHz}$. The results are reported in Figure 4.32.

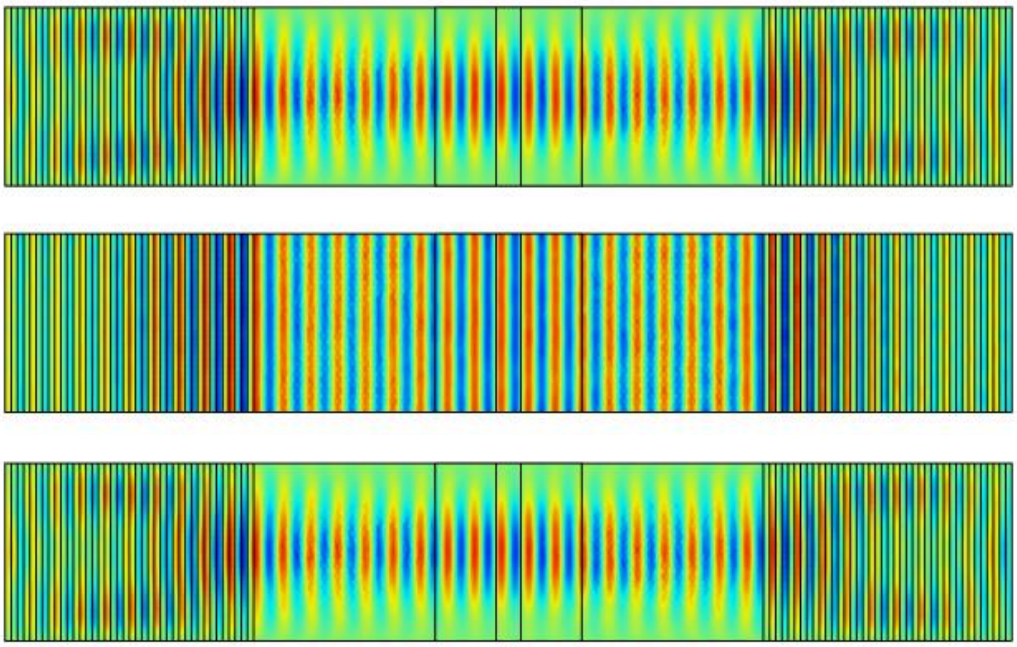

Figure 4.32: z-displacements on the top surface of the piezoelectric substrate. On top the low-reflecting boundary condition is applied, in the middle the symmetry condition is applied, on bottom the continuity condition is used.

The distribution of the waves is the same compared to the low-reflecting condition and the continuity one. This result can be justified considering that the low-reflecting condition allows waves only to pass the boundaries, condition which can be assumed to be equal as simulating a longer and continuous substrate. In these two cases the standing waves are developed but attenuated in the regions near the lateral faces of the substrate. The symmetry condition instead simulates well the waves as being generated by IDTs which are longer than the 2mm modelled. The wave pattern seems to be homogeneous all along the *y*-direction of the substrate.

Then, this condition simulates well the propagation of surface waves as built by longer IDTs. The pressure pattern obtained using the symmetry boundary condition is the same obtained in the previously presented analyses (both magnitude and distribution). Also, the released particles are focused on the central pressure node (Figure 4.33). The low-reflecting boundary condition was exploited in the models reported to have a first part of the channel where particles can move straight being then focused when reaching the pressure field into the channel. Therefore, both the conditions can be considered for the model, providing the same results, but the symmetry boundary condition better simulates longer devices.

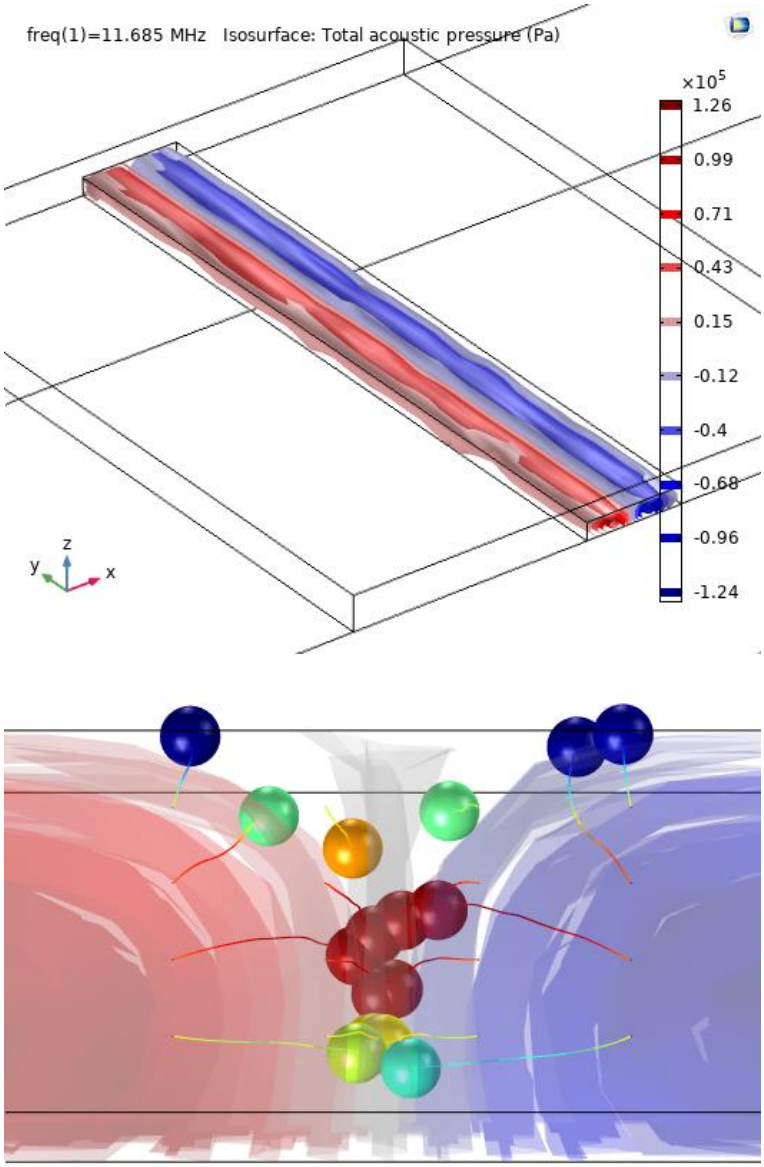

Figure 4.33: Solutions obtained by applying the symmetry boundary condition. (Top) Total acoustic pressure iso-surface plot. (Bottom) Particles trajectories seen from the inlet of the channel.

4.4.4.4 Anisotropic behaviour of the piezoelectric substrate

In this last section related to the particle focusing SAW-based device, the lithium niobate substrate is further investigated by manually modifying the elasticity matrix of the material to see the influence in waves development comparing different material behaviours. The elasticity matrix used for the previous analysis is reported in Section 4.2.2. The anisotropic nature of the material can be recognised by looking at the entries of the matrix (see Section 4.2.2), which provides different values for the diagonal terms and the presence of different non-diagonal terms. The result is the same used for all the previous simulations and is shown again in Figure 4.34.

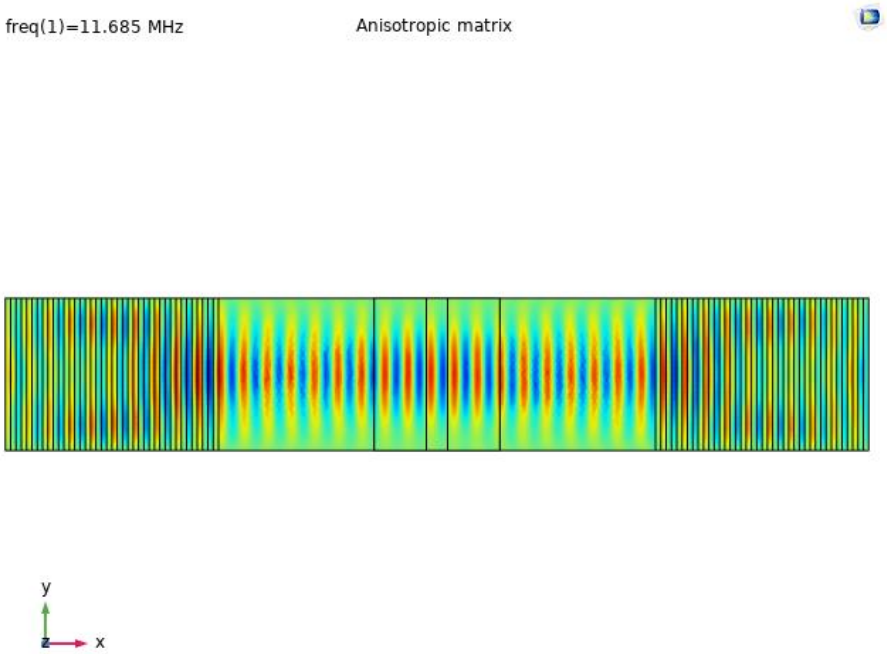

Figure 4.34: z-displacements on the surface of the piezoelectric substrate modelled with an anisotropic elasticity matrix.

To simulate an isotropic mechanical behaviour for the piezoelectric material, the matrix was modified to be:

$$c_{ij} = \begin{bmatrix} 2.029 & 0.749 & 0.749 & 0 & 0 & 0 \\ 0.749 & 2.029 & 0.749 & 0 & 0 & 0 \\ 0.749 & 0.749 & 2.029 & 0 & 0 & 0 \\ 0 & 0 & 0 & 0.599 & 0 & 0 \\ 0 & 0 & 0 & 0 & 0.599 & 0 \\ 0 & 0 & 0 & 0 & 0 & 0.599 \end{bmatrix} [\cdot 10^{11}\text{Pa}]$$

In this case, the diagonal terms have the same value while the non-diagonal terms are equal. Then, the material should behave as an isotropic one. The result is reported in Figure 4.35 showing the development of the standing surface waves differently than the anisotropic case. The waves seem to be attenuated, not interfering correctly to increase the displacements in the channel region. In addition, the interaction with the fluid, considering the pattern reported, should not be effective in particle focusing: the pressure field should present two parts, one at the inlet and the other at the outlet where the focusing should work, while in the mid-length of the channel no focusing effect should be developed (in the green parts, the displacement magnitude is zero).

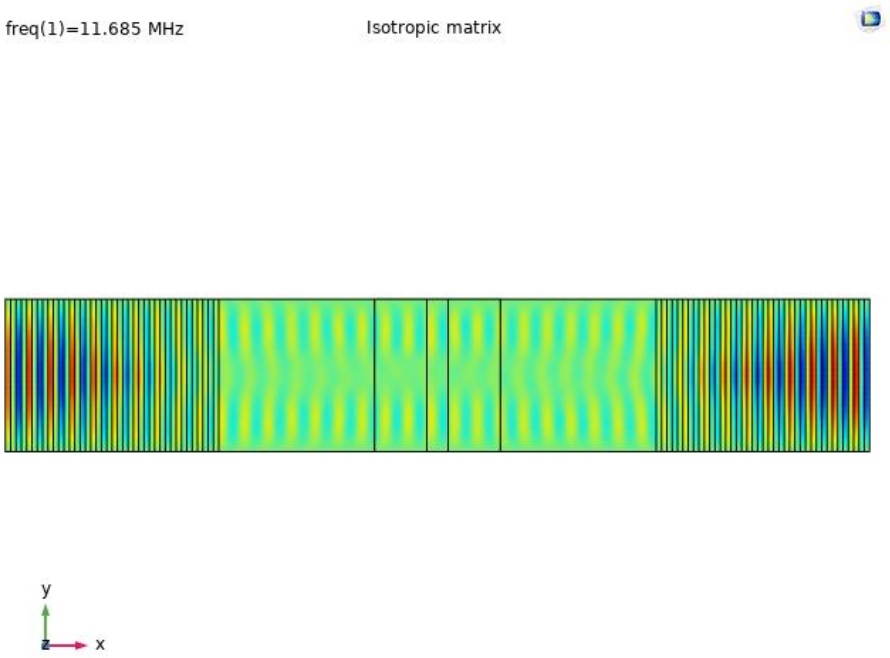

Figure 4.35: z-displacements on the surface of the piezoelectric substrate modelled with an isotropic elasticity matrix.

On COMSOL it is also possible to model one material to be isotropic and define only one value as elastic constant (elastic modulus) to describe it. The value selected is $2.029 \cdot 10^{11}$Pa. The z-displacements are plotted in Figure 4.36. In this case, the standing waves are built on the material but with a non-precise distribution and the interference in the channel region seems not to be constructive.

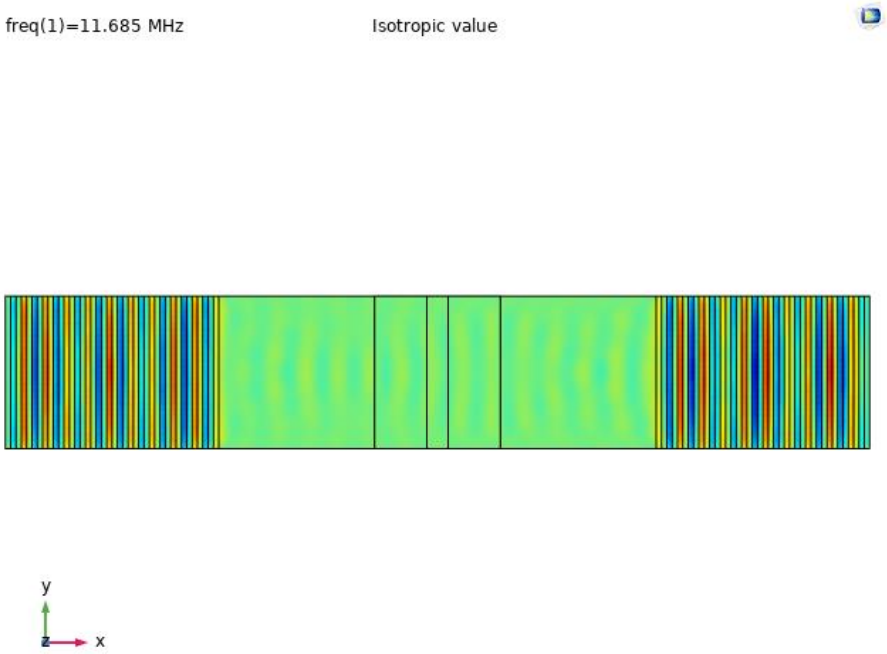

Figure 4.36: z-displacements on the surface of the piezoelectric substrate modelled with just a value to determinate the elastic properties.

These plots show the importance of using an anisotropic material for the propagation of surface acoustic waves, because it provides good interactions, precise and defined propagation.

4.5 IDTs configurations and particle trapping analysis

The three-dimensional analysis performed in Section 4.4 provides interesting results regarding SAW-based devices for particles focusing. As described in Section 4.4.4.4, the anisotropic behaviour of the piezoelectric substrate is one important feature to provide the development of standing waves and a good interaction between the substrate and the fluid. Moreover, the device modelled exploits the use of just two IDTs deposited at the opposite sides of a PDMS channel to generate two counter-propagating waves. Different positioning and number of IDTs to develop different surface wave distributions can be modelled to investigate the interaction between waves. First of all, the configuration used in the following analysis is tilted with respect to the *x*-direction (previously the IDTs were aligned to this direction), another way to investigate the anisotropic behaviour of the material and the electro-mechanical coupling. Then, configurations exploiting the use of four or six IDTs are simulated to see the interaction between propagating waves from different directions. A squared-section lithium niobate substrate is used to perform this analysis. Also, a circular shape IDT is modelled to see the developed field. Finally, exploiting the interaction between the surface waves and fluids generated by a four IDTs configuration, a squared-section PDMS "pool" containing particles is modelled trying to simulate the entrapment of particles within the pressure nodes of the generated pressure field within a static fluid.

4.5.1 Geometry

The geometry of the model is simple, to reduce the computational effort of the software to solve the problem. The model described here refers to the "pool" device for particles trapping (Figure 4.37), the other geometries and features used will be described in the corresponding sections while showing the results. The lithium niobate substrate is a block with a squared section. The block is 500μm thick as in the previous analysis. The length of the four sides of the square section is 8627μm (calculated with the Pythagorean theorem, starting from the wanted length and

distances for the IDTs). 15 couples of fingers constitute each of the four IDTs tilted by 45° with respect to the *x*-direction. The width of the fingers is 70μm and the same distance is used to separate the fingers, developing a wave with 280μm wavelength. On top of the substrate, in the central position, a 100μm high squared PDMS "pool" is modelled (1650μm x 1650μm) with inside water (1400μm x 1400μm). The fluid domain is 50μm high.

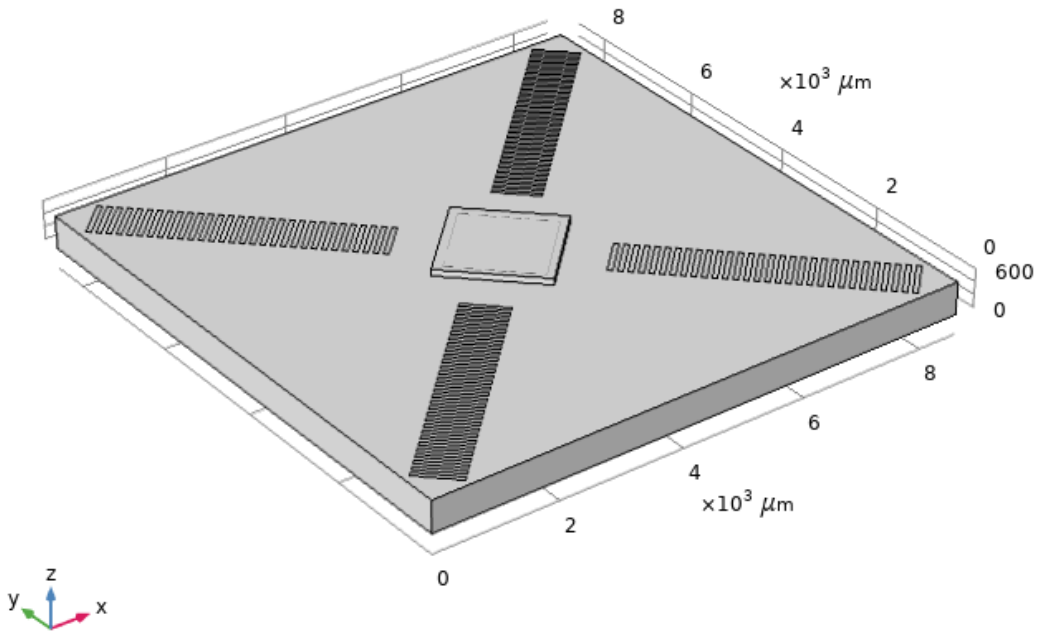

Figure 4.37: Geometry of the "pool" device for particles trapping.

4.5.2 Mesh

The mesh used in this model is the same described in Section 4.4.2. The only difference is that in this case the mesh is unstructured and composed by tetrahedral elements for all the components of the model. The maximum and minimum sizes of the elements composing the "pool" are 17.5μm (corresponding to $\frac{\lambda}{16}$). For the substrate and the PDMS the maximum element dimension is 140μm (which is $\frac{\lambda}{2}$) while the minimum dimension is 35μm (which is $\frac{\lambda}{8}$). To avoid mesh-dependent effects on the solutions, the elements size is always chosen to be a fraction of the wavelength.

4.5.3 Boundary conditions

4.5.3.1 Solid mechanics interface

The low-reflecting boundary condition is applied to the lateral faces and to the bottom surface of the lithium niobate substrate, to avoid the reflection of the waves. The upper surface of the substrate is free. Where the PDMS "pool" is modelled, the upper face of it is low-reflecting while the lateral surfaces are set as free. In the configuration exploiting four 45° tilted IDTs, also a PDMS channel is simulated. Again, the upper surface is associated to the low-reflecting boundary condition while the lateral faces are set as free surfaces.

4.5.3.2 Pressure acoustics interface

The symmetry boundary condition is applied at the inlet and the outlet of the fluid domain, when the channel is modelled, to simulate a more extended domain. The acoustics-structure coupling boundary condition is applied to the walls of the channel because all the boundaries of the fluid are in contact with solid components. The PDMS "pool" is sealed, no inlet and outlet are modelled, then the fluid is static. In this case, all the boundaries of the fluid domain are associated to the acoustics-structure coupling condition.

4.5.3.3 Electrostatics interface

The fingers, composing the IDTs, are alternatively charged and grounded, as in the previous analyses. The voltage applied is the same of the Equation (4.12) with $V_0 = 8V$. The harmonic dependence is automatically added by COMSOL in a frequency domain analysis.

4.5.3.4 Laminar flow interface

The fluid flow interface is used only where the channel is modelled. The velocity of the fluid is set at the inlet to be 1mm/s. A zero-pressure condition is applied at the outlet of the channel. On the sidewalls of the fluid channel the no-slip condition is applied, meaning that the velocity of the fluid goes to zero at the walls.

4.5.3.5 Particle tracing interface

For the configuration exploiting a PDMS channel, a 14x3 (forty-two) grid of 8μm polystyrene particles is released at the inlet, covering the whole inlet surface. The particles move along the channel with the same velocity of the fluid. The freeze condition is applied to the walls of the channel. For the "pool" configuration, thirty-four particles are released at mid-height of the fluid domain to be displaced by the acoustic radiation force. Again, the freeze boundary condition is applied to the walls of the structure. The time simulated is of 10s for both the models.

4.5.4 Analyses and results

4.5.4.1 IDTs configurations

A frequency domain analysis is done using the same value of frequency found in the two-dimensional analysis, $f = 11.685\text{MHz}$. The elasticity matrix associated to the lithium niobate substrate is the same reported in Section 4.2.2, which was chosen to have a good propagation of the waves along the *x*-direction. To investigate the anisotropic behaviour of the material and the interaction between waves, different configurations of the IDTs are considered.

The first analysis is done modelling two opposite IDTs composed by 10 couples of fingers, generating two counter-propagating surface waves. Differently from the three-dimensional analysis previously reported, in this case the IDTs are rotated by an angle with respect to the *x*-direction of the system. The distance between the IDTs is the same modelled for the previously reported analyses. A parametric sweep is used to rotate the IDTs by 15° each step, starting from 0° and finishing to 90°. In Figure 4.38, the more interesting results are reported. The best interaction is obtained by tilting the IDTs with a 45° angle. When the angle is set to 30°, the interaction is good but between the IDTs there are some destructive interferences which reduce the effect. At 60° the interaction is very low. With the angle set to 90°, the interaction is good, but the values of the z-displacements are reduced with respect to the 45° case. The scale, reporting the values for the z-displacements, is the same for all the situations plotted, then the interaction effects can be compared.

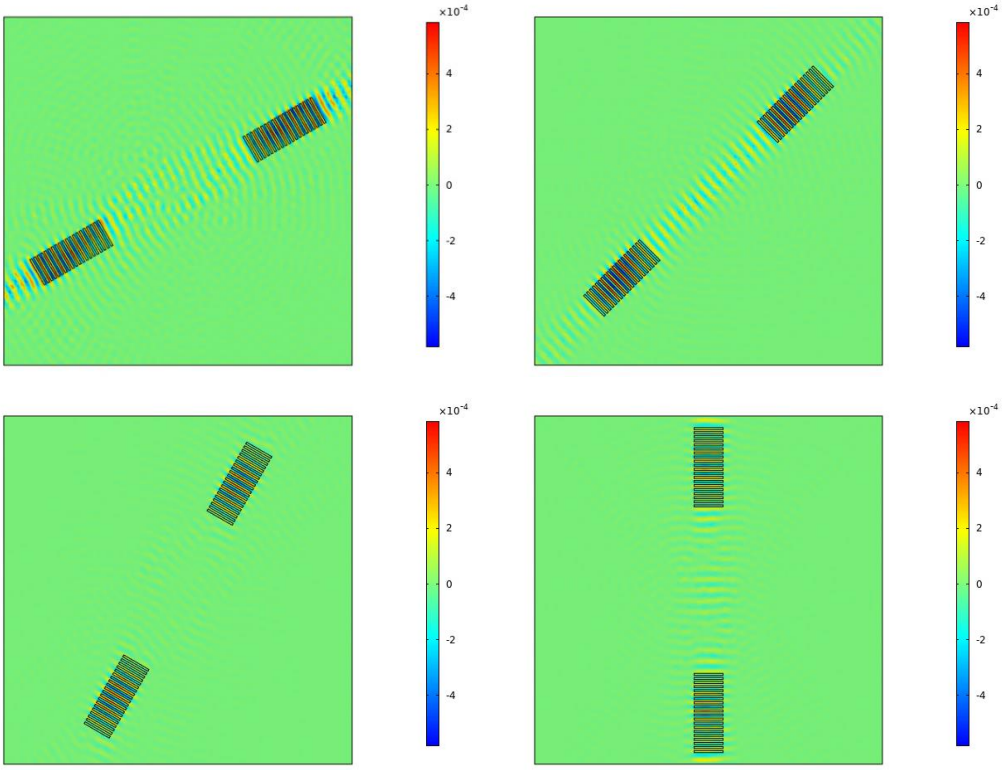

Figure 4.38: Comparison of the z-displacements by tilting the IDTs direction by an angle with respect to the x-direction: (Top-left) the angle is 30°, (Top-right) 45°, (Bottom-left) 60° and (Bottom-right) 90°.

Considering the results obtained by tilting the IDTs direction, two configurations exploiting the use of four and six IDTs are modelled. Being the best interaction plotted in Figure 4.37, the 45° tilted direction is used to position the IDTs. The first configuration is modelled with four IDTs, tilted by a 45° angle and composed by 15 couples of fingers (top image of Figure 4.39). The interaction of the waves, in the region between the four structures, generates a grid pattern composed by a series of nodes and antinodes regularly alternated. If particles manipulation is considered, a trapping effect within the pressure nodes generated in a fluid coupled with this waves pattern can be studied (see Section 4.5.4.2). On the other hand, modelling a channel with a fluid flowing along this pattern, a focusing effect for particles moving towards the nodes of the pressure distribution can be achieved (see Section 4.5.4.2). To model the configuration exploiting six IDTs, four 45° tilted IDTs composed by 10 couples of fingers are used together with other two IDTs (composed by 5 couples of fingers to maintain the same distances), aligned in the *x*-direction for a better propagation. Also in this case, the interaction between waves

is generating a grid pattern. The difference is that the waves interaction is reduced in a smaller region between the IDTs.

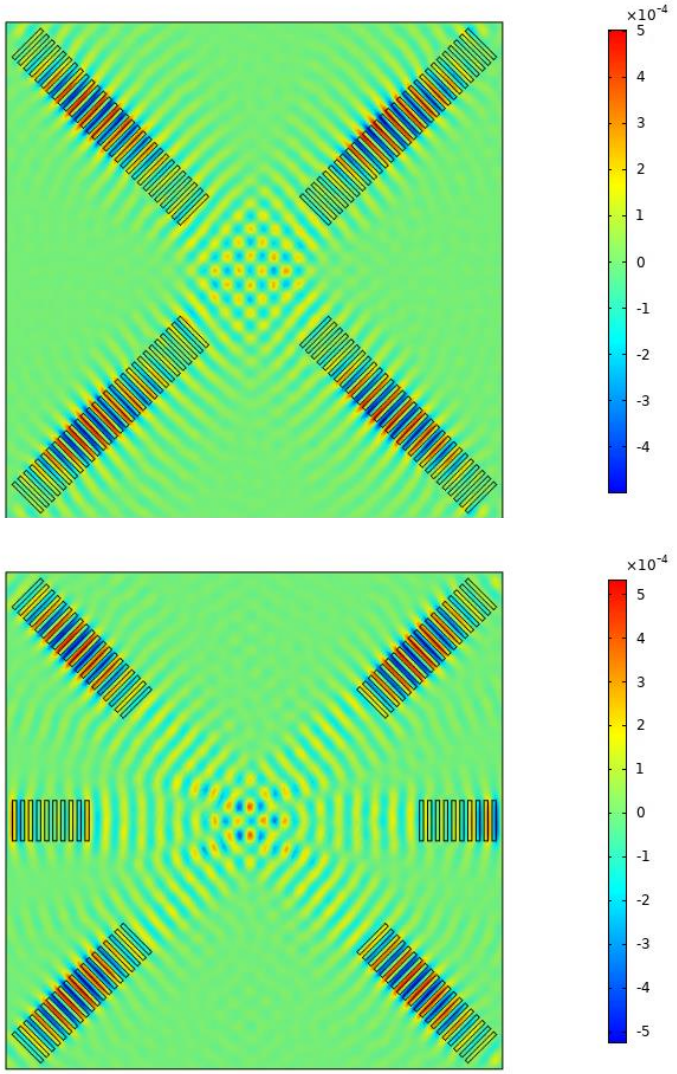

Figure 4.39: Interaction between waves with two different IDTs configurations. (Top) A configuration using 4 IDTs and (Bottom) 6 IDTs.

Other IDTs configurations have been studied just to see the interaction between waves. In Figure 4.40, a circular and a quarter-circular IDTs are modelled. In the case of the circular IDT, the substrate is modelled as a circle to simplify the computation and the dimensions are selected to generate an antinode in the centre of the circle. The pattern of the waves is clearly circular and propagating towards the centre. In Figure 4.40 the circle is cut due to the use of the axial-symmetric geometry to construct the model, but the system is simulated as an entire circle. The

other configuration, exploiting the use of two quarter-circular IDTs, is not generating a precise pattern, as was not expected. This kind of configuration is used to design acoustic tweezers to manipulate single particles. Then, a precise pattern of waves was expected, but not obtained. This result can be correlated to the anisotropic behaviour of the substrate: by managing the properties of the material used, it is possible to control the propagation of the waves to generate the interaction needed for particles manipulation.

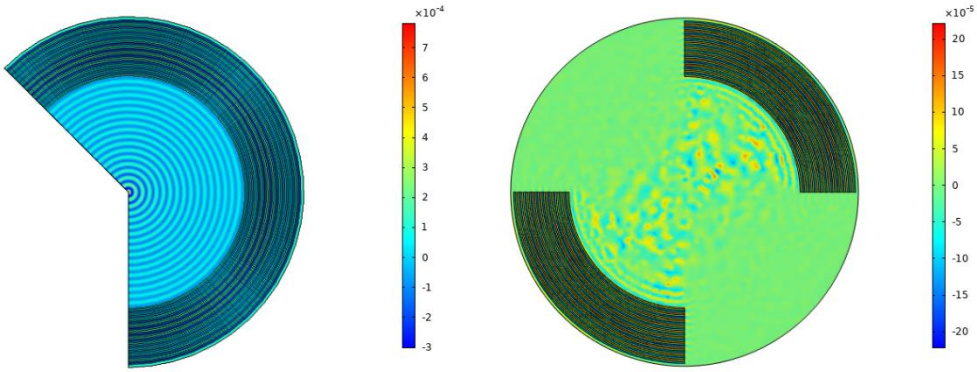

Figure 4.40: Two configurations exploiting the use of circular IDTs. (Left) A circular IDT, (Right) two quarter-circular IDTs.

4.5.4.2 PDMS channel and "pool" models

A PDMS channel and a PDMS squared-section "pool" are added to the model exploiting the co-operation of four IDTs. The interaction between the surface waves and the fluid domain leads to standing pressure waves inside the fluid and this pressure field can be used to manipulate particles.

A PDMS channel (100μm high, 1650μm wide, with the same length of the substrate) is placed on the lithium niobate substrate. The geometry of the channel is the same modelled for the three-dimensional device (50μm high, 280μm wide, with the same length of the substrate). A frequency domain analysis is performed to find the 3D pressure distribution inside the fluid domain which is exploited for particles focusing. Both the iso-surfaces of pressure and the trajectories of particles are reported in Figure 4.41. Two pressure nodes can be seen within the channel width, while along the length other nodes parallel to the x-direction are generated. This field is correlated to the waves pattern reported in Figure 4.39. Several

particles are moved towards the walls of the channel and freeze due to the effect of the vertical component of the acoustic radiation force (blue particles). The other particles, near the pressure nodes, are focalized toward the nodes parallel to the channel longitudinal axis because the fluid is moving along this direction dragging them. Also in this case, even if the pressure pattern is different with respect to the one obtained in the previous analysis (Section 4.4), the particles are moved exploiting the acoustic radiation force towards the pressure nodes being focalized. This result highlights the possibility to exploit the configuration made of four IDTs to improve the focusing effect on particles. Considering the standing surface waves distribution of Figure 4.39, by modifying the position and the width of the PDMS channel on the substrate it is possible to generate more than one pressure nodes.

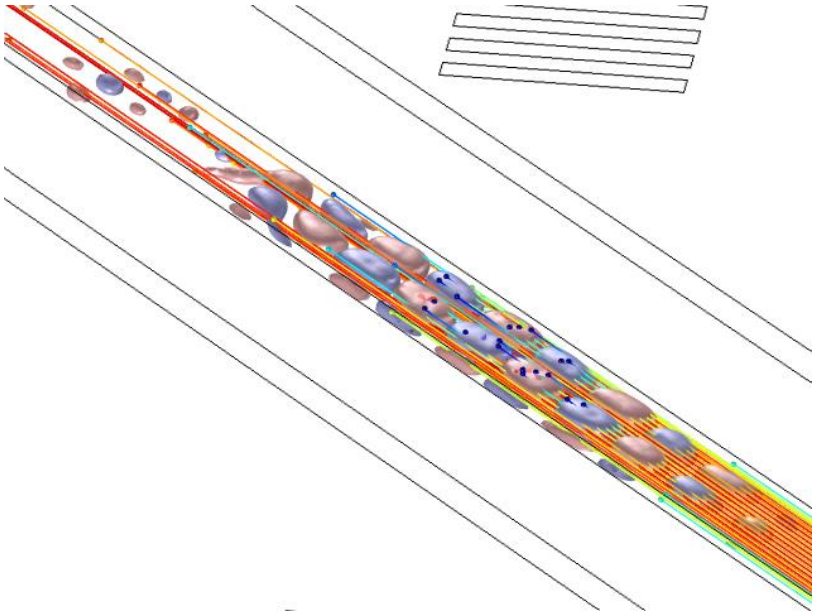

Figure 4.41: Iso-surfaces of pressure field and particles trajectories obtained using the configuration of 4 IDTs.

Finally, a PDMS structure, without the use of inlet and outlet for fluid flow, is considered to study the effect of distributed pressure nodes on particles suspended in a static fluid. Due to its shape, this structure is called “pool” and is simply a square-section PDMS chamber (the geometry is described in Section 4.5.1 and reported in Figure 4.37) containing water. In Figure 4.42, the z-displacements of the lithium niobate surface and the iso-surfaces of the pressure field are plotted. The presence of the PDMS structure influences the waves propagation, being the pattern

of the displacements different with respect to the one of Figure 4.39. The pressure field shows a regular distribution of pressure nodes and antinodes within the fluid domain. Maybe using a more refined mesh, the pressure distribution would be more precise.

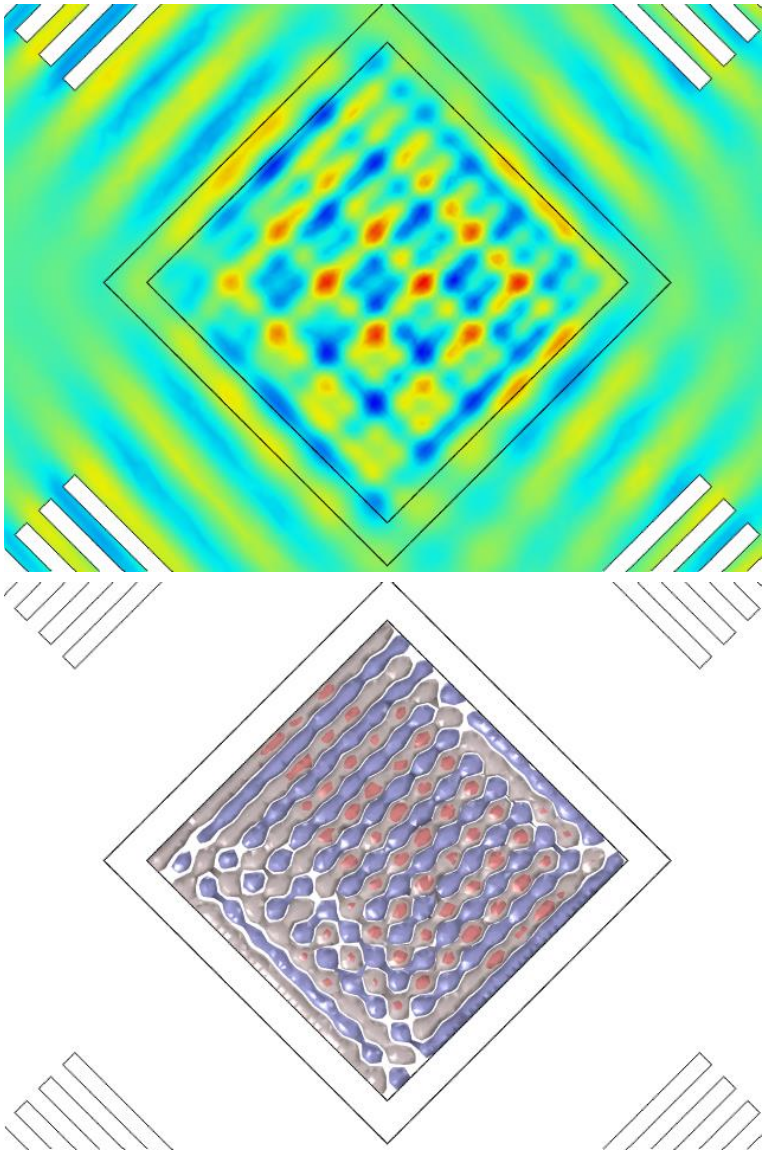

Figure 4.42: (Top) z-displacements and (Bottom) pressure iso-surfaces obtained by simulating a PDMS "pool" above the lithium niobate substrate.

Thirty-four particles are released into the fluid at the mid-height of the fluid domain in a cross shape along the diagonals of the square (seventeen for each diagonal). As seen in the other analysis performed (both the two-dimensional and the three-dimensional), the particles released in a position near the pressure antinodes are

pushed by the acoustic force towards the walls of the PDMS structure. The same effect is obtained in this analysis, except for a single particle (the blue particle in the middle of the images) which remains fixed in a pressure node trapped for all the 10s simulated. The particle moves up and down with little oscillations (in the order of 10μm) but always confined in the pressure node. Four images associated to different time instants are reported in Figure 4.43 (starting from the initial position of release, green particles).

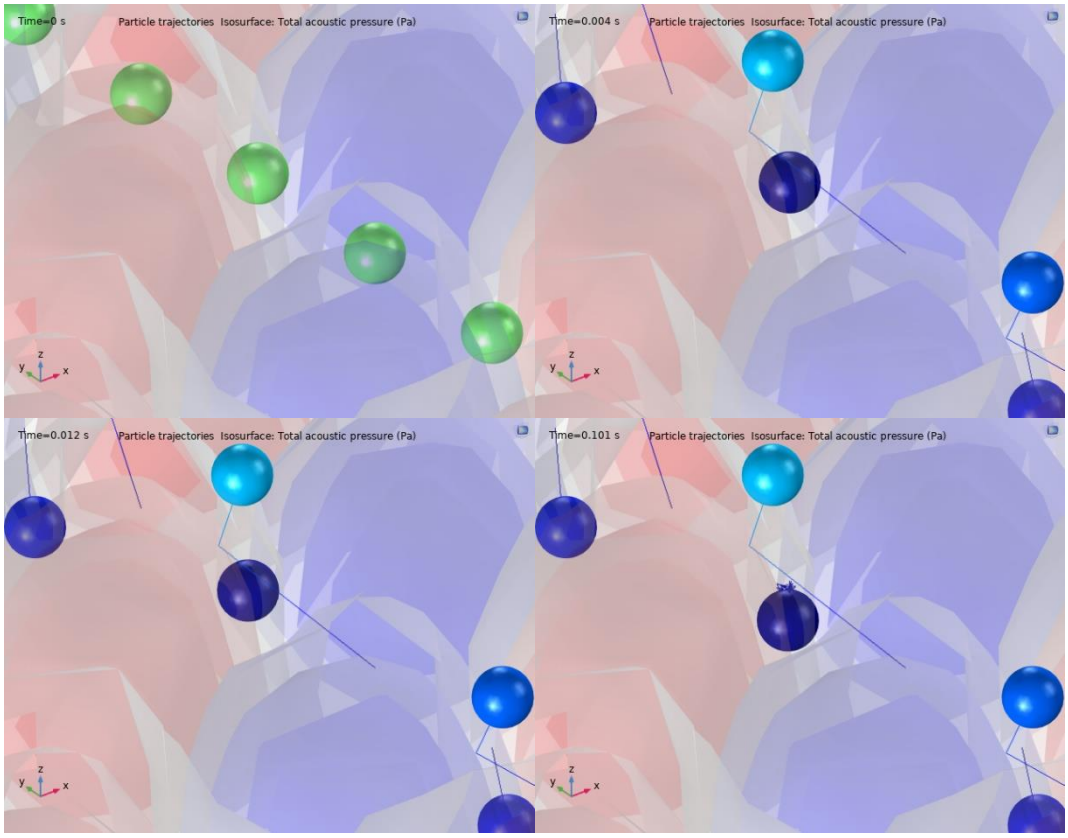

Figure 4.43: Particle trapped in one pressure node. The four instants reported are (Top-left) 0s, (Top-right) 0.004s, (Bottom-left) 0.012s and (Bottom-right) 0.101s.

Maybe, using a more structured and refined mesh, this trapping effect can be seen for more particles and not only one, being the pressure field more precise and structured. But the result obtained is interesting and confirms the possibility to manipulate single particles exploiting SSAW-devices and the correlated acoustophoresis phenomenon. Again, this result extends the versatility of this phenomenon with the possibility to be exploited for a large variety of applications (one example is the development of acoustic tweezers).

4.6 PDMS channel design and fabrication

A collaboration with the French university ESIEE Paris [103] brought to the production of a PDMS channel using maskless technologies to imprint the channel design on a SU-8 mold and exploiting the soft-lithographic technique to build the polymeric structure. All the process was performed in a clean-room (sealed building where a complex ventilation system is used to continuously remove dust and particulates which can interfere with the fabrication of micro-sized products), located in the university. The people coming from outside must clean their hands and their portable objects and completely cover their clothes and their body with an integral suit (from hairs to feet), to avoid the presence of any contaminating agent in the clean-room.
In this section, the design of the PDMS channel and the steps done for its production are reported. No experiments were performed on the fabricated system.

4.6.1 Y-shape channel design

The channel was designed considering a possible application exploiting bulk acoustic waves (BAWs), generated by actuating the PDMS through a piezoelectric transducer attached at the bottom of the structure. This structure should be composed by two parts in PDMS glued leaving the channel in between. The BAWs, travelling inside the PDMS, are transmitted to the fluid contained into the channel to develop pressure waves. To reflect the waves and produce a standing pressure field within the fluid, a glass slide can be placed on top of the structure to reflect back the waves which can interact in the region of the fluid. PDMS was chosen due to the faster process of production with respect to silicon or glass. Also, the PDMS channel can be exploited for the fabrication of a SAW-based device by gluing it on a piezoelectric substrate and generating the surface acoustic waves through IDTs deposed on it.
The formulation which correlates the resonant frequency of the system (and then the frequency of actuation of the piezoelectric transducer) with the width of the channel is:

$$f_n = n \cdot \frac{c}{2L} \tag{4.13}$$

where c is the speed of sound in the medium, L is the width of the channel and n is the number of nodes of the stationary waves within the channel. Therefore, knowing the speed of sound in the PDMS and the frequency of actuation (specific of the piezoelectric transducer used), is possible to evaluate the width of the channel to achieve the wanted number of nodes within the stationary pressure field. In this work, not having purchased a piezoelectric transducer (and then not knowing the frequency of actuation), the calculation has been done to obtain a design where a single pressure node will be achieved having a frequency of actuation around 500kHz. Then, the width of the channel was designed as 1mm and the corresponding frequency is 538kHz.

The channel is shown in Figure 4.44 (reporting a CAD image of the design simply done using Microsoft Office PowerPoint to highlight the dimensions of each part).

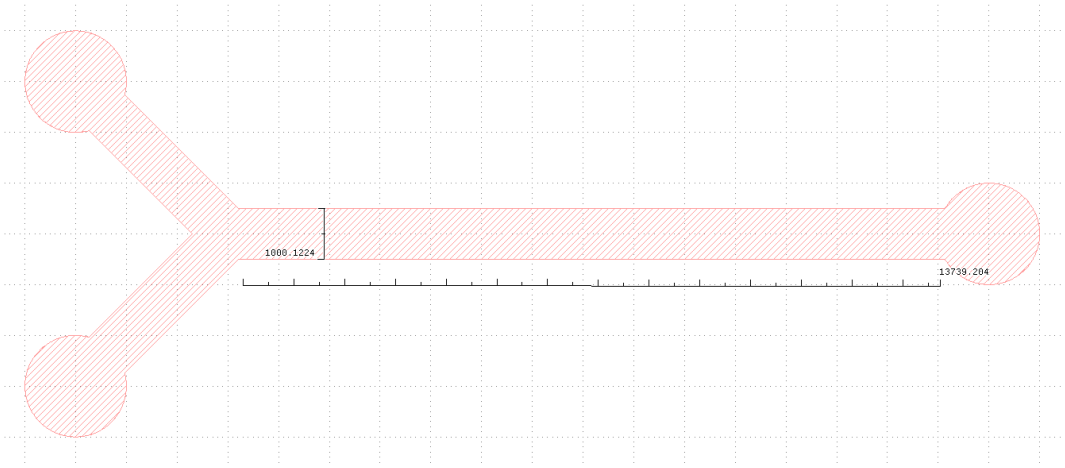

Figure 4.44: CAD design of the microchannel. The values reported are in µm.

Two inlets are provided (on the left) to introduce the fluid alone and the fluid containing particles. The width is around 1mm while the length of the central part is around 1.4cm. On the right, one single outlet can be seen. The system is intended to focus particles on the pressure node generated in the fluid flowing in the central region; therefore, one outlet only is enough. The diameter of the inlets and the outlet is 2mm while the distance between the two outlets is around 5mm.

The wavelength of the acoustic waves travelling in the PDMS is $\lambda = {}^{c}/_{f} = 2mm$. Then, both the PDMS blocks composing the structure, which contains the channel, must be designed with a height proportional to this wavelength to achieve a good interaction where the fluid is placed. Finally, the height of the channel is 25μm. Being this value very small with respect to the width of the channel, some bending instabilities can be generated when attaching the two PDMS parts, causing the upper boundary of the channel to touch the lower one.

4.6.2 SU-8 microfluidic mold

SU-8 2000 is a high contrast, epoxy-based photoresist designed for micromachining and other microelectronic applications, where a thick, chemically and thermally stable image is desired. This material is available with different compositions changing the density and the viscosity. The one used to produce the mold is the SU-8 2025 with a viscosity of 4500cSt and a density of 1.219g/ml.

Before spin-coating the photoresist on a silicon wafer (used as support substrate), the substrate must be polished and dry to obtain maximum process reliability. The silicon wafer undergoes different cleaning steps: first, HF (hydrofluoric acid) 1% solution is applied on the surface of the wafer for 30 seconds, then, two treatments exploiting H_2SO_4 (at 140°C for 3 minutes) and HNO_3 (fuming, for its tendency to release vapours, applied for 3 minutes) are performed and finally, the HF 1% is applied again for 20 seconds. After being polished, the silicon wafer is put into an oven at 250°C for 30 minutes, for the drying step, and then cooled down for 15 minutes.

Now, the SU-8 can be spin-coated on the silicon support. To achieve a height of 25μm, a recommended program is performed: dispense 1ml of resist for each inch of substrate diameter, spin at 500rpm for 5s with acceleration of 100rpm/s and again spin at 3000rpm for 30s with acceleration of 300rpm/s. In this way a uniform 25μm thick SU-8 layer is deposed on top of the silicon wafer. At this point, the system is left relaxing for 15 minutes before performing a soft-bake process, made by applying different temperatures in sequence (65°C for 1min, 95°C for 6min and again 65°C for 1min) to consolidate the SU-8 layer. After soft-bake, the system is relaxed for 5min.

The two-dimensional design of the channel (Figure 4.44) is imprinted on the photoresist with a maskless lithographic technique using the POLOS µPrinter equipment (shown in Figure 4.45) [45] which directly projects the image of the wanted pattern on the SU-8. Based on a µLCD projection technology compatible with a wide range of photoresists and substrates, the POLOS µPrinter equipment is mainly exploited for rapid prototyping with a good resolution down to 2μm. Of course, the greatest advantage of the technique is that no solid mask is needed to project the wanted image on the photoresist, avoiding the step of fabrication of different masks to imprint different patterns (which means time and money saving). Several attempts have been done to successfully achieve the precise image containing four channels disposed on the photoresist. The technology is still under development in the clean-room, then a precise process to work with this equipment is not reported. In the classic procedure the photoresist is impressed using a UV-light with an energy density of 220mJ/cm^2 applied in two steps of 15s. The exposed parts of the photoresist are cross-linked and survive to the chemical attack which will be performed in the development step (negative photoresist).

Figure 4.45: POLOS µPrinter equipment [45].

After the exposure, a post-exposure bake is performed with the same temperature steps used for the soft-bake (65°C for 1min, 95°C for 8min and again 65°C for 1min). After waiting 10min to leave the system relaxing, the development step can be performed. One specific developer formulation is sold together with the photoresist and is applied by immersion or spray to remove the non-exposed SU-8 with strong agitation of the system for 5-8 minutes. Then, rinsing in isopropyl alcohol for 10s is required to remove any residue of the photoresist. To dry the system pressurized air, ejected through a gun, is exploited. Finally, a hard-bake is required to ensure that the properties of the SU-8 do not change during use. Starting with the oven at room temperature, it is increased to 175°C and kept fixed for 30min.

By following all these steps, the SU-8 mold is fabricated on top of a silicon wafer used as solid support. The soft-lithographic technique must be performed now to fabricate the channel in PDMS.

4.6.3 PDMS soft-lithography

The soft-lithographic process is performed to fabricate the PDMS channel exploiting the produced SU-8 mold. The product used is called Sylgard 184 (sold by DOW®) [104], which is a polydimethylsiloxane (PDMS) elastomer. The advantages of this material are the low-cost, the high transparency (allowing easy inspection of the components), the rapid and versatile curing (both at room temperature or by heating) and the easy processing. The steps which must be performed in soft-lithography (see Figure 2.7) are: casting of the silicon polymer on the mold, inlets/outlets drilling, connection of the openings with external tubes and bonding of different parts (PDMS is usually bonded on another PDMS substrate or glass in microfluidic devices). In this section the process followed to fabricate the PDMS channel described in Section 4.6.1 are reported.

The mold is put in HDMS (hexaethyldisilazane, a derivative of ammonia with trimethylsilyl groups in place of two hydrogens) vapours to prepare the surface by removing the oxygen formed on it. HDMS chemically bonds its Si atoms to the oxygen of oxidized surfaces, releasing ammonia. Methyl groups form a hydrophobic surface which improves the resist wetting and adhesion properties.

PDMS must be mixed with a cross-linker. Using a syringe, the PDMS and the cross-linker are collected from their containers and released inside a baker. The PDMS is put into the baker before putting the cross-linker to achieve better results in terms of polymer cross-linking. The composition of the mixture is defined depending on the required properties for the final product which can be softer of harder. With a glass rod, the PDMS and the cross-linker are mixed and, in the solution, can be noticed the presence of some air bubbles. The solution is agitated in an ultrasonic bath (process that exploits ultrasonic waves to agitate fluids) to achieve a strong mixing between the two components. Finally, the solution is sealed in a vacuum chamber for 30min to release the gases.

One plastic box is covered with an aluminium foil, to reduce the adhesion with the PDMS solution, and is placed on the mold. This box is used to avoid PDMS leakages, therefore, the volume of PDMS needed to achieve the wanted dimensions for the PDMS must be calculated with respect to the box size. The PDMS/cross-linker solution is extracted from the vacuum chamber and is slowly poured on the mold, to avoid the generation of air bubbles. The system is then placed into an oven at 75°C for 2h to activate and perform the cross-linking process. The aluminium foil must be slowly and carefully peeled from the cured PDMS which, after that, is stripped from the mold.

For this work, the process stopped at this step, but other passages can be performed to obtain a complete PDMS microfluidic system. In this case, the mold is composed by four channels which should be divided by cutting the PDMS block to achieve the wanted size of the isolated structures. Using a calibrated needle, three holes to connect the outlet and the inlets to external tubes should be made by punching the needle in the circular regions of the design (see Figure 4.44). The last step provides the bonding between the different components of the microfluidic system (which could be made of PDMS or glass). Usually, oxygen plasma bonding is used for this purpose because this technique provides very good sealing avoiding any leaks from the microchannel. The plasma-cleaner available in the clean-room was purchased from Harrick Plasma® [105] and is connected to another machine which controls the injection of gases and the pressure into the vacuum chamber.

The device must be turned on and automatically starts to create vacuum using a build-in pump. The valve on the left of the machine is opened to inject oxygen into the chamber, in this way the vacuum is broken. To build again the vacuum, the valve is closed. This sequence is repeated for three times to inject a good amount of oxygen to generate the plasma. When the oxygen is enough, the wanted level of vacuum (in this case 300mtorr) can be set by opening the second valve on the right of the machine. The plasma is activated through a switch and kept working for 1min. To open the chamber, the atmospheric pressure must be obtained. After the treatment, the surfaces of the materials are activated (OH- groups replace methyl groups) and can be softly pressed together to bond them. To strengthen the bond between the two parts, the system can be placed in oven at 80°C for 20min.

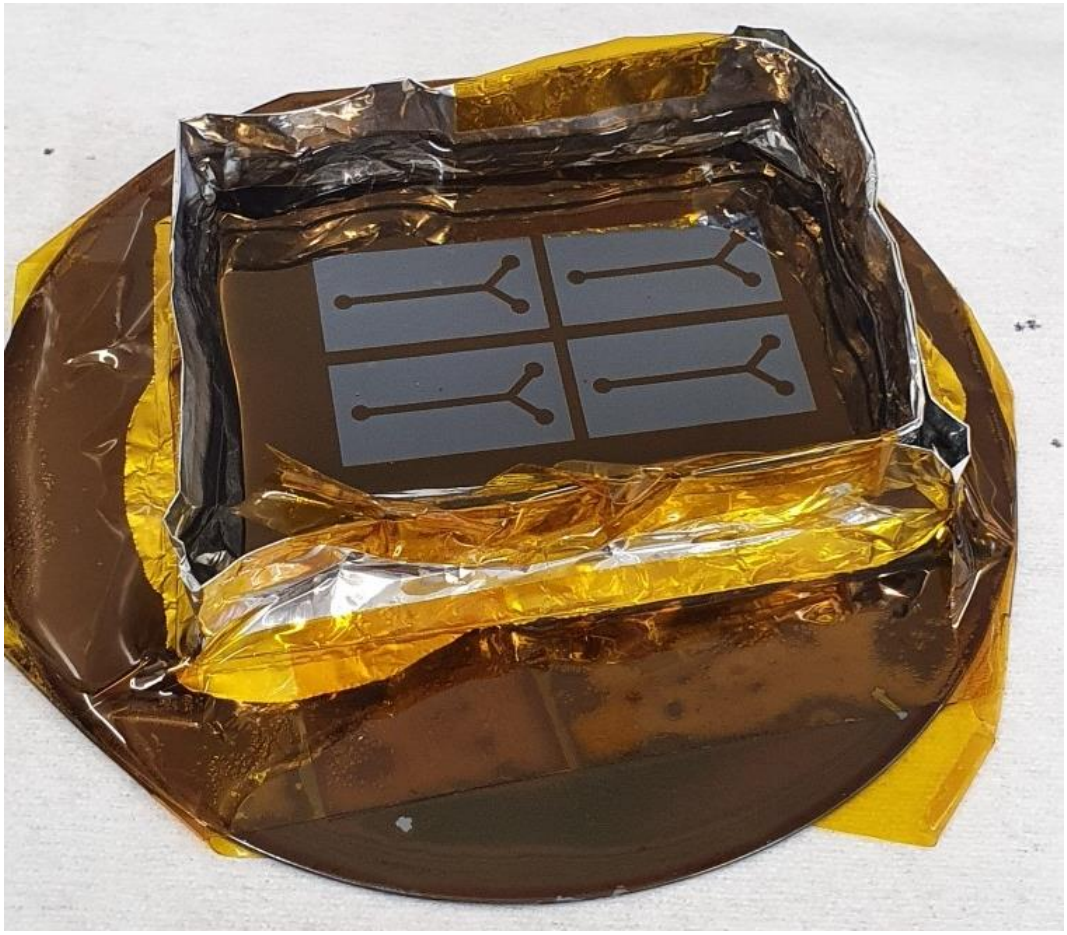

Figure 4.46: The plastic box, covered by an aluminium foil, containing the cured PDMS above the SU-8 mold.

The PDMS channel was only produced (see the PDMS on its mold in Figure 4.46), no experiments were performed exploiting it. Nevertheless, the fabrication of the

channel using soft-lithography was useful to experience the process and the importance of each step. In future, this design can be considered to model microfluidic devices which can be exploited for particles manipulation.

4.7 Summary of the numerical analyses

The results obtained in the different previously described analysis are summarized in the following sections.

4.7.1 Two-dimensional cross-section analyses

Different analyses were done considering different behaviours for the PDMS (non-flowing fluid or solid) and different device geometries. The analyses were performed on the cross-section of a SSAW-device for particles manipulation. One frequency domain analysis, considering the PDMS as a non-flowing fluid, provided a precise pattern for the pressure distribution within the fluid domain and the PDMS with a vertical pressure node in the centre of the channel cross-section. The acoustophoretic phenomenon was reported exploiting a time-domain particle tracing analysis: the particles were displaced by the acoustic radiation force towards the pressure nodes of the pressure distribution. The particles in this case (using the frequency which provided the higher values and the more precise distribution of pressure) were moved towards two regions near the mid-height of the channel, where two horizontal pressure nodes are generated, and they were confined in these regions.

Then, the PDMS was modelled as a linear elastic solid material and the analyses are performed again to compare the results with the PDMS modelled as a non-flowing fluid. The frequency domain analysis provided a precise and more real pattern of pressure, than the one obtained with the PDMS modelled as a fluid, with a pressure node in the centre of the channel. One time-domain analysis was also performed to see the development of the pressure field inside the fluid domain. In the case of solid PDMS, the particles near the centre were moved towards the vertical pressure node, while the other particles, following the shape of the pressure field, were displaced towards the walls of the channel, and then the focusing effect cannot be clearly demonstrated. These results were limited by the geometry of the

system: the 2D analysis done was too simple to simulate the acoustophoretic phenomenon because the drag force caused by the fluid flow was not simulated and the interaction between the components of the system was limited. By moving one IDT, the simulation of a phase shift between the signals applied to the IDTs, in a frequency domain analysis, was obtained. The displacement of the pressure node along the channel cross-section can be seen demonstrating the possibility of exploiting a phase shift of the signal to change the streamlines for the focusing of particles.

A sensitivity analysis on the geometrical features of the fluid domain and on the boundary conditions applied to the upper surface of the PDMS structure was performed. The results clearly show how the pressure field is influenced by the geometry of the channel: the height limit found is of 50μm, above which other lobes of pressure begin to develop generating other pressure nodes. These results were caused by the acoustic pressure waves interacting in the fluid with a specific wavelength and then by changing the geometry of the channel, the waves have different amount of space to interact and build the standing field. Also, the boundary conditions applied to the PDMS interacting with the fluid influence the pressure field. The best way to simulate the waves not being reflected and not generating interferences is to use the low-reflecting boundary condition for the upper boundary of the PDMS.

Finally, another design was modelled exploiting the use of SSAWs to manipulate particles. This “sandwich” design exploited the use of the same design of the cross-section view but mirrored, constructing two lithium niobate substrates interacting with one PDMS channel and the fluid. The pressure pattern obtained shows both a vertical pressure node in the centre of the channel and a horizontal node at the mid-height of the channel. in this way, the particles are supposed to be controlled in both the directions. The simulation of the trajectories of the particles moved them towards the horizontal nodes where are confined, in such a way that they can move along these nodes but never escape. This design cannot be realised as a real device due to the difficulty in actuation of the piezoelectric substrates together, being one of them flipped with respect to the other.

4.7.2 Three-dimensional device analyses

To achieve better results in terms of particles manipulation, a frequency domain analysis was performed on a simple three-dimensional SSAW-based device. Again, the pressure field distribution is precise showing a vertical pressure node in the centre of the channel. In this case, the particles are clearly focalized on the central pressure node being dragged along the channel by the fluid flowing in it.

The good result obtained was investigated by changing the diameter of the particles (8μm and 4μm were used) and the velocity of the fluid (1mm/s and 2mm/s were used). The direct proportionality between the volume of the particles and the acoustic radiation force was confirmed, being the 8μm diameter particles more affected by the acoustic pressure with respect to the 4μm diameter particles. Also, the effect of the drag force on particles focusing is considered by comparing the effect of different velocities for the fluid.

Finally, the lithium niobate substrate was investigated by changing the boundary conditions applied on the lateral surfaces. All the conditions considered (low-reflecting, symmetry and periodic condition of continuity) provided good results in terms of waves propagation and interaction. Also, the anisotropic nature of the lithium niobate was studied by modifying the elasticity matrix of the material. The material was modelled using its anisotropic matrix, a re-arranged isotropic matrix and a single value of elastic constant. The anisotropic material provided the best results, confirming that the characteristic anisotropic behaviour of piezoelectric materials is important to achieve a good interaction between waves to be transmitted to the fluid in the channel.

4.7.3 IDTs configurations and particle trapping analysis

The analysis done on the three-dimensional SSAW-based device was modelled considering the propagation of waves along the *x*-direction of the system and positioning the IDTs to generate waves along this direction. To investigate the anisotropic behaviour of the piezoelectric substrate, the direction of propagation was modified by tilting the IDTs with respect to the *x*-direction. A good interaction between counter-propagating waves was achieved by tilting the IDTs with a 45°

angle. The result obtained by this analysis was exploited to design other configurations for the IDTs to generate different interactions between waves and achieve new patterns on the surface of the substrate. Configurations using four IDTs (all tilted by 45°) and six IDTs (four tilted by 45° and two aligned with the *x*-direction) were modelled. The pattern shows the presence of alternated regions corresponding to nodes and antinodes different with respect to the one obtained in the 3D device analysis: the distribution is not made by parallel lines but more like a grid presenting point regions where the pressure field should show a precise distribution of nodes. Considering these results, two new analyses were performed simulating a PDMS channel and a PDMS squared-section "pool" above the substrate to investigate the shape of the pressure field and the interaction with particles. The pressure field within the channel shows the presence of two pressure nodes. Several particles were injected into the fluid being focused on the nodes of the field, confirming the acoustophoretic phenomenon also for different patterns of acoustic pressure. The pressure field developed within the "pool" (where a static fluid is placed) should be used for particles trapping: the particles should be displaced by the acoustic radiation force to reach the pressure nodes, being then trapped inside these regions. This effect is achieved by one particle only in the analysis performed but is enough to conclude that the trapping phenomenon can be simulated and achieved in reality, by generating specific pressure distributions in fluids.

5 Conclusions and future developments

In this thesis, acoustofluidics exploited for particle manipulation (called acoustophoresis) was investigated. Bulk acoustic waves (BAWs) and surface acoustic waves (SAWs) are two types of waves used to develop acoustofluidic devices. This work focused on the use of standing surface acoustic waves (SSAWs), one type of SAWs, to study the interaction of particles with a generated standing acoustic pressure field within a fluid. Particles and bio-particles are displaced by the acoustic radiation force, developed by the acoustic pressure, towards the pressure nodes, regions of zero pressure.

The intention of this work was to exploit a numerical analysis software (COMSOL Multiphysics) to study the acoustophoretic phenomena dominated by acoustic radiation force in SSAW-based microfluidic devices. One reference paper dealing with a real SSAW-based device was used to critically examine the numerical procedure proposed to model this kind of devices. Several modifications have been done on the model described by the paper (geometry, boundary conditions, mesh elements size). Nevertheless, this reference was useful to have a starting point to understand how to model the problem. The system is composed by a PDMS channel placed between two interdigital transducers (IDTs) deposed on top of a piezoelectric substrate. The application of an external electrical field to the IDTs activates the converse piezoelectric effect to generate surface waves on the surface of the piezoelectric substrate. Different steps were considered to model the device and to provide a complete understanding of the problem. First of all, the transversal cross-section was modelled to investigate the effects of changing geometrical features of the channel and the boundary conditions applied to the components on pressure field developed within the fluid. After that, a three-dimensional analysis on the complete device was performed to correlate all the forces involved in the problem (the drag force generated by the fluid flow and the acoustic radiation force generated by the acoustic pressure field). Finally, different configurations of the IDTs positioning above the piezoelectric substrate have been simulated to investigate the anisotropic behaviour of the material and the interaction of the

waves coming from different directions. Seen the results obtained by this analysis, a device exploiting a PDMS "pool" for particle trapping has been modelled.

The analysis on the cross-section of the device was performed first by modelling the PDMS as a non-flowing fluid (through the pressure acoustics interface) and then by modelling it as a linear elastic solid (through the solid mechanics interface). The first analysis was performed emulating the model proposed in the reference paper [99] but changing some geometrical parameters (the width of the substrate, the distance between the IDTs and the width of the fluid domain). The pattern of the pressure field obtained is precise, showing the sought vertical pressure node in the middle of the channel, and the magnitude of pressure is similar to the one obtained by the reference. The presence of two horizontal pressure nodes near the mid-height of the channel is an important difference achieved with respect to the reference paper: the particles, being displaced by the acoustic radiation force, are displaced towards these horizontal nodes and forced to move along them never escaping. This result is good to demonstrate the effect of the radiation force on the particles but the focusing effect on the central pressure node is not achieved. Then, to simulate a more real situation, the PDMS was modelled as a linear elastic solid to completely describe the interactions between the solid materials, where shear waves can propagate, and the fluid. Also in this case, the pressure distribution is precise showing the central pressure node while the magnitude is reduced. This result can be explained considering the interaction between the fluid and the PDMS, not simulated in the previous analysis where between the fluid and the PDMS a continuity condition was applied. To simulate a phase shift of the signal applied to one IDT, a parametric sweep analysis was done to displace the IDT by fractions of the wavelength. The results demonstrate that by modifying the phase of the signal is possible to manage the trajectory of the particles by moving the central pressure node. The trajectories of the particles, moved by the acoustic radiation force, follow the shape of the pressure field being displaced towards the central node, if released in this region, or towards the upper and lateral walls of the channel, if released far from the central node. The solution modelling the PDMS as a solid is better in terms of particles control and pressure distribution within the fluid, therefore this model is used to investigate how the pressure field changes by modifying some parameters

such as the geometrical features (height and width) of the channel and the boundary conditions applied on the upper boundary of the solid PDMS (low-reflecting, free surface and fixed constraint). The limit value for the height of the channel was found to be around 50μm, above this value other nodes appear in the pressure distribution, changing the effect of the acoustic radiation force. Changing the width, the pressure field generated shows two antinodes and one central node until the width of the channel is equal to the wavelength of the surface waves propagating on the piezoelectric substrate, therefore the channel must be as wide as the wavelength to obtain the pattern with a single central pressure node. The best boundary condition to be used for the upper surface of the PDMS is the low-reflecting one, which makes all the waves being transmitted and never reflected to generate interferences in the pressure field. This boundary condition provides a good solution to the problem and can be achieved in real devices by exploiting thick PDMS structures above the channel cavity. Finally, another geometry consisting of a "sandwich" device is simulated. This model is made by two piezoelectric substrates, actuated by two IDTs, attached to a PDMS channel to generate a pressure field in the fluid. With this specific geometry, one horizontal pressure node and a vertical central node were achieved, and the particles can be controlled in both the directions.

An analysis on the three-dimensional device was performed by extruding the cross-section by a 2mm length. This analysis provides the same results obtained in 2D but with a more precise and complete solution in terms of pressure field and particle manipulation. The acoustophoretic phenomenon of particle focusing on the central pressure node was obtained and the particles are collected at the outlet of the channel being dragged by the flowing fluid. Two different sizes of particles have been released in the channel by changing the diameter (8μm and 4μm) and the acoustic radiation force have been demonstrated to be more effective in displacing bigger particles being directly proportional to their volume. Also, two velocities (1mm/s and 2mm/s) have been applied to the fluid, to investigate the effect of the drag force on the manipulation. The particles travelling for the same distance are less focused when reaching the outlet if dragged by a greater force (being the acoustic radiation force not influenced by the fluid velocity). Two further analyses

were done on the three-dimensional device to investigate the propagation and the interaction of the surface waves by applying different boundary conditions (low-reflecting, symmetry and periodic condition of continuity) to the lateral surfaces of the piezoelectric substrate and by modifying the elasticity matrix to simulate an isotropic material. Again, the low-reflecting boundary condition provides the best results both in terms of displacement and pressure distribution and magnitude. The anisotropic behaviour of the material, from the results, seems to be fundamental to generate and propagate the surface acoustic waves on the substrate. By simulating the material as isotropic, the propagation of the surface waves is limited and the interaction seems not to be constructive in the region where the channel is placed.
Finally, to further investigate the propagation of the waves on an anisotropic material and the interaction between counter-propagating waves, different configurations were analysed by modifying the position of the IDTs on the piezoelectric material. First, the direction of propagation was changed by tilting the IDTs with respect to the *x*-direction of the system (the direction considered for the 3D device of the previous analysis). The best interaction has been obtained tilting the IDTs by a 45° angle. Then, considering this result, two configurations exploiting respectively four and six IDTs were modelled using four 45° tilted IDTs (in the four IDTs configuration) and adding to them two IDTs aligned in the *x*-direction (in the six IDTs configuration). The analysis provides simple patterns generated by the interaction between waves: a sort of grid of nodes and antinodes were generated in the region between the used IDTs. Seen the plot, two analyses were done to position on top of the piezoelectric substrate a PDMS channel and a PDMS squared-section structure containing a static fluid (without inlet and outlet for fluid flow). In the channel, two pressure nodes are obtained where the particles can be focused by the acoustic radiation force. In the squared "pool" several particles have been dispersed with the intention of being trapped inside the pressure nodes of the grid dot-like distribution of the pressure field. Only one particle is successfully controlled remaining fixed in one pressure node (with small oscillations) for the 10s simulated.

The results achieved in this work can be considered to fabricate SSAW-based devices for particles manipulation. The configuration made of two IDTs is effective in focusing particles on the pressure nodes, as demonstrated by the 3D device

model. Moreover, the parametric analyses, performed by changing the geometrical features of the microchannel, show how the pressure field is influenced by the standing surface waves generated on the piezoelectric substrate, providing a tool to design the best structure. Also, the model of the "pool" in the four IDTs configuration provide another interesting solution which can be exploited to trap or agglomerate particles in specific positions where the pressure nodes are located, as shown in the results reporting the trajectories of the particles released in the "pool". The same effect can be achieved exploiting the circular IDT configuration, where the particles should be trapped in the centre of the concentric circular waves pattern. These are kinds of configurations which can be used to fabricate two-dimensional acoustic tweezers (being the standing field produced by actuating the IDTs from two different directions), which can be built to manipulate single particles or generate cell spheroids.

To conclude, the results obtained are interesting and useful to demonstrate the important role of numerical analysis to investigate physical phenomena and real devices. The acoustophoresis applied on solid microparticles have been achieved. Future developments of the model can consider providing a better control on the meshing conditions applied to the components of the device to increase the efficiency of the model. Of course, by improving the meshing conditions, the time required for the simulations and the computation effort requested by the machine will be increased. Nevertheless, this improvement can lead to a more precise and real distribution of the pressure waves within the fluid domain and then to a better control of particles, which could be moved more precisely in the horizontal direction avoiding them being displaced towards the walls of the channel obtaining more real results. For sure, several other geometries can be investigated to obtain new effects caused by the interaction of the surface waves and the fluid. For example, systems exploiting separated regions, where the frequency of actuation of the IDTs is different, can be modelled to sort particles with different physical properties (for example different materials or species) and to collect them at separated outlets. This problem is difficult to be modelled using COMSOL, different software should be considered to improve the analysis. Other geometrical parameters of the device can be modified to investigate the correlated effects: the

distance between the IDTs and the channel, the length and the number of the fingers constituting the IDTs. The final goal of the numerical analyses is to optimize the geometry of the device, precisely control the mesh to avoid mesh-dependent solutions and carefully select the boundary conditions associated to the physics involved in the problem to achieve a high efficiency in particles control. Moreover, different materials can be used, then, a further step to be done exploiting numerical analysis can be a comparison between the effects caused by the use of different materials constituting the microchannel. The material chosen in the reported analyses was PDMS due to the easy fabrication associated to the soft-lithographic technique and the biocompatibility of the material with aqueous fluids. But microchannels can also be made in silicon, glass or SU8 (photoresist), which have different mechanical properties than PDMS leading to different interaction with the fluid. One last development which can be implemented in the numerical analyses is the simulation of non-spherical and deformable particles. This feature is important, for example, to study blood diseases which modify the mechanical properties of the red blood cells. In this case, the particles interact in different ways with the standing pressure field, being differently manipulated. The separation of different cells can be achieved exploiting the acoustic radiation force. Again, this feature cannot be simulated using COMSOL, then another software should be used.

6 Bibliography

[1] R. Habibi, V. He, S. Ghavamian, A. de Marco, T.-H. Lee, M.-I. Aguilar, D. Zhu, R. Lim, A. Neild, "Exosome trapping and enrichment using a sound wave activated nano-sieve (SWANS)", *Lab on a chip*, vol. 20, n. 19, pp. 3633-3643, 2020.

[2] B. Song, J. Yu, Y. Sun, Q. Wang, S. Xu, Y. Jia, S. Lin, Y. Zhang, C. Wang, Y. Zhang, X. Zhang, "Microfluidics for the rapid detection of Escherichia coli O157:H7 using antibody-coated microspheres", *Bioengineered*, vol. 12, n. 1, pp. 392-401, 2021.

[3] G. M. Whitesides, "The origins and the future of microfluidics", *Nature*, vol. 442, n. 7101, pp. 368-373, 2006.

[4] B. Cetin, M. B. Ozer, M. E. Solmaz, "Microfluidic bio-particle manipulation for biotechnology", *Biochemical Engineering Journal*, vol. 92, pp. 63-82, 2014.

[5] D. Erickson, D. Li, "Integrated microfluidic devices", *Analytica Chimica Acta*, vol. 507, pp. 11-26, 2004.

[6] N. Convery e N. Gadegaard, "30 years of microfluidics", *Micro and Nano Engineering*, vol. 2, pp. 76-91, 2019.

[7] B. Yılmaz, F. Yılmaz, "Lab-on-a-chip technology and its applications", *Omics Technologies and Bio-Engineering*, Academic Press, chapter 8, pp. 145-153, 2018.

[8] P. Yager, T. Edwards, E. Fu, K. Helton, K. Nelson, M. R. Tham e B. H. Weigl, "Microfluidic diagnostic technologies for global public health", *Nature*, vol. 442, n. 7101, pp. 412-418, 2006.

[9] L. Chen, J. J. Kim, P. S. Doyle, "Microfluidic platform for selective microparticle parking and paired particle isolation in droplet arrays", *Biomicrofluidics*, vol. 12, n. 2, 2018.

[10] J. Friend e L. Yeo, "Microscale acoustofluidics: microfluidics driven acoustics and ultrasonics", *Review of modern physics*, vol. 83, n. 2, pp. 647-687, 2011.

[11] P. Li, T. J. Huang, “Applications of acoustofluidics in bioanalytical chemistry”, *Analytical Chemistry*, vol. 91, n. 1, pp. 757-767, 2019.

[12] M. Hill, N. R. Harris, R. Townsend, S. Beeby, N. M. White, Y. Shen, W. T. Coakley, J. J. Hawkes “A microfluidic device for ultrasonic separation”, *Forum Acusticum - 3rd EAA European Congress on Acoustics, Sevilla, Spain*, 6 pp, 2002.

[13] N. R. Harris, M. Hill, S. Beeby, Y. Shen, N. M. White, J. J. Hawkes, W. T. Coakley, “A silicon microfluidic ultrasonic separator”, *Sensors and Actuators B: Chemical*, vol. 95, n. 1, pp. 425-434, 2003.

[14] T. Laurell, F. Petersson, A. Nilsson, “Chip integrated strategies for acoustic separation and manipulation of cells and particles”, *Chemical Society Reviews*, vol. 36, n. 3, pp. 492-506, 2007.

[15] A. Fornell, C. Johannesson, S. S. Searle, A. Happstadius, J. Nilsson, M. Tenje, "Trapping of Cell-Laden Hyaluronic Acid-Acrylamide Hydrogel Droplets using Bulk Acoustic Waves", *20th International Conference on Solid-State Sensors, Actuators and Microsystems & Eurosensors XXXIII (TRANSDUCERS & EUROSENSORS XXXIII), Berlin, Germany*, pp. 2352-2355, 2019.

[16] S. Shiokawa, Y. Matsui, T. Moriizumi, “Experimental Study on Liquid Streaming by SAW”, *Japanese Journal of Applied Physics*, vol. 28, n. 1, pp. 126-128, 1989.

[17] A. Wixforth, C. Strobl, C. Gauer, A. Toegl, J. Scriba, Z. Guttenberg, “Acoustic manipulation of small droplets”, *Analytical and Bioanalytical Chemistry*, vol. 379, pp. 982-991, 2004.

[18] T. Uchida, T. Suzuki, S. Shiokawa, "Investigation of acoustic streaming excited by surface acoustic waves," *IEEE Ultrasonics Symposium. Proceedings. An International Symposium, Seattle, WA, USA*, vol.2, pp. 1081-1084, 1995.

[19] G. Simon, Y. Pailhas, M. A. B. Andrade, J. Reboud, J. Marques-Hueso, M. P. Y. Desmulliez, J. M. Cooper, M. O. Riehle, A. L. Bernassau, "Particle separation in surface acoustic wave microfluidic devices using

reprogrammable, pseudo-standing waves", *Applied Physics Letters*, vol. 113, n. 4, 2018.

[20] H. Bruus, "Acoustofluidics 1: Governing equations in microfluidics", *Lab on a Chip*, vol. 11, n. 22, pp. 3742-3751, 2011.

[21] S. C. Terry, J. H. Jerman, J. B. Angell, "A gas chromatographic air analyzer fabricated on a silicon wafer", *IEEE Transactions on Electron Devices*, vol. 26, n. 12, pp. 1880-1886, 1979.

[22] J.C. McDonald, D.C. Duffy, J.R. Anderson, D.T. Chiu, H. Wu, O.J.A. Schueller, G.M. Whitesides, "Fabrication of microfluidic systems in poly(dimethylsiloxane)", *ELECTROPHORESIS*, vol. 21, pp. 27-40, 2000.

[23] A. Fornell, "Acoustic manipulation of cells and microbeads in droplet microfluidics", *Lund: Department of Biomedical Engineering, Lund university*, 2018.

[24] S. Sohrabi, N. Kassir, M.K. Moraveji, "Droplet microfluidics: fundamentals and its advanced applications", *RSC Advances*, vol. 10, pp. 27560-27574, 2020.

[25] J. Novotný, F. Foret, "Fluid manipulation on the micro-scale: Basics of fluid behavior in microfluidics", *Journal of Separation Science*, vol. 40, pp. 383-394, 2017.

[26] Y. A. Cengel, J. M. Cimbala, "Meccanica dei fluidi", *Milano: McGraw-Hill*, 2006.

[27] T. M. Squires, S. R. Quake, "Microfluidics: Fluid physics at the nanoliter scale", *Review of Modern physics*, vol. 77, n. 3, pp. 977-1026, 2005.

[28] D. Huang, K. Wang, Y. Wang, H. Sun, X. Liang, T. Meng, "Precise control for the size of droplet in T-junction microfluidic based on iterative learning method", *Journal of the Franklin Institute*, vol. 357, n. 9, pp. 5302-5316, 2020.

[29] A. Lenshof, C. Magnusson, T. Laurell, "Acoustofluidics 8: Applications of acoustophoresis in continuous flow microsystems", *Lab on a chip*, vol. 12, n. 7, pp. 1210-1223, 2012.

[30] M. Wiklund, R. Green, M. Ohlin, "Acoustofluidics 14: Applications of acoustic streaming in microfluidic device", *Lab on a Chip*, vol. 12, n. 14, pp. 2438-2451, 2012.

[31] M. Wu, A. Ozcelik, J. Rufo, Z. Wang, R. Fang, T. J. Huang, "Acoustofluidics separation of cells and particles", *Microsystem and Nanoengineering*, vol. 5, n. 32, pp. 1-18, 2019.

[32] M. Wiklund, "Acoustofluidics 12: biocompatibility and cells viability in microfluidic acoustic resonators", *Lab on a chip*, vol. 12, n. 11, pp. 2018-2028, 2012.

[33] T. Leong, L. Johansson, P. Juliano, S. L. McArthur e R. Manasseh, "Ultrasonic separation of particulate fluids in small and large scale systems: a review", *Industrial & Engineering Chemistry Research*, vol. 52, pp. 16555-16576, 2013.

[34] Y. Gao, M. Wu, Y. Lin e J. Xu, "Acoustic microfluidic separation techniques and bioapplications: a review", *Micromachines*, vol. 11, n. 10, pp. 900-921, 2020.

[35] A. Arnau, D. Soares "Fundamental of piezoelectricity", in "Piezoelectric transducers and applications", *Springer – Verlag Berlin Heidelberg, second edition*, pp. 1-38, 2008.

[36] A. Čeponis, D. Mažeika, "Piezoelectric systems as an alternative energy source", *Mokslas – Lietuvos Ateitis / Science – Future of Lithuania*, vol. 6, n. 6, pp. 676-681, 2015.

[37] H. Wang, A. Jasim, "Piezoelectric energy harvesting from pavement", *Woodhead Publishing Series in Civil and Structural Engineering, Eco-Efficient Pavement Construction Materials, Woodhead Publishing*, pp. 367-382, 2020.

[38] S. O. R. Moheimani, A. J. Fleming, "Fundamentals of Piezoelectricity" in "Piezoelectric Transducers for Vibration Control and Damping", *Springer – Verlag London*, pp. 9-13, 2006.

[39] S. Sharma, R. Kumar, M. Talha, "Design of spatially varying electrical poling for enhanced piezoelectricity in $Pb(Mg_{1/3}Nb_{2/3})O_3$–

0.35PbTiO$_3$", *International Journal of Mechanics and Materials in Design*, vol. 17, pp. 99–118, 2021.

[40] R. S. Weis, T. K. Gaylord, "Lithium niobate: Summary of physical properties and crystal structure", *Applied Physics A*, vol. 37, pp. 191-203, 1985.

[41] W. Connacher, N. Zhang, A. Huang, J. Mei, S. Zhang, G. Tilvawala, J. Friend, "Micro/nano acoustofluidics: materials,phenomena, design, devices, and applications", *Lab on a Chip*, vol. 18, n. 14, pp. 1952-1996, 2018.

[42] "PDMS microfluidics fabrication", *Baskin Engineering UC Santa Cruz* (https://cleanroom.soe.ucsc.edu/microfluidics).

[43] T. Betancourt, L. Brannon-Peppas, "Micro- and nanofabrication methods in nanotechnological medical and pharmaceutical devices." *International journal of nanomedicine*, vol. 1, n. 4, pp. 483-495, 2006.

[44] R. Menon, A. Patel, D. Gil, H. I. Smith, "Maskless lithography", *Materials Today*, vol. 8, n. 2, pp. 26-33, 2005.

[45] "Maskless lithography system, POLOS μPrinter", *SPS Europe*. (System datasheet: https://devmatech.pl/wp-content/uploads/2605-Datasheet-SPS-2020-POLOS-Micro-Printer.pdf).

[46] B.K. Gale, M.A. Eddings, S.O. Sundberg, A. Hatch, J. Kim, T. Ho, S.M. Karazi, "Low-Cost MEMS Technologies", *Reference Module in Materials Science and Materials Engineering, Elsevier*, ch. 4.1.1, 2016.

[47] G. V. Casquillas, T. Houssin, "Introduction to PDMS soft lithography and polymer molding for microfluidics", *Microfluidic reviews, Elveflow*, *Paris, France*.

[48] A. Shakeri, S. Khan, T. F. Didar, "Conventional and emerging strategies for the fabrication and functionalization of PDMS-based microfluidic devices", *Lab on a chip*, vol. 21, n. 16, pp. 3053-3075, 2021.

[49] A. Jilani, M. S. Abdel-wahab, A. H. Hammad, "Advanced deposition techniques for thin films and coatings", in "Modern technologies for

creating the thin-film systems and coatings", *IntechOpen, London, England,* ch. 8, 2017.

[50] "Liftoff procedure SOP", *University of Louisville, Micro/nano technology center*, 2020 (Liftoff procedure document: https://louisville.edu/micronano/files/documents/standard-operating-procedures/Liftoff_SOP.pdf)

[51] A. Lenshof, M. Evander, T. Laurell, J. Nilsson, "Acoustofluidics 5: Building microfluidic acoustic resonators", *Lab on a Chip,* vol. 12, n. 4, pp. 684-695, 2012.

[52] J. J. Hawkes, M. Groschl, E. Benes, H. Nowotny, T. W. Coakley, "Positioning particles with liquids using ultrasound force fields", *Proceedings: Forum Acusticum, Sevilla, Spain, Special session: Acoustics of Dispersed Particulate Matter*, 2002.

[53] J. J. Hawkes, T. W. Coakley, "Force field particle filter, combining ultrasound standing waves and laminar flow", *Sensor and Actuators*, vol. B, n. 75, pp. 213-222, 2001.

[54] M. Evander, A. Lenshof, T. Laurell, J. Nilsson, "Acoustophoresis in Wet-Etched Glass Chips", *Analytical Chemistry*, vol. 80, n. 13, pp. 5178-5185, 2008.

[55] A. V. Mamishev, K. Sundara-Rajan, F. Yang, Y. Du, M. Zahn, "Interdigital sensors and transducers", *Proceedings of the IEEE*, vol. 92, n. 5, pp. 808-845, 2004.

[56] Y. Q. Fu, J. K. Luo, N. T. Nguyen, A. J. Walton, A. J. Flewitt, X. T. Zu, Y. Li, G. McHale, A. Matthews, E. Iborra, H. Du, W. I. Milne, "Advances in piezoelectric thin films for acoustic biosensors, acoustofluidics and lab-on-chip applications", *Progress in Material Science,* vol. 89, pp. 31-91, 2017.

[57] L. Rayleigh, "On Waves Propagated along the Plane Surface of an Elastic Solid", *Proceedings of the London Mathematical Society*, vol. s1, n. 1, pp. 4-11, 1885.

[58] N. Fourati, J. Fougnion, L. Rousseau, P. Lepeut, O. Français, P. Boutin, C. Vedrine, J. Bonnet, B. Mercier, C. Pernelle, "Surface Acoustic Love

Waves Sensor for Chemical and Electrochemical Detection", *Proceedings of ESDA 2006: 8th Biennial Conference on Engineering Systems Design and Analysis, Torino, Italy*, pp. 973-980, 2006.

[59] X. Ding, P. Li, S. S. Lin, Z. S. Stratton, N. Nama, F. Guo, D. Slotcavage, X. Mao, J. Shin, F. Costanzo, T. J. Huang, "Surface acoustic waves microfluidics", *Lab on a Chip*, vol. 13, n. 18, pp. 3626-3649, 2013.

[60] T. Wang, Q. Ni, N. Crane et al., "Surface acoustic wave-based pumping in a microchannel", *Microsystem Technologies*, vol. 23, pp. 1335–1342, 2017.

[61] M. Gedge, M. Hill, "Acoustofluidics 17: Theory and applications of surface acoustic wave devices for particle manipulation", *Lab on a Chip*, vol. 12, n. 17, pp. 2998-3007, 2012.

[62] G. Destgeer, H. J. Sung, "Recent advances in microfluidic actuation and micro-object manipulation via surface acoustic waves", *Lab on a Chip*, vol. 15, n. 13, pp. 2722-2738, 2015.

[63] A. Doinikov, "Acoustic radiation forces: Classical theory and recent advances", in "Recent Research Developments in Acoustics" *Transworld Research Network*, vol. 1, pp. 39-67, 2003.

[64] B. Jakoby, M. J. Vellekoop, "Properties of Love waves: applications in sensors", *Smart materials and structures*, vol. 6, n. 6, pp. 668, 1997.

[65] M. Puiu et al., "Enhanced sensitive love wave surface acoustic wave sensor designed for immunoassay formats", *Sensors*, vol. 15, n. 5, pp. 10511-10525, 2015.

[66] A. A. Doinikov, "On the radiation pressure on small particles", *The Journal of the Acoustical Society of America*, vol. 100, n. 2, pp. 1231, 1998.

[67] K. Sritharan, C. J. Strobl, M. F. Schneider, A. Wixforth, Z. Guttenberg, "Acoustic mixing at low Reynold's numbers" *Applied Physics Letter*, vol. 88, n. 5, 2006.

[68] R. Shilton, M. K. Tan, L. Y. Yeo, J. R. Friend, "Particle concentration and mixing in microdrops driven by focused surface acoustic waves", *Journal of Applied Physics*, vol. 104, n. 1, 2008.

[69] T. Frommelt, M. Kostur, M. Wenzel-Schäfer, P. Talkner, P. Hänggi, A. Wixforth, "Microfluidic mixing via acoustically driven chaotic advection", *American Physical Society*, vol. 100, n. 3, 2008.

[70] H. Lim, S. M. Back, H. Choi, J. Nam, "Acoustic mixing in a dome-shaped chamber-based SAW (DC-SAW) device", *Lab on a Chip*, vol. 20, n. 1, pp. 120-125, 2020.

[71] C. Westerhausen, L. G. Schnitzler, D. Wendel, R. Krzyszton, U. Lächelt, E. Wagner, J. O. Rädler, A. Wixforth, "Controllable Acoustic Mixing of Fluids in Microchannels for the Fabrication of Therapeutic Nanoparticles", *Micromachines*, vol. 7, n. 9, p. 150, 2016.

[72] A. Wixforth, "Acoustically driven planar microfluidics", *Superlattices and Microstructures*, vol. 33, pp. 389-396, 2003.

[73] M. K. Tan, J. R. Friend, L. Y. Yeo, "Interfacial jetting phenomena induced by focused surface vibrations", *American Physical Society*, vol. 103, n. 2, 2009.

[74] H. Li, J. R. Friend, L. Y. Yeo, "Surface acoustic wave concentration of particle and bioparticle suspensions", *Biomed Microdevices*, vol. 9, pp. 647–656, 2007.

[75] Y. Bourquin, S. Abeer, J. Reboud, L. C. Ranford-Cartwright, M. P. Barrett, J. M. Cooper, "Rare-Cell Enrichment by a Rapid, Label-Free, Ultrasonic Isopycnic Technique for Medical Diagnostic", *Angewandte Chemie: International edition*, vol. 53, n. 22, pp. 5587-5590, 2014.

[76] T. Franke, A. R. Abate, D. A. Weitz, A. Wixforth, "Surface acoustic wave (SAW) directed droplet flow in microfluidics for PDMS devices", *Lab on a chip*, vol. 9, n. 18, pp. 2625-2627, 2009.

[77] T. Franke, S. Braunmüller, L. Schmid, A. Wixforth, D. A. Weitz, "Surface acoustic wave actuated cell sorting (SAWACS)", *Lab on a chip*, vol. 10, n. 6, pp. 789-794, 2010.

[78] Z. Ma, D. J. Collins, Y. Ai, "Detacheble acoustofluidic system for particle separation via a traveling surface acoustic wave", *Analytical Chemistry*, vol. 88, n. 10, 2016.

[79] Y. Chen, A. A. Nawaz, Y. Zhao, P.-H. Huang, J. P. McCoy, S. J. Levine, L. Wang, T. J. Huang, "Standing surface acoustic wave (SSAW)-based microfluidic cytometer", *Lab on a Chip*, vol. 14, n. 5, pp. 916-923, 2014.

[80] J. Shi, S. Yadzi, S. S. Lin, X. Ding, I. Chiang, K. Sharp, T. J. Huang, "Three-dimensional continuous particle focusing in a microfluidic channel via standing surface acoustic waves (SSAW)", *Lab on a chip*, vol. 11, n. 14, pp. 2319-2324, 2011.

[81] R. Guldiken, M. C. Jo, N. D. Gallant, U. Demirci, J. Zhe, "Sheathless size-based acoustic particle separation", *Sensors*, vol. 12, pp. 905-922, 2012.

[82] J. Nam, H. Lim, C. Kim, J. Yoon Kang, S. Shin "Density-dependent separation of encapsulated cells in a microfluidic channel by using a standing surface acoustic wave", *Biomicrofluidics*, vol. 6, n. 2, 2012.

[83] J. D. Adams, H. T. Soh, "Tunable acoustophoretic band-pass particle sorter", *Applied Physics Letters*, vol. 97, n. 6, 2010.

[84] Y. Deng, Y. Guo, B. Xu, "Recent development of microfluidic technology for cell trapping in single cell analysis: a review", *Processes*, vol. 8, n. 10, 2020.

[85] Y. Wu, Z. Ao, B. Chen, M. Muhsen, M. Bondesson, X. Lu, F. Guo, "Acoustic assembly of cell spheroids in disposable capillaries", *Nanotechnology*, vol. 29, n. 50, 2018.

[86] X. Lu, F. Soto, J. Li, T. Li, Y. Liang, J. Wang, "Topographical manipulation of microparticles and cells with acoustic microstreaming", *ACS Applied Material Interfaces,* vol. 9, n. 44, pp. 38870-38876, 2017.

[87] X. Ding, S. S. Lin, B. Kiraly, H. Yue, S. Li, I. Chiang, J. Shi, S. J. Benkovic, T. J. Huang, "On-chip manipulation using surface acoustic waves", *Proceedings of the National Academy of Sciences*, vol. 109, n. 28, pp. 11105-11109, 2012.

[88] J. Shi, D. Ahmed, X. Mao, S. S. Lin, A. Lawit, T. J. Huang, "Acoustic tweezers: patterning cells and microparticles using standing surface

acoustic waves (SSAWS)", *Lab on a chip*, vol. 9, n. 20, pp. 2890-2895, 2009.

[89] M. Wu, Z. Mao, K. Chen et al., "Acoustic Separation of Nanoparticles in Continuous Flow", *Advanced Functional Materials*, vol. 27, n. 14, 2017.

[90] B. Hammaström, T. Laurell, J. Nilsson, "Acoustic trapping of bacteria and nanoparticles in disposable glass capillaries using seed particles", *15th International Conference on Miniaturized System for Chemistry and Life Science, Seattle, Washington, USA*, 2011.

[91] D. J. Collins, Z. Ma, J. Han, Y. Ai, "Continuous micro-vortex-based nanoparticle manipulation via focused surface acoustic waves", *Lab on a Chip*, vol. 17, n. 1, pp. 91-103, 2017.

[92] L. Ren, Y. Chen, P. Li, Z. Mao, P.-H. Huang, J. Rufo, F. Guo, L. Wang, J. P. McCoy, S. J. Levine, T. J. Huang, "A high-throughput acoustic cell sorter", *Lab on a Chip*, vol. 15, n. 19, pp. 3870-3879, 2015.

[93] H. Felton, R. Hughes, A. Diaz-Gaxiola, "Negligible-cost microfluidic device fabrication using 3D-printed interconnecting channel scaffolds", *PLoS ONE*, vol. 16, n. 2, 2021.

[94] J. K. Luo, X. He, J. Zhuo, W. Wang, W. Xuan, J. Chen, H. Jin, Y. Xu, S. Dong, "Flexible and transparent surface acoustic wave microsensors and microfluidics", *Procedia Engineering*, vol. 120, n. 1877-7058, pp. 717-720, 2015.

[95] M. Barnes, S. M. Sajadi, S. Parekh, M. M. Rahman, P. M. Ajayan, R. Verduzco, "Reactive 3D printing of shape-programmable liquid crystal elastomer actuators", *ACS Applied Materials & Interfaces*, vol. 12, n. 25, pp. 28692-28699, 2020.

[96] J. Dual, T. Schwartz, "Acoutofluidics 3: Continuum mechanics for ultrasonic particle manipulation", *Lab on a Chip*, vol. 12, n. 2, pp. 244-252, 2012.

[97] H. Bruus, "Acoustofluidics 2: Perturbation theory and ultrasound resonance modes", *Lab on a Chip*, vol. 12, n. 1, pp. 20-28, 2012.

[98] H. Bruus, “Acoustofluidics 7: The acoustic radiation force on small particles”, *Lab on a Chip*, vol. 12, n. 6, pp. 1014-1021, 2012.

[99] J. Guo, Y. Kang, Y. Ai, “Radiation dominated acoustophoresis driven by surface acoustic waves”, *Journal of Colloid and Interface Science*, vol. 455, pp. 203-211, 2015.

[100] M. Travagliati, R. J. Shilton, M. Pagliazzi, I. Tonazzini, F. Beltram, M. Cecchini, “Acoustofluidics and Whole-Blood Manipulation in Surface Acoustic Wave Counterflow Devices”, *Analytical Chemistry*, vol. 86, n. 21, pp. 10633-10638, 2014.

[101] *COMSOL Multiphysics*®, Stockholm, Sweden: COMSOL AB.

[102] Z. Ni, Y. Chuhao, X. Guangyao, X. Linzhou, J. Huang, S. Liu, J. Tu, X. Guo, D. Zhang, “Modelling of SAW-PDMS acoustofluidics: physical fields and particle motions influenced by different descriptions of the PDMS domain”, *Lab on a Chip*, vol. 19, n. 16, pp. 2728-2740, 2019.

[103] *ESIEE Paris,* 2 boulevard Blaise Pascal, 93162 Noisy-le-Grand Cedex, France.

[104] *DOW*®, 2211 H.H. Dow Way, Midland, MI, USA.

[105] *Harrick Plasma*®, 120 Brindley Street, Ithaca, NY, USA.